This is to certify that the

thesis entitled

A MULTI-PREFERRED FIBER ORIENTATION CONSTITUTIVE MODEL FOR FIBER MAT REINFORCED THERMOPLASTICS WITH A RANDOM ORIENTATION APPLIED TO THE STAMP THERMO-HYDROFORMING PROCESS

presented by

Michael A. Zampaloni

has been accepted towards fulfillment of the requirements for

PhD degree in Mechanical Engineering

F. Barlat

Major professor

Date 1/21/03

A MULTI-PREFERRED FIBER ORIENTATION CONSTITUTIVE MODEL FOR FIBER MAT REINFORCED THERMOPLASTICS WITH A RANDOM ORIENTATION APPLIED TO THE STAMP THERMO-HYDROFORMING PROCESS

By

Michael A. Zampaloni

A DISSERTATION

Submitted to
Michigan State University
in partial fulfillment of the requirements
for the degree of

DOCTOR OF PHILOSOPHY

Department of Mechanical Engineering

2003

ABSTRACT

A MULTI-PREFERRED FIBER ORIENTATION CONSTITUTIVE MODEL FOR FIBER MAT REINFORCED THERMOPLASTICS WITH A RANDOM ORIENTATION APPLIED TO THE STAMP THERMO-HYDROFORMING PROCESS

By

Michael A. Zampaloni

This work focuses on the development of a constitutive relationship for the modeling of a multi-preferred fiber orientation sheet that has several different primary fiber orientations, none of which are necessarily mutually perpendicular prior to, or during, deformation. One of the goals was to develop the constitutive relationship for the deformation behavior of the fiber mat reinforced thermoplastics with a random orientation, a material that is starting to gain in popularity but has not been extensively investigated. Two different types of mat fiber reinforced material were investigated; one a continuous fiber mat and one a chopped fiber mat, both with a polypropylene matrix. Both materials were characterized through a series of squeeze flow and uniaxial tensile tests to determine the preferred fiber orientations as well as the material properties. The constitutive model was implemented through a user-subroutine into the commercial finite element analysis code ABAQUS/Explicit and the numerical results were validated against experimental stamping results. Overall, the multi-preferred fiber orientation constitutive relationship was able to accurately capture the material instabilities that occurred during the stamping process. Since the

mat fiber reinforced materials have not been extensively investigated this research creates one of the building blocks that can be used to develop more accurate models in the future. With the addition of a constitutive relationship for the interaction between the layers, this single layer model could be expanded into a constitutive relationship for the full sheet.

In addition to the constitutive modeling aspect of this work there is also an experimental portion that deals with the development, design, build and verification of a new processing method for the shaping and forming of fiber reinforced thermoplastic materials, stamp thermo-hydroforming. Experimentation demonstrated that the process provides a 7-10 percent increase in draw depth when applying small levels of counteracting pressure. In addition, the use of a counteracting hydrostatic pressure during forming led to less delamination of the material. Overall the experimental results demonstrate that the stamp thermo-hydroforming process is a viable method for shaping thermoplastic materials that warrants additional attention. When the numerical and experimental portions are coupled together a unique design tool is created. The numerical results can be used to eliminate some of the trial and error associated with experimental work and the experimental portion can be used to validate changes to the numerical simulation.

To Suzanne and Andrew, thank you for all your love, support and patience

ACKNOWLEDGMENTS

I would like to express my deepest appreciation to Dr. Farhang Pourboghrat for all of his support and guidance provided during the course of my graduate studies. Without his encouragement and leadership the research could not have progressed. His guidance and wisdom will stay with me throughout my professional career. I would also like to thank the members of my Ph. D. committee: Dr. Ronald Averill, Dr. Charles MacCluer and Dr. Thomas Pence for their constructive criticism and suggestions throughout the course of this work.

Special thanks are due to Dr. Woong-Ryeol Yu who helped guide my progression over the course of this research. Without his assistance this research would not have progressed as far or as fast. The time he took to work with me and all the knowledge he shared is greatly appreciated.

I would also like to thank Nader Abedrabbo and Yabo Guan for all their assistance and for their hard work in support of both the experimental and numerical aspects of this research.

The research was made possible through funding received from the Composite Material and Structures Center (CMSC) at Michigan State University and through the Manufacturing Research Consortium (MRC) at Michigan State University. Their support is greatly appreciated.

I would also like to acknowledge Mr. Ken Forden and Dr. Paul Bristow of Azdel Inc. for the generous resources provided in support of the stamp thermo-hydroforming research effort. In addition, I would like to thank Mr. Dave Gearing and Mr. Matt Klepp of Interlaken Technology for all their assistance during the course of this work.

Most importantly, I would like to thank my wife Suzanne and my son Andrew for all their patience, encouragement, support and sacrificed weekends and evenings during the course of my graduate work. This journey would have been impossible without them standing by my side. Thank you so much, I love you both tremendously.

TABLE OF CONTENTS

LIST OF TABLES

LIST OF FIGURES

NOMENCLATURE

E_{11} – Longitudinal Young's Modulus

E_{22} - Transverse Young's Modulus

E_{ii} - Young's Modulus for the i Fiber Direction

E_f - Young's Modulus of the Fiber

E_m - Young's Modulus of the Matrix

G_{12} - Shear Modulus

G_f - Shear Modulus of the Fiber

G_m - Shear Modulus of the Matrix

N - Number of Plies

Q - Modulus Matrix

S - Compliance Matrix

T- Transformation Matrix

t – Ply Thickness

V_{fo} - Original Fiber Volume Fraction

V_f - Fiber Volume Fraction

ε – Strain Tensor

γ - Angle Between Fibers

ν_{12} - Poisson's Ratio

ν_f - Poisson's Ratio of the Fiber

ν_m - Poisson's Ratio of the Matrix

θ - Angle Between Material Frame and Fiber Directions

ρ_a - Areal Density

ρ - Density of Fiber Reinforced Material

σ – Stress Tensor

ξ - Geometrical Factor

Chapter 1

INTRODUCTION

There exists an abundance of fiber-reinforced thermoplastics that exhibit material properties such as strength and modulus that are either comparable to or better than traditional metallic materials. Typically, the composite materials have better strength to weight ratios and modulus to weight ratios than metals and can also possess excellent fatigue strength to weight ratios. Therefore, fiber-reinforced thermoplastics have been gaining popularity as substitutions for many of the weight critical components in the aerospace and automotive industries [1].

These reinforced materials can exhibit the same strength properties as sheet steel, but at a fraction of the weight [2]. Currently in production there are already several composite automobile parts such as suspension springs, space frames, body panels, and entire assemblies. There are also a multitude of others that are being planned in the near future; including the introduction of an automobile body frame created entirely from fiber reinforced composite materials [3].

The fibers are the primary constituent of the fiber-reinforced material, occupying the largest volume fraction and sharing the majority of the load acting on the material. There are multitudes of commercially available reinforcing fibers ranging from glass to kevlar fibers. The choice of the type of reinforcing fiber

depends greatly on the material properties desired from the finished product. The second constituent that makes up the composite material is the polymeric matrix. The matrix serves three distinct functions; it is responsible for distributing the stresses between the reinforcing fibers, it protects the surface of the fibers from abrasion, and it protects the fibers from the adverse environmental effects.

The polymeric matrix can be split into two general categories, thermosets and thermoplastics. The thermoset polymers consist of molecules that are chemically bonded by cross-links forming a three-dimensional network structure. Thermoplastic polymers consist of individual molecules that form a linear structure with no chemical linking, these molecules are held together by weak secondary bonds such as van der Waals bonds and hydrogen bonds. Once formed, thermoset materials cannot be melted and reshaped whereas a thermoplastic polymer can be melted and reshaped as often as desired [1].

The use of a thermoplastic matrix lends itself very easily to the various high-volume and accuracy production rates that are required in the automotive industry. Some of the advantages of a thermoplastic matrix over a thermoset matrix includes: a controllable, constant molding behavior, even after being stored for long periods of time, parts can be reformed as needed, can be joined by hot-welding methods, can be bent, twisted, or otherwise hot-formed, better impact resistance and there is typically no cure time associated with these materials, thereby allowing for a much quicker forming time.

One of the unique aspects of designing parts with fiber reinforced composite materials is that the mechanical properties of the material can be tailored to fit a certain application. By changing the orientation or placement of the fibers the material can be designed to exhibit properties that are isotropic or highly anisotropic depending on the desired end result. A major drawback of this customization is the economic costs that may be associated with this processing method. While customizing individual parts may be appropriate when working with low production level parts when the idea is extrapolated to higher production parts the customizing process becomes highly cost prohibitive. For higher production parts the use of thermoplastic sheets that have a pre-existing fiber orientation is a much more cost-conscious choice.

Currently there is a wide range of orientation methods that can be used for the fiber reinforcement of the thermoplastic matrices including unidirectional, woven, and reinforced mat with random and preferred fiber orientations. A unidirectional material implies that the fibers within the matrix are aligned in a single direction. The advantage of this type of alignment is that along this alignment direction the strength and stiffness of the material is optimized when compared to the other types of reinforcements. The major drawback of this type of material is that while the longitudinal properties are optimized, the transverse properties (normal to the alignment direction) and the off-axis directions depend solely on the material properties of the matrix. As mentioned earlier the moduli of

the matrix are typically 100 times lower and the strength of the matrix is typically 5 times lower than metals so some performance is sacrificed in these directions when utilizing unidirectional materials.

Woven fabric reinforced materials consist of two fibers interwoven together, typically at right angles to one another. The fiber in the longitudinal (x) direction is typically termed the warp and the fiber in the transverse (y) direction is usually termed the weft. The primary strength of these fibers can be found along these warp and weft directions while material properties in the off-axis directions depend solely on the material properties of the matrix. These types of reinforcements provide a significant amount of design flexibility. The warp and weft fibers can be designed with the same material or, if the application requires, different types of fibers could be utilized. In addition, there are a multitude of weave patterns that can be utilized to alter the material properties. The major drawback of this type of reinforcement is the fact that the warp and weft fibers are woven together so there is a cross-over point where the fibers interact and could lead to some undesired behavior such as buckling in the through-thickness (z) direction.

Random fiber mat reinforced thermoplastics differ from both unidirectional and woven fabric structures in that the fibers are distributed in a random manner. These materials are not designed to provide directional strength and stiffness but to ensure that the load is transferred to the fibers instead of the matrix while the

part is being utilized. Theoretically, a thermoplastic that has a truly random fiber orientation should provide isotropic material properties. As will be shown in subsequent chapters, the material manufacturing process does impart some directionality to the material so the material will not behave in an isotropic manner but rather as a material with a number of preferred fiber orientations.

Numerous studies have been conducted focusing on the behavior of unidirectional laminates and there has also been considerable work on the evaluation of the highly structured woven fabric reinforced composites, work that will be cited in more detail in Chapter 3. The use of continuous fiber reinforcements with a random orientation has not been widely addressed due to the complicated nature of the fiber structure (see Figure 3 as an example). Since few assumptions can be made about the material, the characterization of its deformation behavior is complicated.

One of the most important steps in the development of a new product is determining a numerical method for the prediction of final part geometry and for the optimization of the process to meet certain product specifications. When working with composite materials this becomes even more critical since these types of materials are prone to wrinkling and buckling during the manufacturing process. In addition, when altering composite materials, anisotropy may be introduced in the part by the rearranging of the fibers within the matrix.

Many different constitutive models and characterization methods have been developed to represent the unique response of specific woven fabric and glass mat reinforced composites. The purpose of this research is to focus on the derivation and the scientific and mathematical description of the three-dimensional deformation behavior of thermoplastic composites reinforced with preferred or randomly oriented fibers of any size or shape during manufacturing. The main thrust of this work will be on the development of constitutive relationships for the randomly oriented mat cases while also touching on the research conducted on the woven fabric reinforced materials with the ultimate goal of building a unified constitutive model to design and optimize the stamp thermo-hydroforming process for shaping textile composites. Two different types of mat reinforcements will be evaluated: continuous glass fiber and chopped glass fiber, both with a random orientation. In addition, the modeling of the highly structured woven fabric reinforcements will be addressed.

Chapter 2

BACKGROUND

Even though fiber reinforced thermoplastic composite materials may present distinct advantages over the traditional metal materials, there is still the issue of manufacturing the parts while still achieving the same level of volume and accuracy. Over the years numerous manufacturing processes have been proposed to shape thermoplastic composite materials, ranging from injection molding to sheet stamping and filament winding. Shaping operations such as sheet forming, thermoforming, match die molding, contact molding, and resin transfer molding have been studied fairly extensively and are currently used by industry to manufacture polymer reinforced products of varying quality.

Due to its high success with metals, various attempts have been made to apply sheet-stamping techniques to composites. A difficulty in using thermoplastics in stamping, however, is the inflexibility of the thermoplastic material prior to heating and the heating requirements necessary to bring the matrix material to its glass transition temperature, enabling the part to be formed. The forming of straight, continuous fiber or woven fiber composite sheets typically results in wrinkling of the fibers and distortions. Randomly oriented fibers have provided good formability, but without the advantages of the highly directional properties often desired in composite parts. The more formable sheets

that consist of aligned, discontinuous fibers appear to have been used with more success than continuous fibers [4].

There are a number of factors that could influence the ability to process fiber reinforced composite materials. One of the most important factors is the effect that temperature has on the formability of the material. Fejes-Kozma et al. (1994) [5] and Czigany et al. (2000) [6] determined that the fracture-toughness response of unidirectional fiber reinforced composites was strongly affected by changes in temperature. Chow et al. (2001) [7] and Gorczyca et al. (2001) [8] also evaluated the temperature effects during the shearing of co-mingled woven glass thermoplastic composites. These studies demonstrated the importance that temperature has when processing fiber reinforced composite materials.

The second important factor impacting the deformation behavior of fiber-reinforced composites is strain rate. Davis et al. (1990) [9] performed a series of squeezing flow tests on glass mat fiber reinforced composites treating the GMTs as viscous, incompressible Newtonian fluids. They determined that as GMTs were deformed they appeared to strain harden. Gorczyca et al. (2001) [8] evaluated the effect of strain rate on woven glass fiber reinforcements and also found a very strong relationship between strain rate and material behavior during forming.

The third factor that significantly influences the deformation behavior of the composite during processing is hydrostatic pressure. Chen et al. (1993) [10] concluded that plastic deformation behavior of unidirectional composites is typically due to the behavior of the matrix and the exclusion of the hydrostatic stresses is not valid. On the microscopic scale they were able to deduce that the plastic strains were not incompressible due to the fact that the hydrostatic stresses were producing plastic deformations. Zinoviev et al. (2001) [11] further evaluated the effect of hydrostatic pressures on high-strength unidirectional composite materials. They found that the longitudinal moduli of elasticity were essentially pressure independent while the longitudinal tensile strength showed a strong dependence on the hydrostatic pressures.

McClintock (1968) [12] and Rice and Tracey (1969) [13] conducted studies on sheet metal blanks that demonstrated rapidly decreasing fracture ductility as a hydrostatic pressure, applied across the material, was increased. Clift et al. (1990) [14] and Hartley et al. (1992) [15] demonstrated that for sheet metal draw blanks, the use of a hydrostatic pressure prevented the initiation and spreading of microcracks within the metallic material. Based on the success found with using a hydrostatic pressure to delay the onset of fracture within metallic materials the same idea was extrapolated to the possible use of a hydrostatic force during the processing of thermoplastic materials. This led to the idea of adopting the use of stamp hydroforming currently used by sheet metal industries as a means of processing fiber reinforced thermoplastic composite sheets. The

stamp thermo-hydroforming process will be discussed in greater detail in Chapters 12 and 13.

One type of reinforced thermoplastic composite material that is becoming increasingly popular is glass-mat thermoplastics (GMTs). Due to their low weight, ease of processing, recyclability, noise suppression and price the use of these types of materials is beginning to gain favor with the automotive industry when creating some structural components such as bumpers or as backing for some interior components such as headliners. Glass mat thermoplastics are much easier to manufacture than most other composite materials. Rollers typically compress the reinforced mats and the resin. Once the material hardens it can be cut to the appropriate sheet size and shipped to the end-user. The material is easily recycled back into the process after shaping so the cost savings is significant. The major disadvantage of the material is the significant lofting that occurs after the resin material is heated to its glass transition temperature; see Figure 1 for an example. Due to this lofting it is very difficult to achieve a class A finish with this material so its typical applications include mostly structural parts or parts that are not on the exterior of the vehicle.

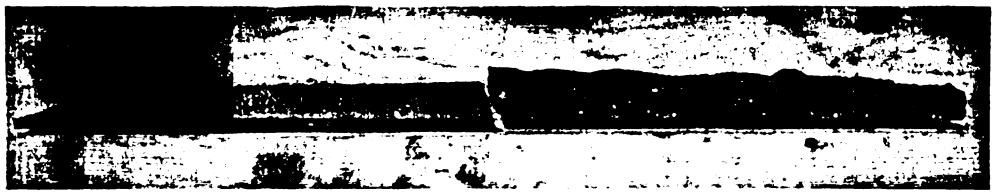

Figure1. Illustration of the lofting associated with glass mat reinforced thermoplastics. Part on the left is unheated and the part on the right is after the material has been heated to its forming temperature.

As mentioned previously a truly random fiber orientation would allow for the assumption that the material properties were isotropic. In an attempt to validate this assumption some preliminary numerical modeling was performed using the commercial code MARC. Initially the focus was placed on modeling hemispherical cups formed from random continuous fiber reinforced polypropylene matrix composite material, arranged without any prescribed directionality during the manufacturing process. The material properties that were utilized to characterize the composite sheets came through a series of uniaxial tensile tests performed at different temperatures for the continuous fiber (random orientation) reinforced polypropylene matrix material.

The material deformation process was modeled using a rigid-plastic, incremental analysis that used large displacements and an updated Lagrangian procedure. Modeling was conducted for a part that was drawn to depths varying from 30 to 75 mm (1.2 – 3 inches). The boundary conditions utilized included the restriction of the y-direction movement of the lower end of the axisymmetric part

to account for the axis of symmetry within the material. This allowed for a further simplification by analyzing only half of the sheet and assuming symmetric behavior of the overall part. Figure 2 illustrates a sheet that is being stamped to a depth of 75 millimeters (mm) (3 inches (in)).

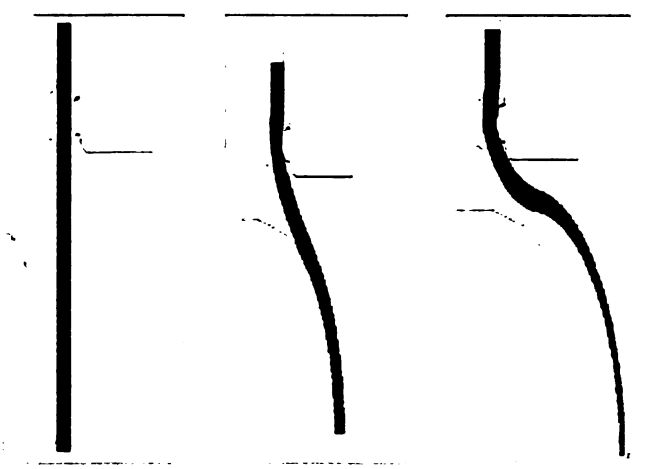

Figure 2. Two-Dimensional modeling results for the stamping process using a continuous fiber reinforced glass mat with a random orientation.

One of the major assumptions that went into the creation of this model was that the material was isotropic. While this could theoretically be the case for this type of material the actual manufacturing process does impart some directionality to the material as it is manufactured. Figure 3 is an Environmental Scanning Electron Microscopy (ESEM) image taken of the material prior to deformation. As can be shown from this figure, there does seem to be some directionality, especially in the general x-direction, and the assumption that the material is isotropic is invalid. In addition, even if the two-dimensional isotropic model did

provide some results that were consistent with the expected and with the experimental results, information regarding the fiber orientation after deformation would be unavailable.

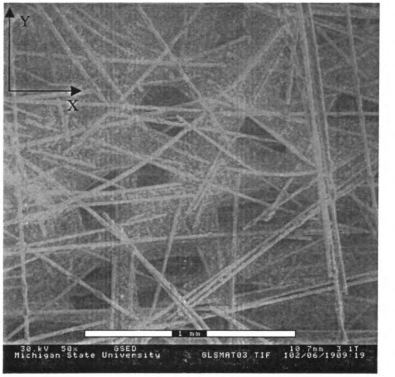

Figure 3. Environmental Scanning Electron Microscopy (ESEM) image of an undeformed glass mat fiber reinforced thermoplastic with a random orientation.

The two-dimensional model could provide a quick method of evaluation but would not be very useful for an in-depth analysis of material behavior and material property changes after undergoing deformation (specifically fiber orientation and the main strength areas of the material). Therefore, a different modeling approach is needed so that accurate information regarding fiber

orientation after deformation and changes to the overall strength or other material properties can be determined during the design phase.

Chapter 3

CONSTITUTIVE MODELING LITERATURE REVIEW

Before describing the proposed methodology, the state-of-the-art on constitutive modeling for textile composites will be reviewed according to reinforcement type. Works on constitutive modeling of preform without resin, which is useful in the RTM (Resin Transfer Molding) type of process modeling, will be omitted.

3.1. Unidirectional Structures

Based on the simplified geometry of the unidirectional fiber reinforcement numerous studies have been conducted focusing on the behavior of unidirectional laminates. Most of this work provides the basis for the more complicated reinforcement methods so the details of these past works will be omitted from this work. The major papers that focused on the behavior of unidirectional laminates that were used during the course of this research study will be mentioned in detail as they apply to either the woven or the mat structured materials. Otherwise the majority of these works were not directly utilized except where they formed the basis for the more complicated fiber reinforcement arrangements.

3.2. Woven Structure (Anisotropic Preferred Fiber Orientation)

The research on constitutive modeling for woven fabric reinforced composites (FRT) can be classified into two general categories; continuum mechanics and non-continuum mechanics models. The non-continuum approach is used for the modeling of textile preform without resin. This enables draping simulation before resin injection in RTM, with the dynamics of particles representing the intersection points between warp and weft threads (Breen et al., 1994 [16]). For woven FRT, the continuum model is preferred due to its complex deformation behavior during manufacturing. Therefore, the rest of this research will focus solely on the use of the continuum-based model. In general, for composite modeling the material can be treated as either homogenous or non-homogeneous. Based on non-homogeneous concepts, truss and shell (membrane) elements are used to model textile structure and resin matrix, respectively (Sidhu et al., 2001 [17], Billoet et al., 2000 [18]).

Many models assuming homogeneous material properties have been developed utilizing the well-defined mathematical theory (e.g. orthotropic constitutive equation) thereby reducing the computational cost (Luca et al., 1998 [19]). These studies assume the preservation of the initial orthotropy of woven FRT during all forming processes, which is a common practice in sheet metal forming analysis. This assumption is not proper for the analysis of woven FRT, since the change in fiber angles is significant (Dong et al., 2001 [20]).

Several efforts have been made to develop numerical models capable of capturing the fiber angle evolution. This resulted in non-orthogonal continuum constitutive equations for unidirectional composites that maintained fiber inextensibility and incompressibility assumptions (O'Bradaigh et al., 1991 [21]). This approach has been applied to the diaphragm forming analysis of unidirectional thermoplastic composites and recently has been extended to thermoplastic composites with woven fabric reinforcements (Spencer, 2000 [22]).

A great deal of research has been devoted to using homogenization methods to account for the evolution of micro-structural parameters, such as fiber angle, to predict the macroscopic deformed shape of composites. Homogenization methods consist of modeling a unit cell in 3D and then solving a set of governing equations to obtain the homogenized material properties of the composite based on the geometrical description of the unit cell (Hsiao et al., 1999 [4]). In spite of the computational disadvantages, including long computational time, the homogenization method has been used to model a multitude of domains such as micro-level of fiber and meso-level of fabric (Takano et al., 1999 [23]).

Recently, a new method has been developed that reduces computational costs and accounts for micro-structural effects on the forming behavior of thermoplastic composites. The method utilizes numerical experimental techniques to extract the nonlinear elastic material properties based on the

homogenization method, all under a continuum mechanics framework (Peng et al., 2000 [24]).

3.3. Mat Structure (Anisotropic Random Fiber Orientation)

While mat structure materials have not been extensively investigated there is still some work being accomplished that can provide a starting point for further investigations. Sikarskie (1998) [82] has investigated the failure process for random mat structured materials. The investigation focused on determining a global failure theory that required a thorough understanding of the material's behavior during uniaxial tensile testing, specifically post peak stress-strain behavior. Several problems were encountered during the experimentation phase resulting in no clear indication of the post peak stress-strain behavior for the random mat structures.

The anisotropic modeling of isothermal squeezing flow for GMT was investigated using a transversely isotropic incompressible Newtonian fluid model (Dweib et al., 1998 [2]) and non-Newtonian fluid model (Dweib et al., 1999 [25]) based on the work of Rogers (1989) [26]. These works characterized the viscous flow properties of GMT using compression molding. Results showed very good agreement with the experiments but the feasibility of the model's application to thermoforming was not included.

While the above research was focusing on the macro-mechanical behavior to develop viscous material laws for GMT, several works have looked at the fiber orientation through squeezing flow experiments (Dweib et al., 2000 [27]) and tensile testing (Lee et al., 1999 [28]). This resulted in the conclusion that the optimal strength occurs at a volume fraction of approximately 20%. Research on fiber orientation in mat structures has been widely performed in textile manufacturing, especially for short fibers (Lee et al., 1992a, 1992b [29, 30]). For GMT composites a few works (McGee et al., 1983 [31], Advani et al., 1987 [32]) have focused on characterizing the material using the fiber orientation distribution function (ODF). Kitano et al. (2000) [33] evaluated the influence of different types of fibers on the mechanical properties of mat structures for hybrid composites.

A transversely isotropic model for the mechanical response of fiber mats was developed to simulate the compression in RTM (Pillai et al., 2001 [34]). The model includes a nonlinear function for the compressive stresses due to changes in mat thickness, ignoring other responses. The focus was on predicting the deformation during the compression of dry preform mats without resin matrix. The constitutive model for the glass mat was developed based on classical nonlinear elasticity.

3.4. Strain Rate and Temperature Dependent Constitutive Modeling

To apply numerical models to the stamp thermo-hydroforming, it might be necessary to take into account the effect of strain rate and temperature on constitutive modeling due to the polymeric nature of composites (Ebewele, 2000 [35]). There have been numerous studies performed for deformation behavior during cases of high strain rates such as Goldberg et al. (2000, 2001) [36, 37] and Tsai et al. (2000) [38]. While some of these investigations may provide insight into the incorporation of strain rate dependence into a constitutive model, the high strain rates studied corresponded to single events such as bird strikes in an aircraft engine, blast loading of a submarine hull, or some other dynamic loading events. The strain rates investigated were at levels much higher than those typically encountered in material forming.

There are a few works that considered strain rate effects on composites undergoing simultaneous heating conditions. A viscoplastic model was developed using a one-parameter flow law for unidirectional thermoplastic composites at forming temperatures (Wang et al., 1997 [39]). The viscoplastic model developed showed limitations in its application to woven fabric reinforced composites (Thiruppukuzhi et al., 2000 [40]).

Several works have been dedicated to characterizing the anisotropic viscous properties of composites considering strain rate effects at several different

temperatures (McGuinness et al., 1997a, 1997b [41, 42]). The parameters of an anisotropic viscous fluid law were obtained by fitting the constitutive equation to the experimental data. Recently, the shear behavior of woven co-mingled glass reinforced thermoplastics was investigated. The main focus of the work was on the reproducibility of picture frame tests. Results showed that some mechanical pre-conditioning improves repeatability of shear tests, and that temperature strongly affects the stress-strain response of the composite (Chow et al., 2001 [7]).

Chapter 4

CONSTITUTIVE MODELING BACKGROUND

A review of the past and present literature shows that no attempt has yet been made to develop a constitutive model that can be applied to the deformation response of a wide range of materials ranging from the highly structured woven fabric composites that have a series of two preferred fiber orientations to the continuous fiber reinforced materials with a random orientation that may have several different preferred fiber orientations. This work focuses on the development of a constitutive relationship for the modeling of a multi-preferred fiber orientation sheet that has several different primary fiber orientations.

Since the bulk of the work conducted in the past focuses on the behavior of the highly structured woven composites some continuum-based, non-orthogonal constitutive models that were derived for those materials will be utilized with new definitions of the concept of primary fiber orientations for GMT to characterize its anisotropy. The advantages of this constitutive model are that continuum based models: (a) are computationally efficient, (b) can accurately predict fiber orientation and strength by tracking the evolution of non-orthogonal preferred directions, (c) can be applied to a wide range of composite materials and (d) are easily implemented into finite element analysis codes through user defined material subroutines. Details of this new model will be discussed in Chapter 5.

4.1. Orthotropic Constitutive Modeling

For some initial validation, and to create a baseline to compare future results against, the use of an orthotropic constitutive model was explored. The orthotropic consideration assumes that there are two preferred directions, both mutually perpendicular to one another, even after deformation. An orthotropic material model was created using the commercial code ABAQUS/Explicit and used to model a variety of fiber mat reinforced materials. Results for these models can be found in Chapter 11.4.

4.2. Non-Orthogonal Constitutive Modeling

The main source of the anisotropic behavior of textile composites is the preferred directions (warp and weft) for woven FRT and the preferred fiber orientations for GMT. The fiber orientations can be treated as material axis, which determine the symmetrical properties of the material, thus enabling the textile composites to be treated as orthotropic materials. As reviewed in the previous section, this assumption would only be true if the deformation was such that it preserved the orthogonality of fiber directions. However, in real forming

situations, such as in the stamp thermo-hydroforming process, the orthogonality of the fibers will not be preserved due to rheological flow of resin matrix.

Therefore, the constitutive modeling should be based on the non-orthogonality of fiber directions, maintaining preferred fiber orientations as main variables for describing the deformation behavior of textile composites. The majority of yield functions used in metal forming and composite mechanics were developed based on orthotropic anisotropy. Therefore, the development of a constitutive model based on the non-orthogonality concept will be of great benefit to both metal and polymeric material science.

Chapter 5

UPDATED MATERIAL LAW WITH CONSTANT MATERIAL PROPERTIES

Dong et al. (2001) [20] developed a constitutive modeling approach for the draping of dry woven fabrics that demonstrated the importance of non-orthogonality on material behavior during deformation. The term updated material law refers to the fact that the constitutive relationship is changing as the material deforms. The constitutive relationship is based on a series of fiber directions. As the material deforms these fiber directions move thereby changing the overall material properties that form the basis for the model, hence the term updated material law. Dong et al. focused on the investigation of a woven fabric reinforced material but the research conducted as a part of this study investigated the behavior of preferred fiber directions that were not necessarily orthogonal prior to, or even during, deformation.

The approach involved the consideration of a fiber reinforced material as a series of two unidirectional layers, illustrated schematically in Figure 4. Each layer was analyzed individually and then a global stiffness matrix was created based on the summation of these two layers.

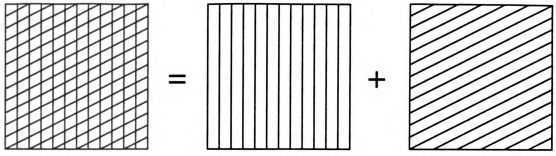

Figure 4. Schematic illustration of the basic theory behind the constitutive relationship developed by Dong et al. for evaluating the draping behavior of dry woven fabrics.

The theory started with the most general form of Hooke's law with linear elastic anisotropic material properties that can be found in Equation 1.

$$[\sigma] = [Q][\varepsilon] \tag{1}$$

Where σ is the stress tensor, Q is the modulus matrix and ε is the strain tensor.

The inverse of [Q] can be written as shown in Equation 2, where [S] is termed the compliance matrix.

$$[S] = [Q]^{-1} \tag{2}$$

Using Equation 2 to rewrite Equation 1 results in Equation 3.

$$[\varepsilon]=[S][\sigma] \tag{3}$$

For a three-dimensional stress state the generalized Hooke's law relationship can be written as illustrated in Equation 4.

$$\begin{bmatrix}\varepsilon_{11}\\ \varepsilon_{22}\\ \varepsilon_{33}\\ \varepsilon_{23}\\ \varepsilon_{31}\\ \varepsilon_{12}\\ \varepsilon_{32}\\ \varepsilon_{13}\\ \varepsilon_{21}\end{bmatrix}=\begin{bmatrix} S_{1111} & S_{1122} & S_{1133} & S_{1123} & S_{1131} & S_{1112} & S_{1132} & S_{1113} & S_{1121}\\ S_{2211} & S_{2222} & S_{2233} & S_{2223} & S_{2231} & S_{2212} & S_{2232} & S_{2213} & S_{2221}\\ \vdots & \vdots & \vdots & \vdots & \vdots & \vdots & \vdots & \vdots & \vdots\\ \vdots & \vdots & \vdots & \vdots & \vdots & \vdots & \vdots & \vdots & \vdots\\ \vdots & \vdots & \vdots & \vdots & \vdots & \vdots & \vdots & \vdots & \vdots\\ \vdots & \vdots & \vdots & \vdots & \vdots & \vdots & \vdots & \vdots & \vdots\\ \vdots & \vdots & \vdots & \vdots & \vdots & \vdots & \vdots & \vdots & \vdots\\ \vdots & \vdots & \vdots & \vdots & \vdots & \vdots & \vdots & \vdots & \vdots\\ S_{2111} & S_{2122} & S_{2133} & S_{2123} & S_{2131} & S_{2112} & S_{2132} & S_{2113} & S_{2121}\end{bmatrix}\begin{bmatrix}\sigma_{11}\\ \sigma_{22}\\ \sigma_{33}\\ \sigma_{23}\\ \sigma_{31}\\ \sigma_{12}\\ \sigma_{32}\\ \sigma_{13}\\ \sigma_{21}\end{bmatrix} \tag{4}$$

As shown in Equation 4 there are 81 separate elastic constants that are needed to solve the constitutive relationship. This is much too unwieldy to use as a constitutive model for more than one specific material so some simplifying assumptions need to be made. As shown by Tsai et al. (1968) [43] the stress, strain, compliance and stiffness matrices are symmetrical. Therefore, using the relationships outlined in Equation 5, and the simplifying notation outlined in Equation 6, a constitutive relationship containing only 21 independent elastic constants can be created, Equation 7.

$$\sigma_{12} = \sigma_{21}$$
$$\sigma_{13} = \sigma_{31}$$
$$\sigma_{23} = \sigma_{32}$$

$$\varepsilon_{12} = \varepsilon_{21}$$
$$\varepsilon_{13} = \varepsilon_{31} \qquad (5)$$
$$\varepsilon_{23} = \varepsilon_{32}$$

$$S_{1122} = S_{2211}$$
$$S_{1121} = S_{2111}$$
etc.

$$\begin{aligned} \sigma_{11} &= \sigma_1 & \varepsilon_{11} &= \varepsilon_1 \\ \sigma_{22} &= \sigma_2 & \varepsilon_{22} &= \varepsilon_2 \\ \sigma_{33} &= \sigma_3 & \varepsilon_{33} &= \varepsilon_3 \\ \sigma_{23} &= \sigma_4 & \varepsilon_{23} &= \varepsilon_4 \\ \sigma_{13} &= \sigma_5 & \varepsilon_{13} &= \varepsilon_5 \\ \sigma_{12} &= \sigma_6 & \varepsilon_{12} &= \varepsilon_6 \end{aligned} \qquad (6)$$

$$\begin{bmatrix} \varepsilon_1 \\ \varepsilon_2 \\ \varepsilon_3 \\ \varepsilon_4 \\ \varepsilon_5 \\ \varepsilon_6 \end{bmatrix} = \begin{bmatrix} S_{11} & S_{12} & S_{13} & S_{14} & S_{15} & S_{16} \\ S_{12} & S_{22} & S_{23} & S_{24} & S_{25} & S_{26} \\ \vdots & \vdots & \vdots & \vdots & \vdots & \vdots \\ \vdots & \vdots & \vdots & \vdots & \vdots & \vdots \\ \vdots & \vdots & \vdots & \vdots & \vdots & \vdots \\ S_{16} & S_{26} & S_{36} & S_{46} & S_{56} & S_{66} \end{bmatrix} \begin{bmatrix} \sigma_1 \\ \sigma_2 \\ \sigma_3 \\ \sigma_4 \\ \sigma_5 \\ \sigma_6 \end{bmatrix} \qquad (7)$$

Halpin (1984) [44] proved that a plane of symmetry could be assumed as shown in Figure 5. Based on this plane of symmetry Equation 7 can be reduced to Equation 8, which has 13 independent elastic constants. Extending this

concept to assume 3 planes of symmetry, typically called the orthotropic assumption, Equation 8 can be reduced further to Equation 9, which has only 9 independent elastic constants.

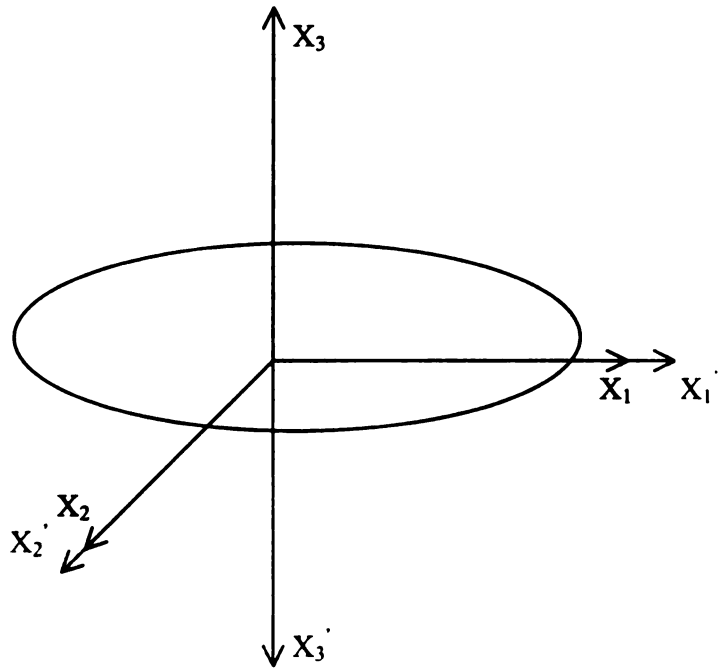

Figure 5. Plane of material symmetry.

$$\begin{bmatrix} \varepsilon_1 \\ \varepsilon_2 \\ \varepsilon_3 \\ \varepsilon_4 \\ \varepsilon_5 \\ \varepsilon_6 \end{bmatrix} = \begin{bmatrix} S_{11} & S_{12} & S_{13} & 0 & 0 & S_{16} \\ S_{12} & S_{22} & S_{23} & 0 & 0 & S_{26} \\ S_{13} & S_{23} & S_{33} & 0 & 0 & S_{36} \\ 0 & 0 & 0 & S_{44} & S_{45} & 0 \\ 0 & 0 & 0 & S_{45} & S_{55} & 0 \\ S_{16} & S_{26} & S_{36} & S_{46} & S_{56} & S_{66} \end{bmatrix} \begin{bmatrix} \sigma_1 \\ \sigma_2 \\ \sigma_3 \\ \sigma_4 \\ \sigma_5 \\ \sigma_6 \end{bmatrix} \quad (8)$$

$$\begin{bmatrix} \varepsilon_1 \\ \varepsilon_2 \\ \varepsilon_3 \\ \varepsilon_4 \\ \varepsilon_5 \\ \varepsilon_6 \end{bmatrix} = \begin{bmatrix} S_{11} & S_{12} & S_{13} & 0 & 0 & S_{16} \\ S_{12} & S_{22} & S_{23} & 0 & 0 & S_{26} \\ S_{13} & S_{23} & S_{33} & 0 & 0 & 0 \\ 0 & 0 & 0 & S_{44} & 0 & 0 \\ 0 & 0 & 0 & 0 & S_{55} & 0 \\ S_{16} & S_{26} & S_{36} & 0 & 0 & S_{66} \end{bmatrix} \begin{bmatrix} \sigma_1 \\ \sigma_2 \\ \sigma_3 \\ \sigma_4 \\ \sigma_5 \\ \sigma_6 \end{bmatrix} \tag{9}$$

Since each individual layer of a composite material is very thin it is safe to assume a state of plane stress since the stresses within the plane are going to be at least an order of magnitude larger than the through-thickness stresses. This reduces Equation 9 to Equation 10.

$$\begin{bmatrix} \varepsilon_1 \\ \varepsilon_2 \\ \varepsilon_6 \end{bmatrix} = \begin{bmatrix} S_{11} & S_{12} & 0 \\ S_{12} & S_{22} & 0 \\ 0 & 0 & S_{66} \end{bmatrix} \begin{bmatrix} \sigma_1 \\ \sigma_2 \\ \sigma_6 \end{bmatrix} \tag{10}$$

Using Equation 2 on Equation 10 results in Equation 11.

$$\begin{bmatrix} \sigma_1 \\ \sigma_2 \\ \sigma_6 \end{bmatrix} = \begin{bmatrix} Q_{11} & Q_{12} & 0 \\ Q_{12} & Q_{22} & 0 \\ 0 & 0 & Q_{66} \end{bmatrix} \begin{bmatrix} \varepsilon_1 \\ \varepsilon_2 \\ \varepsilon_6 \end{bmatrix} \tag{11}$$

Potter (1970) [45] showed that for woven fabric composites that the primary deformation mode during draping was the pure shear of the fabric. Illustrated in Figure 6 is an element undergoing pure shear with a shear force applied along all four sides of the element, where N_p and N_t denote the initial warp and weft

directions, respectively, for a woven fabric case and the original material directions are shown by M_1 and M_2. After deformation n_p and n_t denote the new directions of the warp and weft respectively and the new material frame is denoted by m_1 and m_2. Figure 7 is a different pure shear case where the initial warp fiber direction coincides with the deformed warp direction. In this case the material frame has rotated as well as the weft direction.

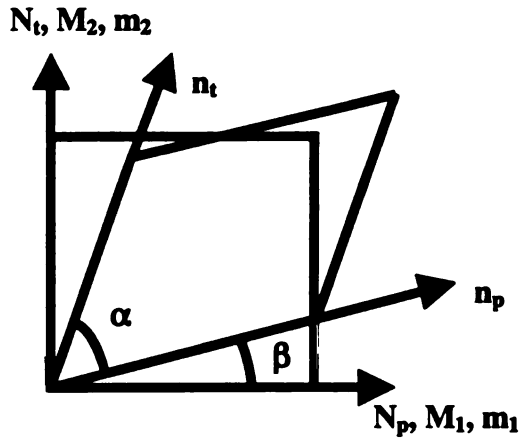

Figure 6. Illustration of an element undergoing pure shear. Material frame before and after deformation remains coincidental.

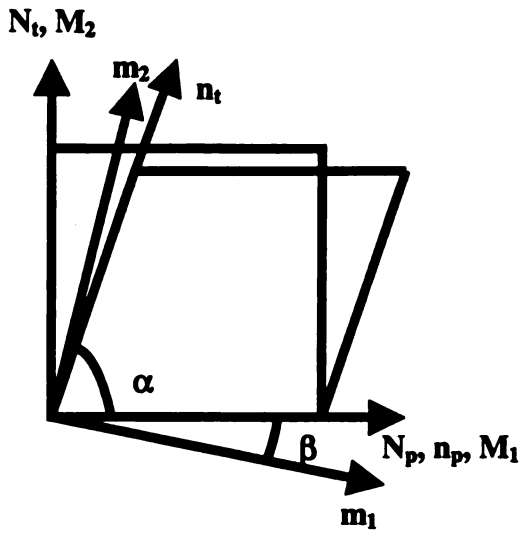

Figure 7. Illustration of an element undergoing pure shear. Material frame before and after deformation rotates while the warp fiber direction before and after deformation remains coincidental.

The stiffness matrix [Q] can be determined based on its principal geometrical axes for each preferred fiber direction, Equation 12, based on the following assumptions; (a) that the reinforced sheet has a plane of symmetry coinciding with the median plane of the sheet, (b) that the preferred fiber orientations are balanced so that the sheet can be considered symmetric and (c) that the thickness of the sheet is much less than the width and length of the sheet. Note that for ease of writing the subscript 6 was changed to subscript 3.

$$\left[Q_{ij}\right]=\begin{bmatrix} Q_{11} & Q_{12} & Q_{13} \\ Q_{21} & Q_{22} & Q_{23} \\ Q_{31} & Q_{32} & Q_{33} \end{bmatrix} \tag{12}$$

As shown by Halpin (1984) [44], the components of the stiffness matrix can be rewritten in terms of the engineering constants of the fiber reinforced thermoplastic as illustrated in Equation 13.

$$
\begin{aligned}
Q_{11} &= E_{11}/(1-\upsilon_{12}\upsilon_{21}) \\
Q_{22} &= E_{22}/(1-\upsilon_{12}\upsilon_{21}) \\
Q_{12} &= \upsilon_{12}E_{11}/(1-\upsilon_{12}\upsilon_{21}) \\
Q_{33} &= G_{12} \\
Q_{13} &= Q_{31} = Q_{23} = Q_{32} = 0 \\
Q_{21} &= Q_{12}
\end{aligned}
\qquad (13)
$$

Where E_{11} represents the Young's Modulus of the fiber in the 1-direction, E_{22} represents the Young's Modulus of the matrix material in the normal to the 1-direction. ν_{12} is the Poisson's Ratio for the fiber in the 1-direction and G_{12} is the Shear Modulus for the fiber in the 1-direction. When working with the second preferred fiber orientation unidirectional layer the same definitions hold, E_{11} is the Young's Modulus of the fiber, E_{22} is the Young's Modulus of the matrix, ν_{12} is the major Poisson's Ratio and G_{12} is the Shear Modulus for the fiber in the second preferred fiber orientation.

Plugging Equation 13 into Equation 12 yields Equation 14. This equation can be considered a special orthotropic case as illustrated in Figure 8. A fictitious fiber direction is assumed normal to each individual preferred fiber orientation or preferred fiber direction (PFD). This fictitious normal direction represents the matrix material in the unidirectional layer. The relationship between this fictitious

layer and the preferred fiber orientation is orthotropic; hence Equation 14 can be considered a special orthotropic case whereas the preferred fiber orientations do not need to remain orthotropic. Therefore, the deformation behavior of each fiber is tracked individually instead of as a unit.

$$\left[Q_{ij}\right]=\begin{bmatrix} E_{11}/(1-\upsilon_{12}\upsilon_{21}) & \upsilon_{12}E_{11}/(1-\upsilon_{12}\upsilon_{21}) & 0 \\ \upsilon_{12}E_{11}/(1-\upsilon_{12}\upsilon_{21}) & E_{22}/(1-\upsilon_{12}\upsilon_{21}) & 0 \\ 0 & 0 & G_{12} \end{bmatrix} \tag{14}$$

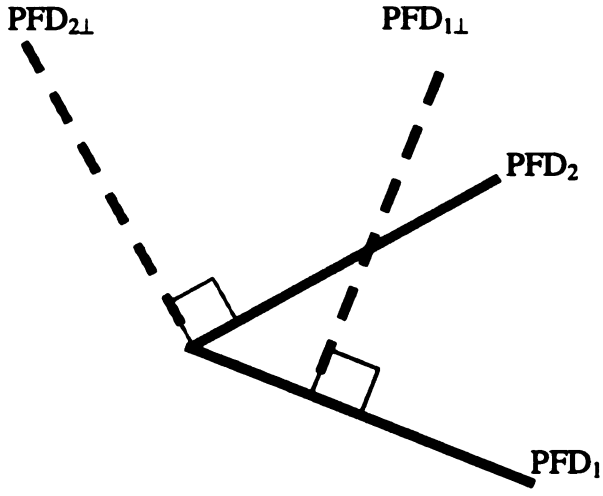

Figure 8. Orthotropic relationship built into the constitutive modeling theory.

For both preferred fiber orientations the minor Poisson's Ration can be determined from the relationship outlined in Equation 15.

$$\nu_{21} = \frac{\nu_{12} E_{22}}{E_{11}} \tag{15}$$

Since the material properties are measured along the fiber axes it is imperative that the stiffness matrix after each deformation is transformed back to the material frame so that there can be continuity with regard to the point of reference. A simple transformation matrix is illustrated in Equation 16.

$$T(\theta) = \begin{bmatrix} m^2 & n^2 & 2mn \\ n^2 & m^2 & -2mn \\ -mn & mn & m^2 - n^2 \end{bmatrix} \tag{16}$$

Where the angle θ is based on the relationships between the material frame and the fiber directions according to Figures 6 and 7. For example, for a woven fabric material the warp direction would have a corresponding angle, θ=β and the weft direction would have an angle, θ=α+β, m = cos (θ) and n = sin (θ).

Based on Equation 12 and Equation 16, Equation 11 can be rewritten as Equation 17.

$$[\sigma]_k = [T]^{-1}[Q]_k[T][\varepsilon]_k \tag{17}$$

Where $[T]^{-1}$ can be represented by Equation 18.

$$[T]^{-1} = [T(-\theta)] = \begin{bmatrix} m^2 & n^2 & -2mn \\ n^2 & m^2 & 2mn \\ mn & -mn & m^2 - n^2 \end{bmatrix} \tag{18}$$

Using Equation 17 each term of Equation 12 can be written as shown in Equation 19 to represent the transformed stiffness matrix for a single preferred fiber orientation direction.

$$\begin{aligned}
\bar{Q}_{11} &= Q_{11}m^4 + 2(Q_{12} + 2Q_{33})n^2m^2 + Q_{22}n^4 \\
\bar{Q}_{22} &= Q_{11}n^4 + 2(Q_{12} + 2Q_{33})n^2m^2 + Q_{22}m^4 \\
\bar{Q}_{12} &= (Q_{11} + Q_{22} - 4Q_{33})n^2m^2 + Q_{12}(n^4 + m^4) \\
\bar{Q}_{33} &= (Q_{11} + Q_{22} - 2Q_{12} - 2Q_{33})n^2m^2 + Q_{33}(n^4 + m^4) \\
\bar{Q}_{13} &= (Q_{11} - Q_{12} - 2Q_{33})nm^3 - (Q_{22} - Q_{12} - 2Q_{33})n^3m \\
\bar{Q}_{23} &= (Q_{11} - Q_{12} - 2Q_{33})mn^3 - (Q_{22} - Q_{12} - 2Q_{33})m^3n
\end{aligned} \tag{19}$$

Using Equation 19 the constitutive model for a single fiber orientation can be written as shown in Equation 20, where the k represents a single preferred fiber orientation.

$$[\sigma]_k = \begin{bmatrix} \bar{Q}_{11} & \bar{Q}_{12} & \bar{Q}_{13} \\ \bar{Q}_{21} & \bar{Q}_{22} & \bar{Q}_{23} \\ \bar{Q}_{31} & \bar{Q}_{32} & \bar{Q}_{33} \end{bmatrix}_k [\varepsilon]_k \tag{20}$$

For materials with more than one preferred fiber orientation, basically anything other than a unidirectional case, a combination stiffness matrix will need

to be created that takes into account the behavior in multiple directions. For a material with only two preferred fiber orientations this combination is shown in Equation 21.

$$\bar{Q}_{ij} = \bar{Q}_{ij}^{p}(\beta) + \bar{Q}_{ij}^{t}(\alpha+\beta) = \left[\bar{Q}\right] \tag{21}$$

So, the final constitutive relationship for the deformation behavior of fiber reinforced thermoplastics with two preferred fiber orientations can be represented as illustrated by Equation 22.

$$[\sigma] = \left[\bar{Q}\right][\varepsilon] \tag{22}$$

5.1. Incorporating Fiber Interaction into the Constitutive Relationship

There are a couple of limitations associated with this constitutive model. The first and most obvious is that by assuming two semi-independent unidirectional layers the interaction between the fibers that may occur during deformation has been removed. For the random fiber mat reinforced materials this may not pose as severe a problem as in the woven fabric reinforced cases. For the woven cases the fibers are physically limited in their motion by the interaction point at the juncture point of the weave. The random mat fibers are not physically tied together so the same type of behavior is not anticipated.

To incorporate shear stiffness into Equation 22, due to either friction at the interaction point of the woven fibers or due to the shear viscosity of resin matrix, shear properties of the material could be utilized. Preferred fiber orientations updated according to the deformation of the reinforced material allow for the calculation of the rotation of the fibers at a crossing point. This rotation allows for the calculation of the shear strain by comparing the old and new configurations of the two fibers. That is, the change in the fiber angle between the preferred fiber orientations represents the shear strain of the fiber reinforced material.

Corresponding to the shear strain, a shear stress could be calculated using experimentally measured shear stress-strain relationships (e.g., obtained from a picture frame shear test). This stress will be assumed to act along a local orthogonal coordinate system that causes the pure shear deformation of the material. To define this local coordinate system, the bisect axis (positioned between 2 preferred fiber orientations), shown in Figure 9 can be utilized.

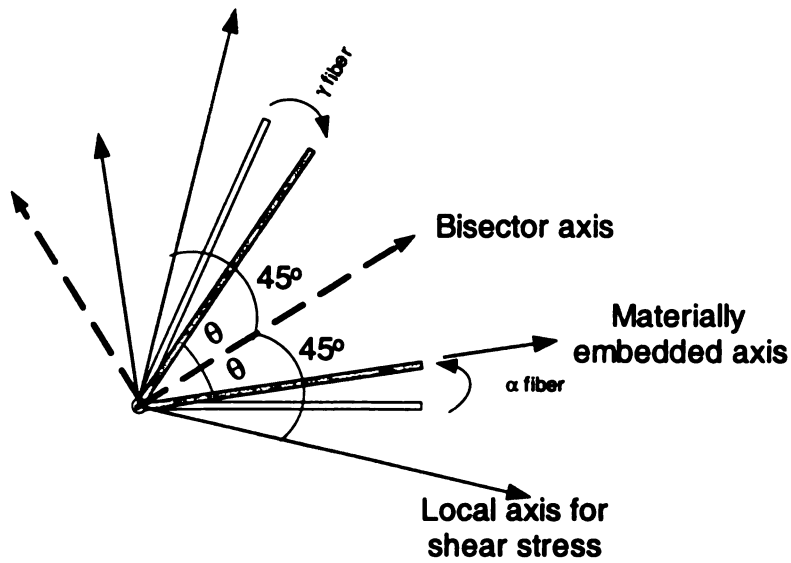

Figure 9. Illustration of the bisector coordinate system used to calculate the shear stiffness between 2 preferred fiber orientations.

One of the axes of the local coordinate system will be located 45° counter clockwise (CCW) from the bisect axis, and the other axis will be located 45° clockwise (CW) from the bisector axis. The shear stress defined along this local orthogonal coordinate axis can be transformed back into the materially embedded coordinate system and added to the constitutive equation to account for the shear stiffness.

The second limitation is associated with the material properties and how they are incorporated into the model. According to Equation 14, the stiffness matrix is based on a set of constant material properties such the Young's modulus along the preferred fiber orientation. Presently there is no mechanism within the model

to account for the evolution of the material properties as the material undergoes deformation. This limitation will be addressed in more detail in Chapter 6.

5.2. Results for the Updated Material Law with Constant Material Properties Constitutive Model

The initial results utilizing the updated material law with constant material properties did not match the results that were illustrated in the work by Dong et al. [20]. Figure 10 is a plot of the shear stress versus shear angle for a variety of constant material properties, including the values given in the paper. The dashed line in the plot represents the experimental data they were using as a baseline for their numerical modeling. The test was a simple pure shear test following the guidelines in Figure 7.

The discrepancy between the numerical and experimental results can be attributed to a couple of different reasons. The first, most obvious reason, is that the article did not include all the test data such as sample size, density etc. Some assumptions had to be made regarding these parameters so some error is anticipated. The largest discrepancy is probably in the general trend exhibited by each case. As evidenced by the results there seems to be some type of work hardening occurring during the numerical analysis. This can be attributed to the use of a constant material property. As the part is sheared the material properties should be changing. For example, the strength in the 2-direction

should not contribute anything to the strength in the 1-direction until deformation has begun. As the angle between the fibers decreases from 90° the strength in the 1-direction should be getting larger and the strength in the 2-direction should be getting smaller. This result was not exhibited by this numerical analysis.

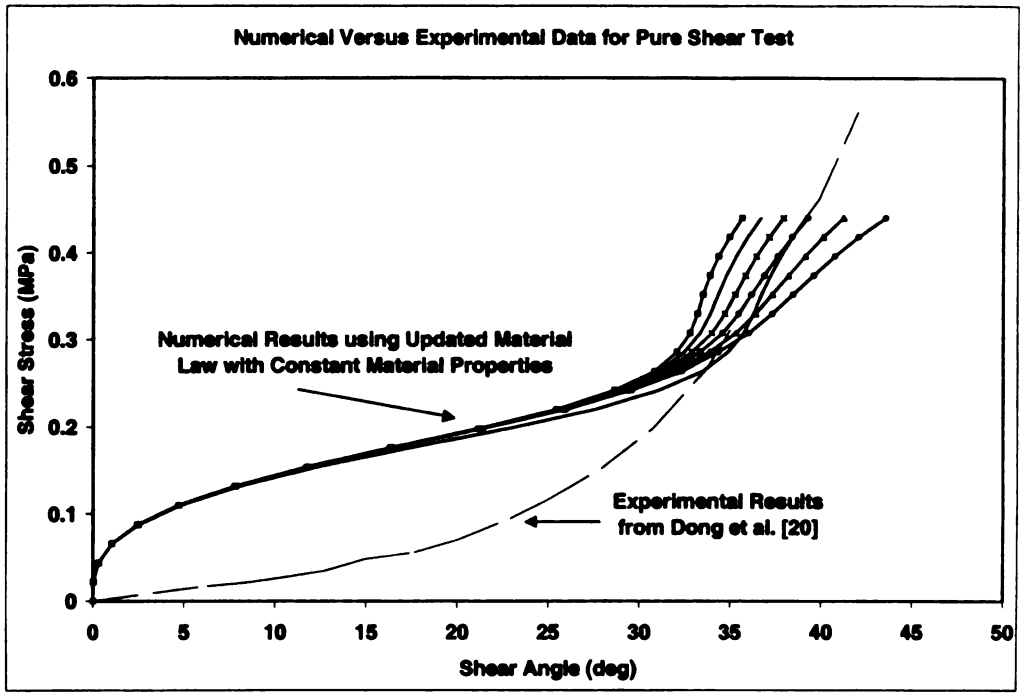

Figure 10. Plot of shear stress versus shear angle for the pure shear case. The dashed line is the experimental data provided by Dong et al. [20] in their paper.

Chapter 6

UPDATED MATERIAL LAW WITH VARYING MATERIAL PROPERTIES

As illustrated by the results outlined in Chapter 5, the constitutive relationship from Equation 22 does not accurately represent the material behavior during deformation. One of the major reasons discovered for this discrepancy is the effect of changes in fiber angle with respect to material properties. For the purpose of explanation consider the pure shear deformation illustrated in Figure 7 for a woven fabric material. As the material begins to undergo shear deformation the angle between the two preferred fiber orientations begins to change. If, for example, the first preferred fiber direction was taken as the 1-fiber direction then as the second fiber is deformed and no longer normal to the 1-fiber direction the strength in the 1-direction will increase, i.e. it will take more applied force to shear the material further in the 1-direction. This will increase, theoretically, until the 1 and 2 fiber directions are aligned thereby giving the maximum theoretical strength of the material in a single direction. The same idea will hold for the other material properties, basically they will all become a factor of the changes in the fiber angle between the preferred fiber orientations.

To that end Mohammed et al. (2000) [46] worked on a model for dry fabrics that was based on material properties that changed with respect to the angle between the fibers. Their work was applied only to dry woven fabrics but was based on a similar theory that was proposed by Dong et al. (2001) [20].

Essentially what they were trying to show was that two unidirectional layers, one for the warp and one for the weft of a woven fabrics reinforced material could be used to represent the deformation behavior of dry woven fabrics.

Some assumptions that were made as a part of this theory include the fact that the fabric element deforms following pure shear, the lengths of its sides do not change during the shearing, there is no compression and the that the element thickness remains unchanged. Therefore, through simple mass continuity, the fiber volume fraction can be determined as illustrated in Equation 23.

$$V_f = \frac{V_{fo}}{\sin \gamma} \tag{23}$$

Where V_{fo} is the original fiber volume fraction, V_f is the fiber volume fraction after shear deformation, and γ is the angle between the warp and weft fibers. The original volume fraction is easily determined from a calculation illustrated in Equation 24, based on four material specific constant values, the areal density of the fabric, ρ_a, the density of the fiber material, ρ, the number of plies, N and the thickness of each ply, t.

$$V_{fo} = \frac{N \rho_a}{t \rho} \tag{24}$$

Assuming no voids in the material leads to Equation 25.

$$V_f + V_m = 1 \tag{25}$$

Since the fiber volume fraction will change with respect to changes in the fiber angle, the material properties can be rewritten in terms of the fiber volume fraction, V_f, through Equation 25 following the Rule of Mixtures as shown in Equations 26 through 29.

$$E_{11} = E_f V_f + E_m (1 - V_f) \tag{26}$$

$$\frac{1}{E_{22}} = \frac{V_f}{E_f} + \frac{(1 - V_f)}{E_m} \tag{27}$$

$$\upsilon_{12} = \upsilon_f V_f + \upsilon_m (1 - V_f) \tag{28}$$

$$\frac{1}{G_{12}} = \frac{V_f}{G_f} + \frac{(1 - V_f)}{G_m} \tag{29}$$

Where E_{ii} represents the Young's Modulus in the i fiber direction, E_f and E_m are the Young's Modulus of the fiber and matrix respectively. ν_{12} is the major Poisson's Ratio while ν_f and ν_m represent the Poisson's Ratio of the fiber and the

matrix. G_{12} is the Shear Modulus of the fabric whereas G_f and G_m are the Shear Modulus of the fiber and the matrix. E_f, E_m, ν_f, ν_m, G_f and G_m are material specific constants that can be determined at the beginning of the analysis and will not need to be re-evaluated with regard to changes in shear angle.

Equations 26-29 are used to determine the material properties E_{11}, E_{22}, ν_{12} and G_{12} for each change in γ, thereby making the stiffness matrix a function of γ, i.e. $Q_{ij}=Q_{ij}(\gamma)$. The same theory outlined in Equations 13 through 20 will hold for the deformation of fiber reinforced thermoplastics with 2 preferred orientations. The stiffness matrix resulting from this theory is shown in Equation 30.

$$\left[\bar{Q}_{ij}\right]_{sheet} = \left(\left[\bar{Q}_{ij}\right]_k + \left[\bar{Q}_{ij}\right]_l\right) \tag{30}$$

With the final constitutive relationship for a thermoplastic composite with two preferred fiber orientations written as shown in Equation 31.

$$[\sigma] = \left[\bar{Q}_{ii}\right]_{sheet} [\varepsilon] \tag{31}$$

6.1. Results for the Updated Material Law with Varying Material Properties Constitutive Model with Two Preferred Fiber Orientations

The results from the updated material law using material properties that changed with respect to changes in the shear angle showed trends that were more in line with the pure shear experimental results, Figure 11. This validated the idea that material properties that vary with changes in shear angle may have a significant effect on the modeling behavior of fiber reinforced thermoplastics.

While these results more closely represented the experimental behavior there still seemed to be some discrepancies. One of the major reasons for these discrepancies can be traced back to the lack of modeling data such as sample size, shearing force and specific material properties. Without the accurate modeling data used by the authors there was great difficulty associated with trying to correlate the modeling results against the experimental results taken from the paper.

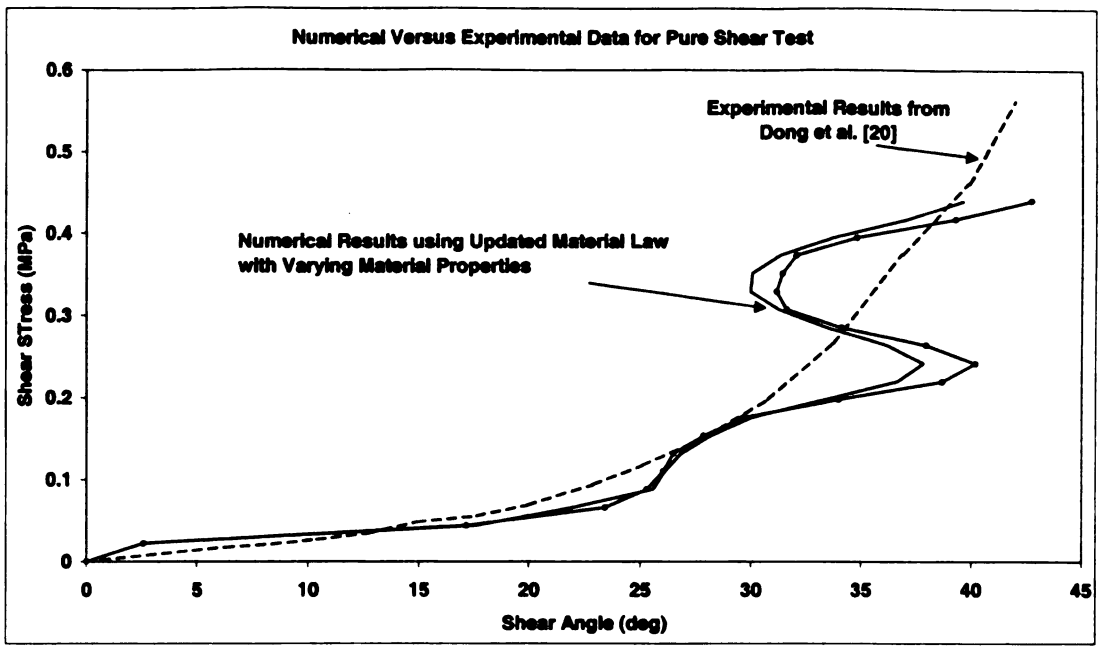

Figure 11. Illustration of the effect of varying material properties on the shear stress versus shear angle behavior of the fiber reinforced thermoplastic.

6.2. Updated Material Law with Multiple Preferred Fiber Orientations

For more than two preferred fiber orientations such as in the case of the continuous fiber materials with a random orientation, Figure 12, Equation 30 could be changed to account for the number of preferred fiber orientations as illustrated in Equation 32.

$$\left[\bar{Q}\right]_{sheet} = \left(\left[\bar{Q}\right]_1 + \left[\bar{Q}\right]_2 + \ldots + \left[\bar{Q}\right]_n\right) \tag{32}$$

Thereby resulting in the constitutive relationship shown in Equation 33.

$$[\sigma]=\left[\bar{Q}\right]_{sheet}[\varepsilon] \tag{33}$$

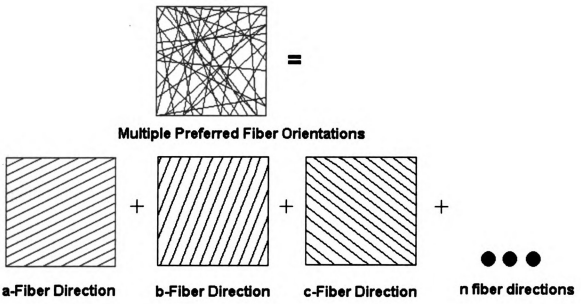

Figure 12. Multiple preferred fiber orientation illustration.

Chapter 7

INCORPORATING CONSTITUTIVE MODEL INTO A COMMERCIAL FINITE ELEMENT PACKAGE

One of the goals of this research was to develop a constitutive modeling approach that could be incorporated in a commercial finite element package such as ABAQUS or LS-DYNA. Since the constitutive equation is given as an explicit form it is suitable for any commercial explicit code. For the purposes of this research ABAQUS/Explicit was chosen due its well-defined handling of user subroutines. Figure 13 is a flow chart illustrating the flow of information with respect to the use of a VUMAT for ABAQUS/Explicit.

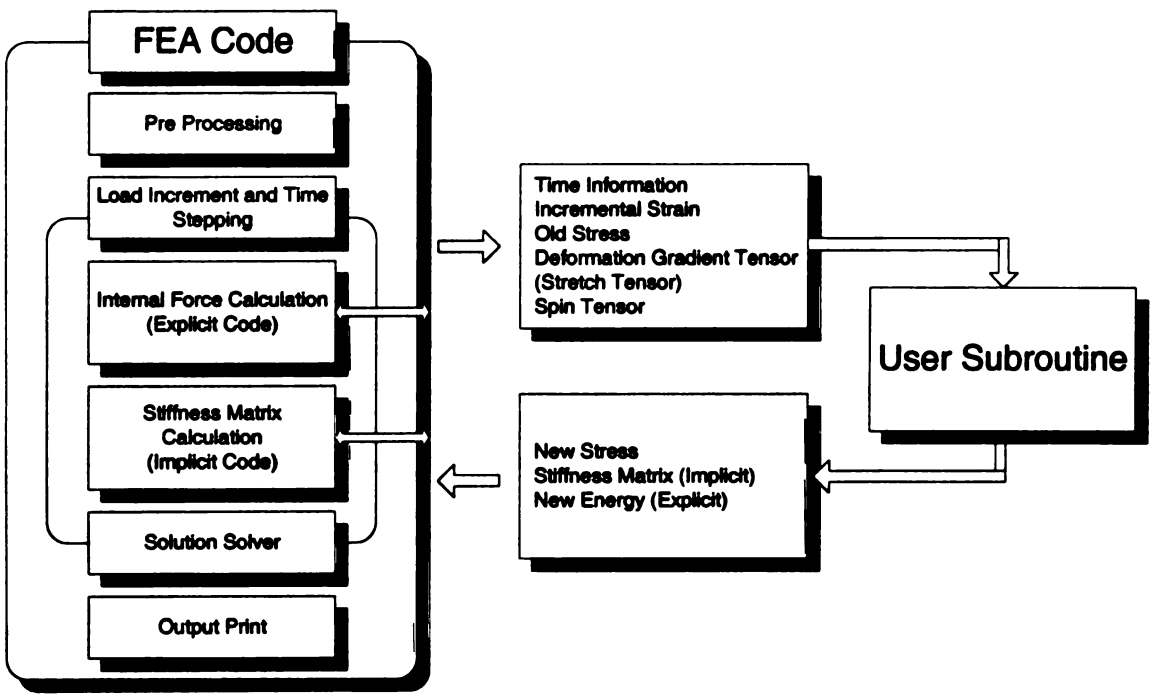

Figure 13. Flow chart illustrating the incorporation of the constitutive model into the commercial finite element package ABAQUS/Explicit.

Essentially the user subroutine could be thought of as the material box within the flow chart. From ABAQUS information such as time, stresses, incremental strains, and stretch and spin tensors are taken from the commercial code. This information is brought into the subroutine and is used to calculate new stress and energy values. These new values are then sent back to ABAQUS and the iteration continues until the simulation is completed.

One of the main reasons for incorporating the constitutive relationship into a commercial finite element package is that the use of a commercial code allows for the incorporation of contact and strain rate effects without the need to write additional subroutines covering these complicated aspects of material deformation. In addition, a commercial code makes the constitutive model more accessible for validation and speeds up the processing and debugging time.

A major disadvantage of using a commercial code is the determination of the proper reference frame. It is imperative that the methods used by the commercial code to calculate stresses and strains is well understood so that the proper transformations can be addressed within the user subroutine. As shown in Figure 14, for a material with 2 preferred fiber orientations, the fibers do not always align with the material axes after deformation. In addition, the material axes themselves have been rotated. Therefore, it is crucial to understand how the commercial code interprets this rotation (i.e. globally or locally) so that the proper stress and strain transformations can be made within the user subroutine.

Figure 15 illustrates the rotations and transformations associated with a material that has three preferred fiber orientations. As is evident from the illustration, as the number of preferred fiber directions increases, the effort and importance of tracking these coordinate axes becomes even more important to ensure that the proper stresses and strains are calculated and incorporated into the deformation behavior.

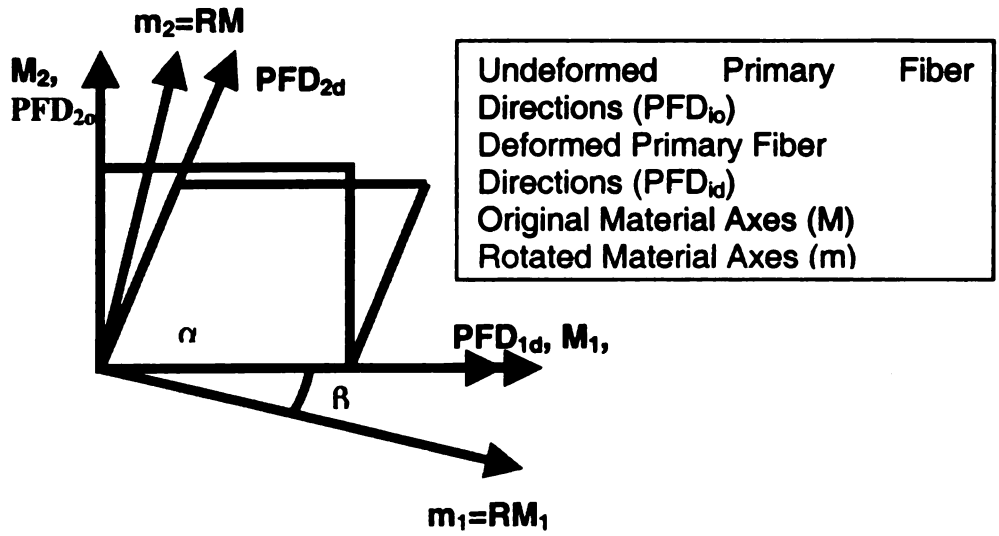

Figure 14. Illustration of the rotating fiber directions and material axes for transforming stresses and strains within the user subroutine.

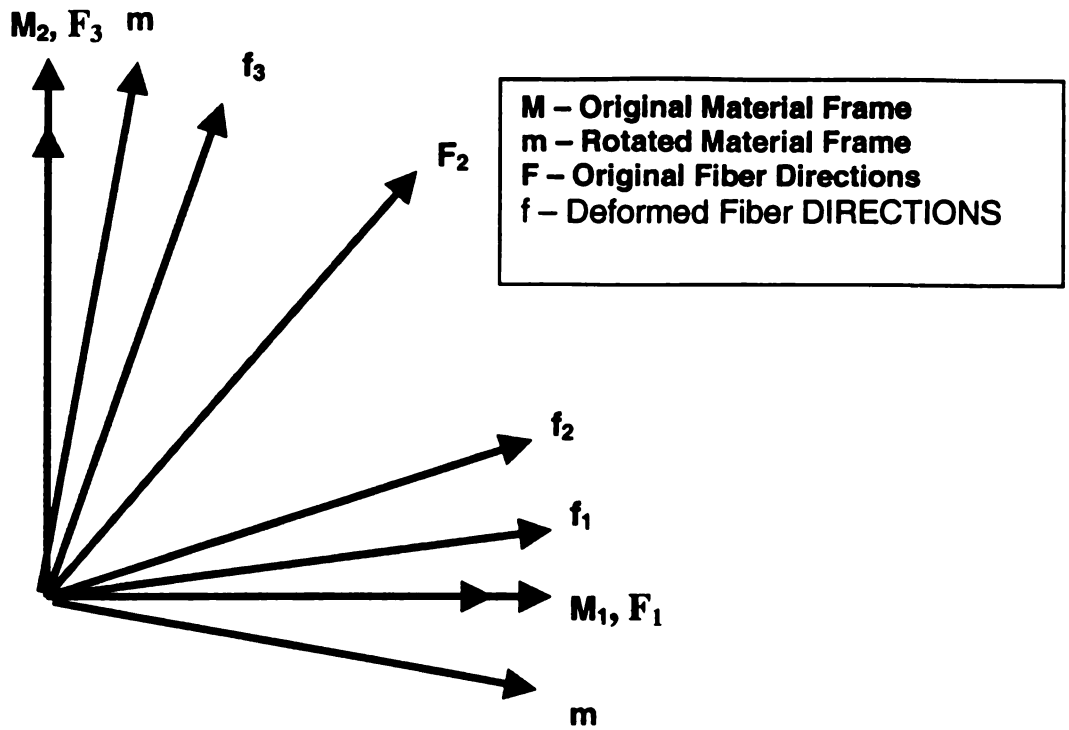

Figure 15. Material axes and fiber location tracking for a material with three preferred fiber orientations.

Chapter 8

MATERIAL CHARACTERIZATION

Material characterization is a vitally important step in the link between the numerical and experimental aspects of this work. The numerical data that results from the analysis is only going to be relevant for the material properties incorporated into the model. If the properties are not reflective of the actual material being tested than a direct comparison between the two methods is rendered irrelevant. So, in order to properly characterize the material behavior during deformation, there existed the need to perform a series of different material tests including compression (or squeeze flow) tests and multi-axis uniaxial tension tests in order to determine the material properties to be used for the numerical analysis.

8.1. Fiber Mat Reinforced Material

Before delving into the material characterization methods it is important to provide a little background on the fiber mat material that is being studied as a part of this work. There are two primary types of fiber mat materials that are going to be characterized, both supplied through a partnership with Azdel, Inc. The first is the R401, continuous fiber mat reinforced thermoplastic and the second is the C321, long chopped fiber mat reinforced thermoplastic, both with a random fiber orientation. The continuous fiber strand mat has a polypropylene

matrix and contains approximately 40% glass while the chopped fiber mat also has a polypropylene matrix and is approximately 32% glass.

8.2. Squeeze Flow Tests

A squeeze flow test or a compression test, as illustrated in Figure 16, is a test method that was utilized in order to determine the preferred fiber orientations for both the chopped and continuous fiber reinforced materials. A 75 mm (3 in) diameter specimen was cut from the material and the material axis corresponding to the zero degree direction was labeled. The part was placed between two heated platens and heated to a forming temperature of 190° Celsius (375° F). Once the material had reached the forming temperature a load of 2224 N (500 lb) was placed on the part and held for 60 seconds. The part was then unloaded and allowed to cool to room temperature within the mold thereby ensuring it would retain its deformed shape. Figure 17 illustrates a pre and post test sample for the R401-B01, continuous fiber material while Figure 18 illustrates the pre- and post test sample for the C321-B01, chopped fiber reinforced thermoplastic samples.

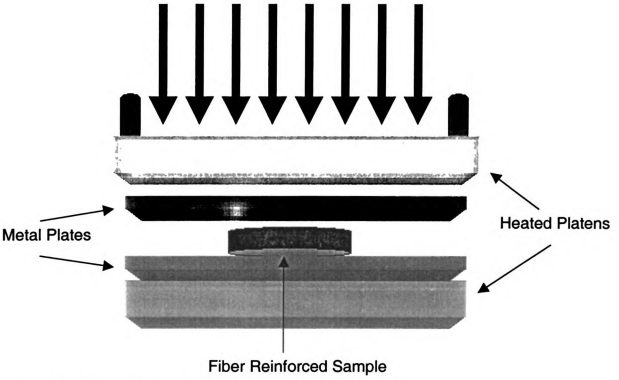

Figure 16. Squeeze flow test diagram.

Figure 17. Squeeze flow results for R401-B01, continuous fiber glass mat reinforced thermoplastic, sample on bottom is original 75 mm disc, on top is the final compressed shape.

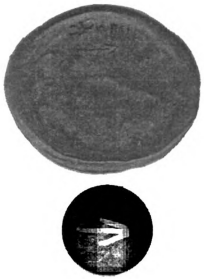

Figure 18. Squeeze flow results for C321-B01, chopped fiber glass mat reinforced thermoplastic, sample on bottom is original 75 mm disc, on top is the final compressed shape.

As shown by Figures 17 and 18 both the continuous mat and the chopped fiber mat deformed anisotropically, the original circular blanks ended up forming an elliptical shape. This confirms the assumption that there is some directionality associated with the fiber arrangements within the matrix and demonstrates that the flow velocity and strain rate are not a constant within the material and vary with respect to an angle ϕ. An isotropic part would have resulted in a circular sample at the completion of the compression process instead of the elliptical behavior found with these samples; therefore these tests confirm the anisotropic nature of the material.

Assigning a polar coordinate system based on ϕ, as outlined in Figure 19, lines were drawn on the deformed parts corresponding to 5° increments. Figures 20 and 21 illustrate this technique for the continuous and chopped fiber glass reinforced materials, respectively, starting at the initial 0° direction line that was marked on the material prior to compression, and proceeding around to the full 360°. The lengths of these lines, measured from the original center point of the material to the edge of the compressed sample were recorded and plotted as shown in Figures 22 and 23.

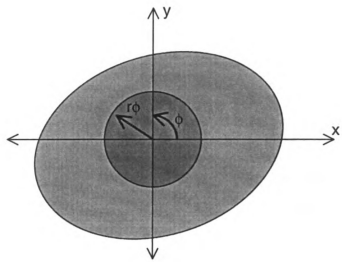

Figure 19. Polar coordinate system used as a reference for the squeeze flow experiments.

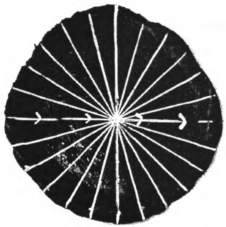

Figure 20. Polar coordinate system drawn on the R401, continuous fiber mat reinforced thermoplastic used to determine the preferred fiber orientations. The arrow on the part represents the 0° direction.

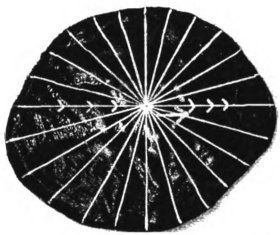

Figure 21. Polar coordinate system drawn on the C321, chopped fiber mat reinforced thermoplastic used to determine the preferred fiber orientations. The arrow on the part represents the 0° direction.

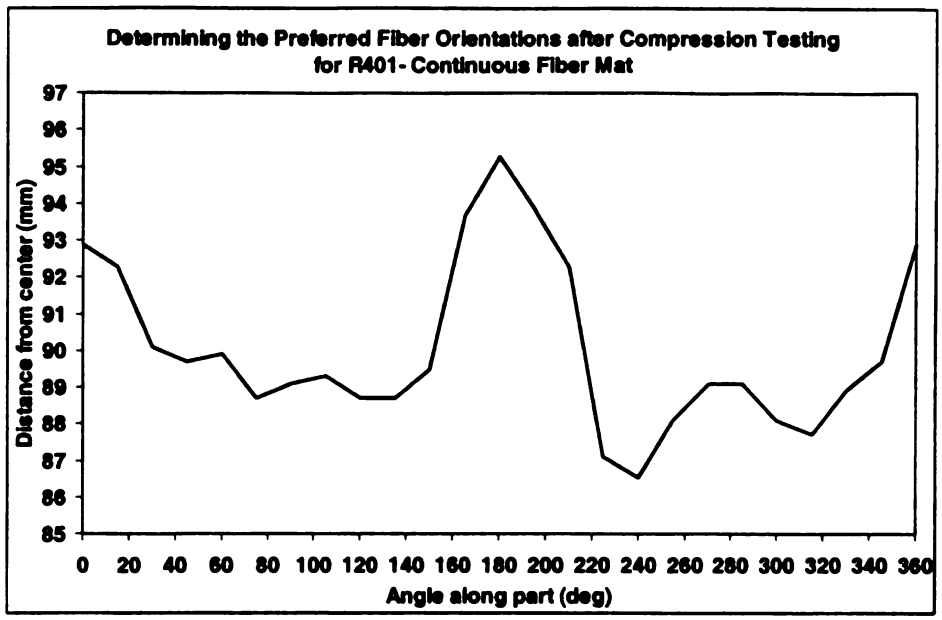

Figure 22. Length from center point to edge of compressed part along ϕ direction for R401-B01, continuous fiber mat.

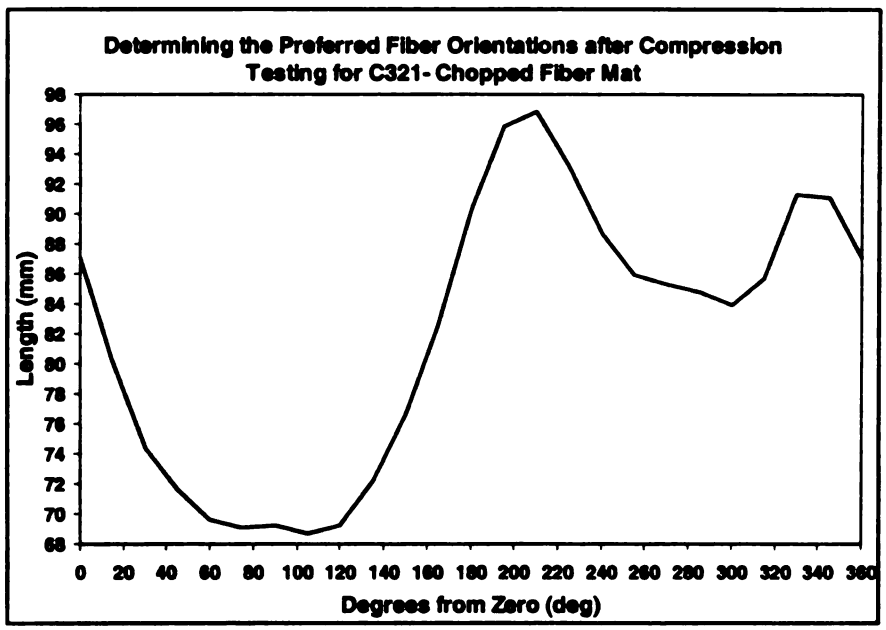

Figure 23. Length from center point to edge of compressed part along ϕ direction for C321-B01, chopped fiber mat.

From Figure 22, the squeeze flow test for the continuous fiber mat reinforced thermoplastic showed an almost quasi-isotropic type of flow behavior. Even though the length changes are small compared to the chopped fiber mat case the plot illustrates that there are some subtle differences between the directions, especially at the 180° direction thereby confirming the anisotropic nature of the material. For the chopped fiber reinforced mat materials there are some distinct minimum and maximums shown so there is definite anisotropic flow behavior occurring for this material during deformation.

Using these plots the preferred fiber orientations could be determined by looking at the maximum and minimum points on the plot. Since the random fiber reinforced materials are layered there are a large number fibers that are not aligned with the x and y plane. By compressing the samples the fibers are forced to align within this plane thereby providing a general method for determining the preferred fiber orientations during deformation for each mat fiber reinforced material type. This leads to the theory that these maximum and minimum points can be used as preferred fiber orientations for the material and can be utilized to determine the material properties. For the continuous fiber material there are 3 distinct points corresponding to the 0°, 60° and 90° degree directions. For the chopped fiber mat, C321-B01, there are two distinct peaks at 30° and 105° with two lesser peaks at 120° and 150°.

8.3. Determining Material Properties

Uniaxial tensile tests can be used to determine a significant amount of information regarding material behavior especially in regard to determining the material properties. Through tensile testing of fiber reinforced materials material properties such as Young's modulus, Poisson's ratio, ultimate tensile strength, and ultimate tensile strain.

For the glass mat fiber reinforced materials uniaxial tensile testing was performed based on the preferred fiber orientations determined through the squeeze flow tests. Tensile tests were conducted using the setup depicted in Figure 24 that included a United testing machine along with a laser extensometer system to measure longitudinal extension within the gage area of the test sample.

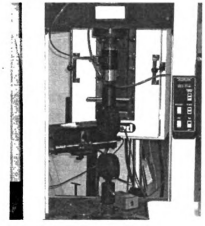

Figure 24. Tensile testing setup used for evaluating the glass mat reinforced thermoplastic composites.

All tests were performed following the guidelines outline in ASTM standard D 3039/D 3039M–95a. Initially tests were performed with the samples held at room temperature (23° C) with a constant strain rate of 5 mm/min. Figure 25 illustrates a sample test coupon after testing while Figures 26-28 contain the results for the R401-B01, continuous fiber mat material along the preferred fiber orientations while Figures 29-32 contain the uniaxial tensile testing results for the C321-B01, chopped fiber mat samples.

Figure 25. Tensile test coupon at the completion of the test cycle at room temperature. The reflective tape is used by the laser extensometer system to measure changes in the longitudinal extension of the material.

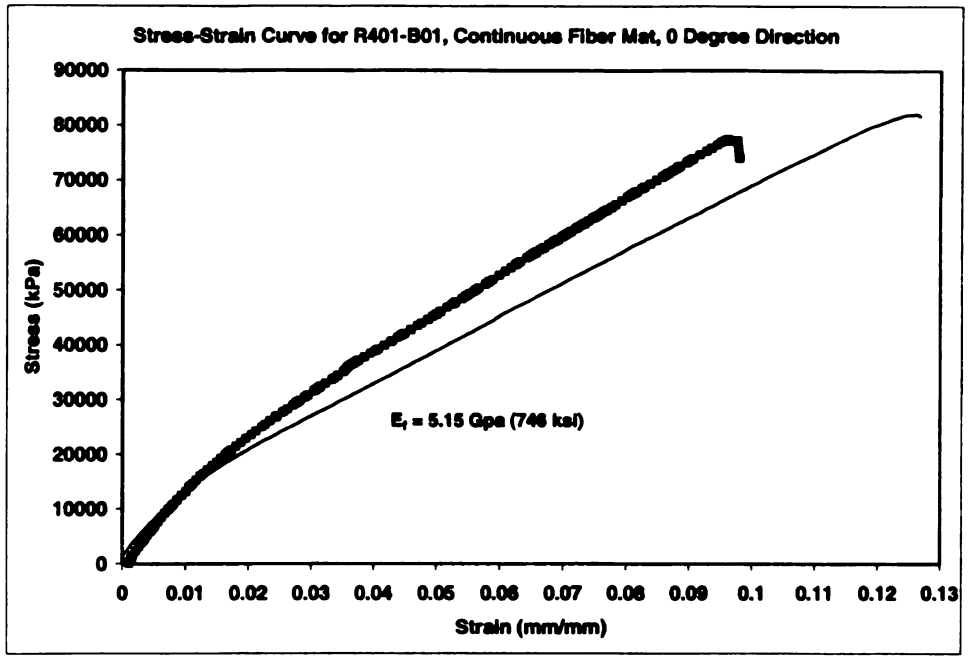

Figure 26. Stress-Strain plot for R401-B01, continuous fiber mat reinforced thermoplastic, 0° direction.

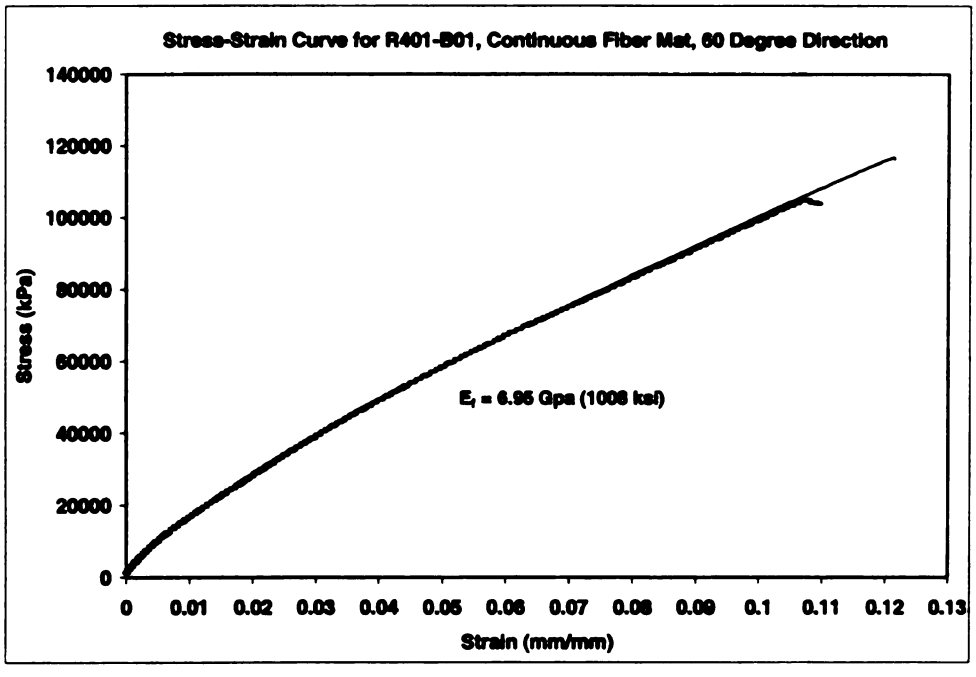

Figure 27. Stress-Strain plot for R401-B01, continuous fiber mat reinforced thermoplastic, 60° direction.

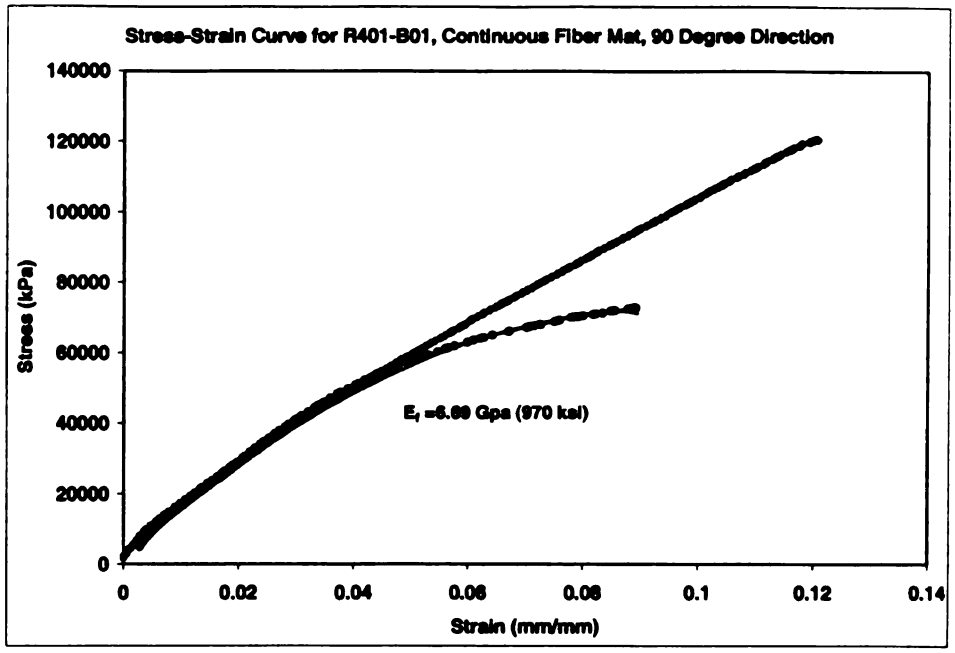

Figure 28. Stress-Strain plot for R401-B01, continuous fiber mat reinforced thermoplastic, 90° direction.

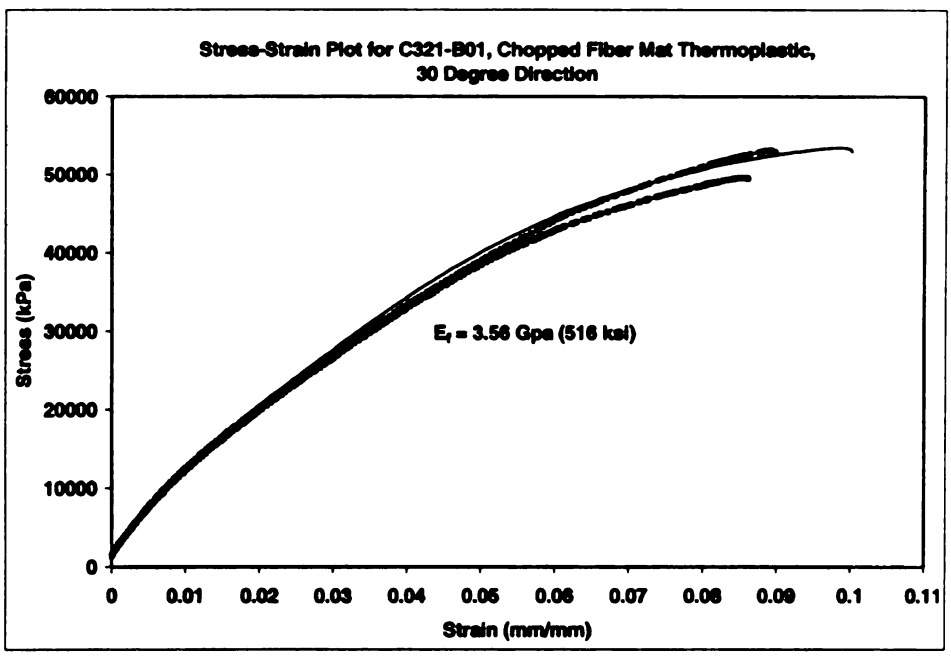

Figure 29. Stress-Strain plot for C321-B01, chopped fiber mat reinforced thermoplastic, 30° direction.

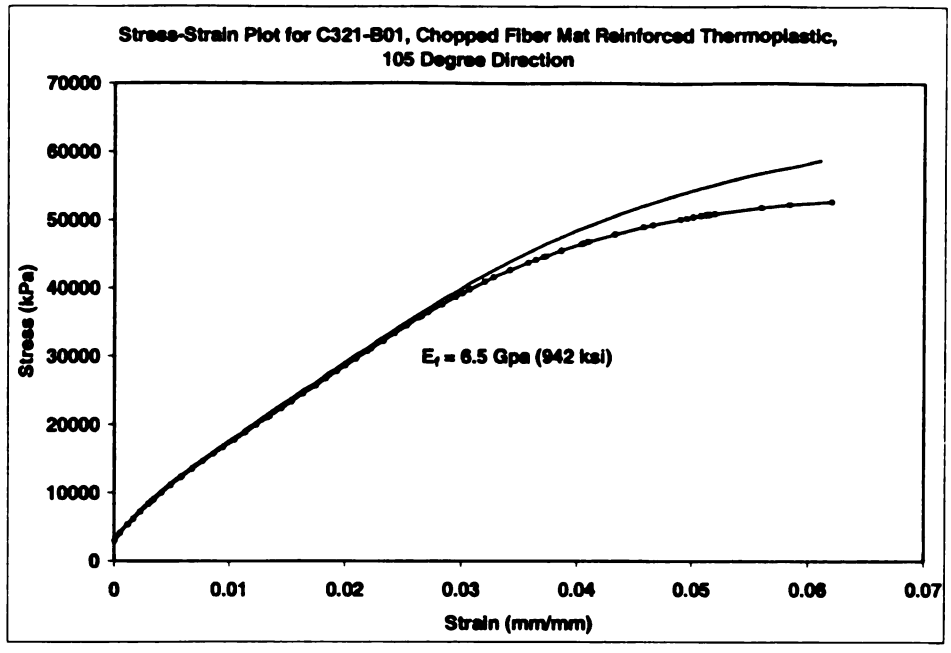

Figure 30. Stress-Strain plot for C321-B01, chopped fiber mat reinforced thermoplastic, 105° direction.

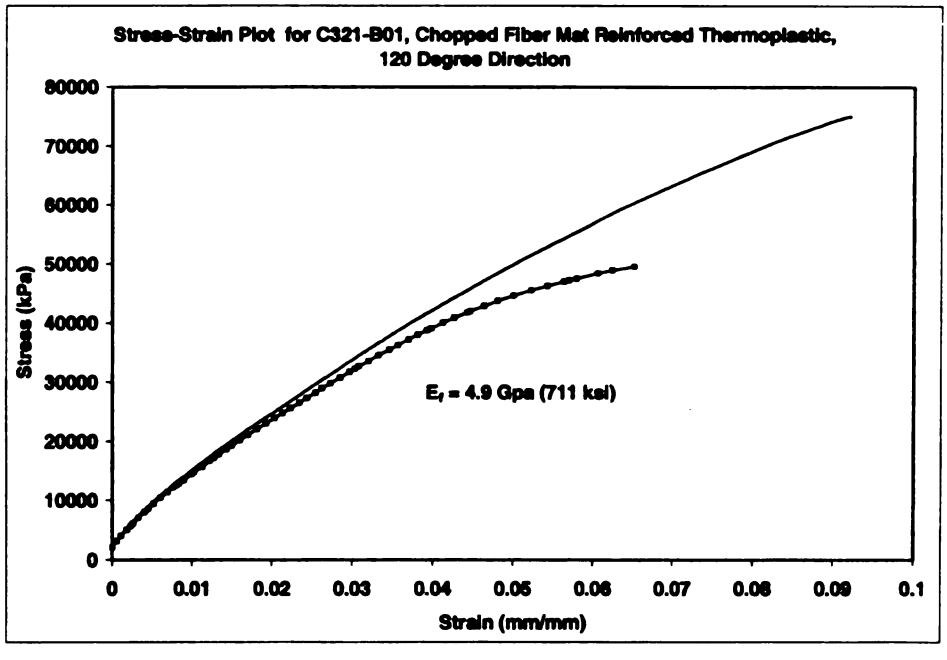

Figure 31. Stress-Strain plot for C321-B01, chopped fiber mat reinforced thermoplastic, 120° direction.

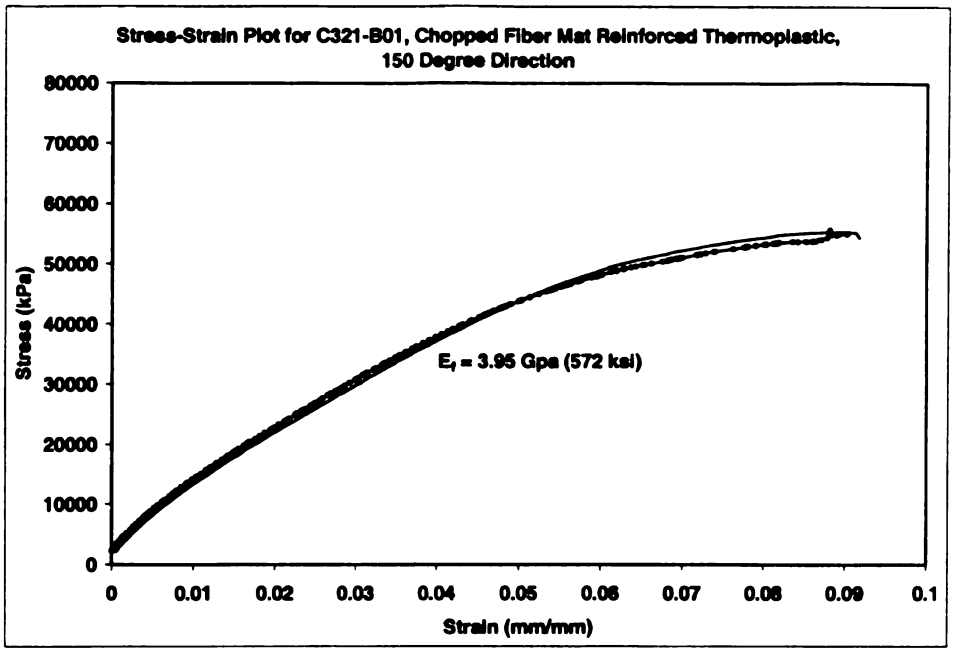

Figure 32. Stress-Strain plot for C321-B01, chopped fiber mat reinforced thermoplastic, 150° direction.

8.3.1. Longitudinal Young's Modulus, E_{11}

From the tensile test data the Young's modulus for each preferred fiber orientation could be easily determined. Once these values were determined they were used as input representing the Young's modulus of the fibers, E_f values that are used in Equations 26-29. Typically E_f is considered a constant that is derived from the behavior of the reinforcing fiber, i.e. e-glass fiber or carbon fiber Young's modulus. Since the theory is based on material properties that vary with respect to the fiber orientation, this assumption of a constant Young's modulus does not hold up. Using constant values within the same set of equations characterizing

the behavior of each unidirectional layer would result in behavior that would not accurately reflect the behavior of the fibers during deformation.

Based on the measured values of E_f the empirical relationship for E_{11} could be evaluated. For the longitudinal Young's modulus along the preferred fiber orientation, E_{11}, Mohammed (2000) [46] showed that the relationship outlined in Equation 26, based on the rule of mixtures, was adequate for describing the material's behavior. This was confirmed by other studies such as those by Okoli and Smith (2000) [51] and Pinfold (1995) [52].

8.3.2. Transverse Young's Modulus, E_{22}

The second material property that is needed for the constitutive model is the Young's modulus in the transverse direction or also termed, the Young's modulus of the matrix, E_m. This value can be determined either experimentally or empirically. Experimentally the material property is determined using the same method outlined for determining the longitudinal Young's modulus, E_f. Test coupons could be cut from the material normal to the preferred fiber orientations and then tested using the uniaxial testing procedures. From these tests the varying nature of E_m could be determined. Since these values are typically two orders of magnitudes less than the longitudinal properties the assumption for E_m was that it could be assumed as constant and then changed if the results did not bear out this assumption.

The empirical relationship for the transverse Young's modulus, E_{22}, proposed by Mohammed (2000) [46], Equation 27, was discovered, through subsequent studies, to provide some errors of up to 15% when applied to the randomly oriented fiber reinforcements. Okoli et al. (2000) [51] and Pinfold (1995) [52] worked on developing the empirical relationships for E_{22} that matched more experimental results for continuous fiber reinforced materials with a random orientation. They concluded that the least amount of error was introduced when using the relationship outlined in Equation 35. Therefore this relationship was adopted and implemented into the updated material law constitutive model with varying material properties based on the assumed values of the matrix shear modulus, E_m and the experimentally determined values of E_f.

$$E_{22} = E_m\left(\frac{1+ABV_f}{1-B\psi V_f}\right) \tag{35}$$

Where A =0.5 , B is defined by Equation 36 and ψ is defined by Equation 37.

$$B = \frac{\left(\frac{E_f}{E_m}\right)-1}{\left(\frac{E_f}{E_m}\right)+A} \tag{36}$$

$$\psi = 1+V_f\left(\frac{1-\varphi_m}{\varphi_m^2}\right) \tag{37}$$

Where φ_m=0.82 for a random array (Nielsen, 1974 [53]).

8.3.3. Poisson's Ratio, ν_{12}

Due to limitations with the equipment the only material property that could be measured from these tests was the Young's modulus along the preferred fiber orientation. The laser extensometer system used to measure the extension within the gage is limited to reading only a single direction during the testing process. In addition, the reflective tape used by the laser system as a measuring gage facilitates its use in measuring only the extension along the length of the test coupon, not across the width as would be required to determine Poisson's ratio. Therefore, instead of experimentally determining the Poisson's ratio for this material, empirical methods for determining this material property were investigated.

Through a search of existing empirical relationships it was determined that there are a large number of existing methods for determining this material property. Pinfold (1995) [52] evaluated the various empirical methods that were applicable to random fiber arrangements and determined that only three equations gave reasonable results when compared to experimental data. Of those three equations some would overestimate and some would underestimate the Poisson's ratio. The study found that the most accurate equation provided an average error of 11% when the results were compared against the experimental data. Okoli and Smith (2000) [51] continued this study and came to the same

conclusions with respect to determining the Poisson's ratio for random fiber reinforced material. So based on these studies, and in the absence of accurate experimental data for this material type, the empirical relationship was assumed to follow the rule of mixtures as used by Mohammed et al. (2000) [46] and is shown in Equation 28.

$$\upsilon_{12} = \upsilon_f V_f + \upsilon_m (1 - V_f) \tag{28}$$

8.3.4. Shear Modulus, G_{12}

The fourth and final material property needed for the constitutive modeling is the longitudinal or in plane shear modulus, G_{12}. In order to determine G_{12} of the fiber mat reinforced material the experimental procedures are much more complicated than the tensile testing that can be used to determine the other properties. For the highly structured materials such as woven fabric reinforced composites a picture-frame experiment is used to determine the in plane shear modulus. A picture-frame test involves the pure shear deformation of a square sample, potentially at room or even elevated temperatures. The main obstacle to overcome when performing these types of test is the attachment of the material sample to the test fixture. The samples need to be attached in a way such that the boundary conditions imposed will not restrict the deformation of the material during the test. This same test could potentially be used for the evaluation of glass mat fiber reinforced materials but as of yet it has not been attempted.

During the course of this study this possibility was investigated but experimental material restrictions limited the capability for this type of experimental evaluation so other methods had to be investigated.

Halpin (1984) [44] suggests a pure torsion test conducted on a solid circular cylindrical rod for the evaluation of the in plane shear modulus. This experimental procedure was also investigated but, again, there are practical material restrictions that prohibit this type of test from being performed. The material that is supplied through our partnership with Azdel is manufactured only is sheet form. It would have become economically unfeasible to create the circular cylindrical rod samples needed for these experiments and the accuracy may have been compromised due to the changes in manufacturing processes.

Instead of experimental methods some empirical methods were investigated in order to determine the in plane shear modulus for the fiber mat reinforced materials. From Pinfold (1995) [52] Equations 38 and 39 were considered based on an extensive literature review and for their applicability to the prediction of material properties for random oriented materials.

$$G_{12} = E_f V_f / 8 \tag{38}$$

Where E_f is the Young's modulus of the fiber, determined through tensile tests and V_f represents the volume fraction, as defined in Equation 23.

$$G_{12} = \frac{E_{11}}{8} + \frac{E_{22}}{4} \tag{39}$$

Where E_{11} and E_{22} are Young's modulus of the longitudinal and transverse direction respectively. These are defined in Equations 26 and 35 and will change with respect to the preferred fiber orientation.

Equation 40 is a semi-empirical relationship derived by Halpin and Tsai (1969) [54] and is used for predicting the longitudinal shear modulus for unidirectional fiber reinforced materials.

$$G_{12} = G_m \left(\frac{1 + \xi \eta V_f}{1 - \eta V_f} \right) \tag{40}$$

Where G_m represents the shear modulus of the matrix, ξ is a geometrical factor and η is defined below in Equation 41.

$$\eta = \frac{G_f - G_m}{G_f + \xi G_m} \tag{41}$$

Where G_f is the shear modulus of the fiber.

The fourth relationship was used by Mohammed et al. (2000) [46] and is derived from the rule of mixtures, Equation 29.

$$\frac{1}{G_{12}} = \frac{V_f}{G_f} + \frac{(1-V_f)}{G_m} \tag{29}$$

Figure 33 is a plot of all four in plane shear modulus empirical relationships versus changes in volume fraction, V_f for the R401-B01, continuous fiber mat reinforced thermoplastics. As is evident from this plot, both Equations 38 and 39 are inappropriate for this study since, at the two extreme values of volume fraction, V_f, equivalent to 0 and 1, the equations fail to predict the expected values.

A volume fraction equivalent to zero implies that the material consists of only matrix material, whereas a volume fraction equal to one implies a material has no matrix and consists of only fibers. Therefore, at these two extremes of 0 and 1, the empirical relationship should be predicting shear modulus values equivalent to the shear modulus of the matrix and the shear modulus of the fiber, respectively.

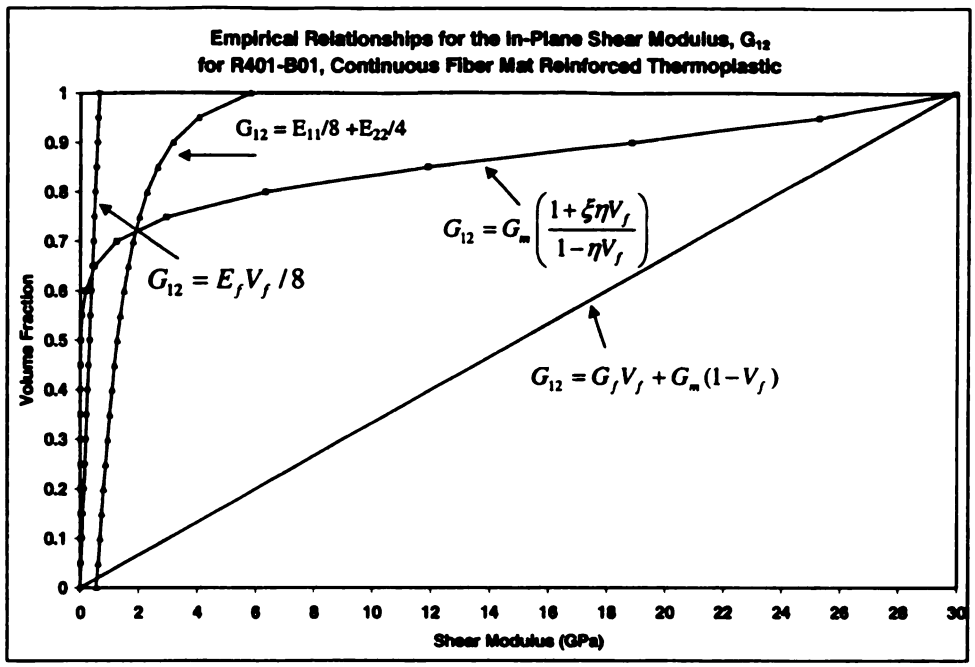

Figure 33. Shear modulus versus volume fraction for the four empirical relationships. Based on material properties for R401-B01, continuous fiber mat thermoplastic.

Figures 34 and 35 are plots of the two remaining empirical relationships plotted against volume fraction for each material type, continuous fiber mat and chopped fiber mat, respectively. As is illustrated in these figures, both relationships predict the boundary values of 0 and 1 correctly but there are some significant differences between the paths in between these points. According to both Pinfold (1995) [52] and Okoli and Smith (2000) [51] Equation 40 corresponds fairly well with experimental data (approximate error of 5-8 %) as long as the appropriate geometrical factor, ξ, is chosen. Halpin-Tsai (1969) [54] recommends a ξ value of 1.0. Studies have shown that this may be appropriate

for certain volume fractions but for some values the error introduced could be over 20% (Hewitt and Malherbe, 1970 [55]). A more appropriate choice for the geometrical factor, ξ, and the one used in this study, comes from both Pinfold (1995) [52] and Okoli and Smith (2000) [51] and is illustrated in Equation 42. This relationship provides a more accurate representation of the random fiber geometry and showed less error for a wider range of volume fractions than for the other studied relationships.

$$\xi = 5 + 10^5 V_f^{10} \tag{42}$$

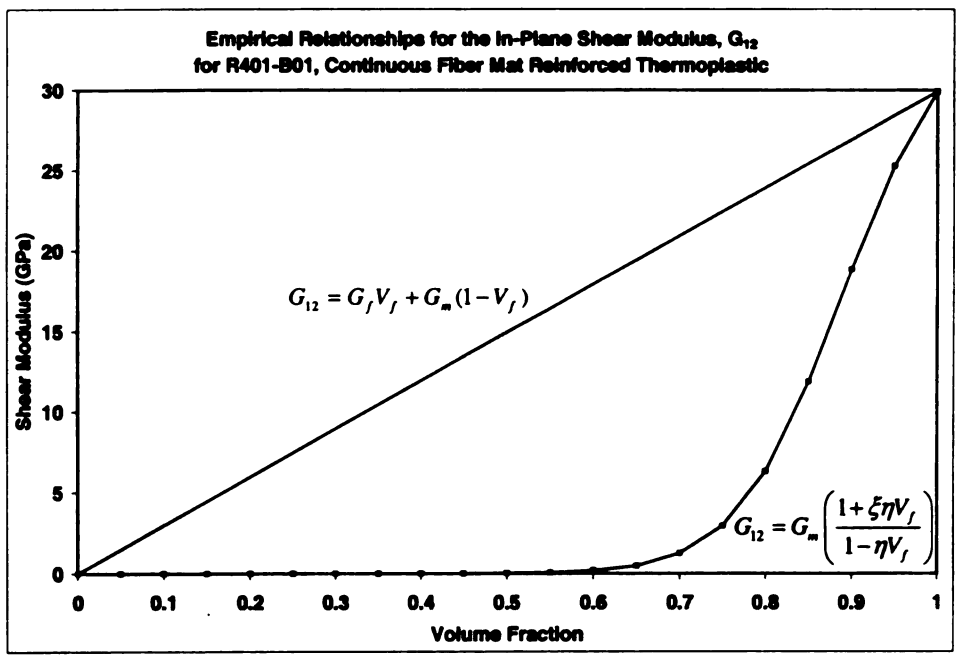

Figure 34. Shear modulus versus volume fraction for the two valid empirical relationships for R401-B01, continuous fiber mat thermoplastic.

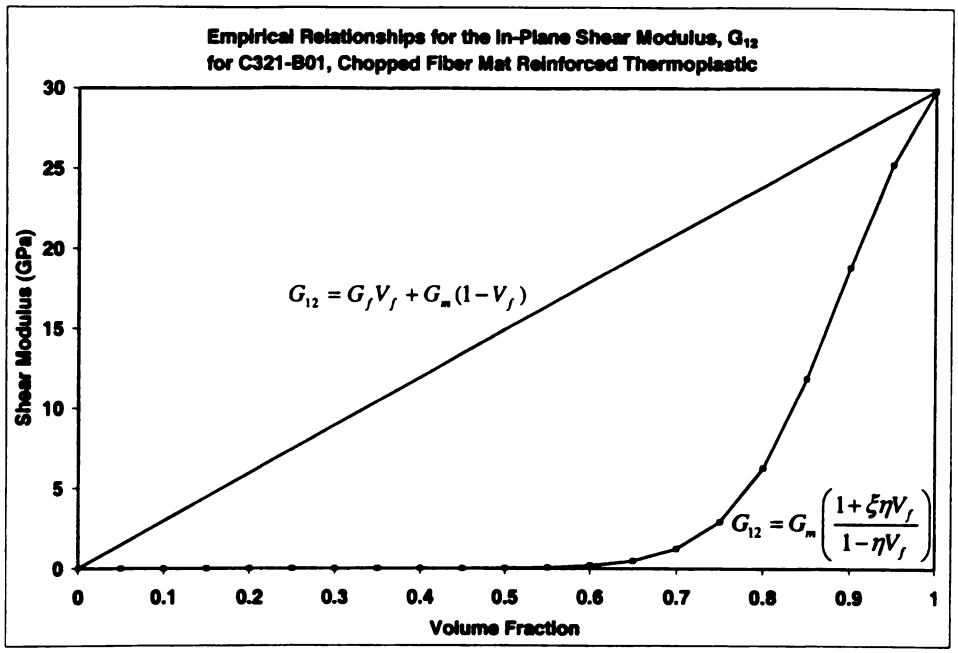

Figure 35. Shear modulus versus volume fraction for the two valid empirical relationships for C321-B01, chopped fiber mat thermoplastic.

Through these characterization methods the material properties for the R401, continuous fiber mat and the C321, chopped fiber mat were determined and are summarized in Table 1 below. These values will be used as inputs for the numerical simulations that will be discussed in the next chapter.

Table 1. Material properties derived through material characterization.

R401, Continuous Mat	
$E_{f,0}$	5.15 GPa
$E_{f,60}$	6.95 GPa
$E_{f,90}$	6.69 GPa
$E_{m,all}$	1.5 GPa
$\nu_{f,all}$	0.361
$\nu_{m,all}$	0.1
$G_{f,all}$	29.9 GPa
$G_{m,all}$	0.2 MPa
C321, Chopped Mat	
$E_{f,30}$	3.56 GPa
$E_{f,105}$	6.5 GPa
$E_{f,120}$	4.9 GPa
$E_{f,150}$	3.95 GPa
$E_{m,all}$	1.5 GPa
$\nu_{f,all}$	0.317
$\nu_{m,all}$	0.1
$G_{f,all}$	29.9 GPa
$G_{m,all}$	0.2 MPa

Chapter 9

NUMERICAL AND EXPERIMENTAL RESULTS

In order to validate the multiple preferred fiber orientation constitutive model there was the need to compare the results obtained numerically versus those acquired through experimentation. A numerical simulation was built to model the three-dimensional deformation behavior of both the continuous and the chopped fiber glass mats as they were formed into 100 mm (4 in) hemispherical cups by stamping. Models were built to simulate isotropic materials, orthotropic materials, woven fabric materials, materials with two preferred fiber orientations and materials with multiple preferred fiber orientations. Stamping experiments were performed for both the continuous and the chopped fiber mats and the results were compared against the numerical results.

9.1. Experimental Stamping Results

Stamping experiments were performed in order to provide some baseline experimental results to validate against the constitutive modeling results. The experiments were performed utilizing the stamp thermo-hydroforming press that will be discussed in greater detail in Chapter 11. Initially the fiber reinforced thermoplastic sheets were placed in an oven and heated to a forming temperature of 190° C (375° F). Once the matrix had melted the parts were transferred to the press and the stamping process commenced.

A 100 mm (4 in) diameter hemispherical punch was used to shape the parts without the presence of a female die. No resisting material was used to constrict the material behavior as it was formed. The blank holder and the die were maintained with a gap of 19 mm (0.75 in) so that the material would be allowed to draw into the chamber as the part was formed, thus allowing for the investigation of the wrinkling behavior of the material. Each part was drawn to a depth of 46 mm (1.8 in) and allowed to solidify before the punch was drawn down, the die halves opened and the part removed. The stamping process setup is shown schematically in Figure 36.

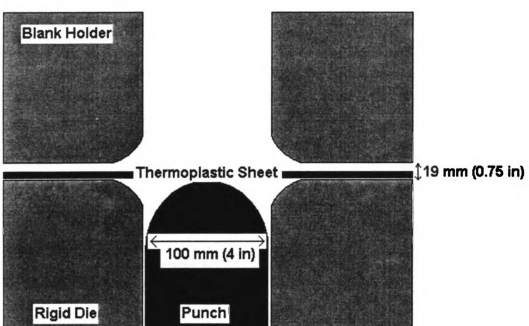

Figure 36. Schematic of the stamping experimental setup and of the numerical simulation process design.

To better illustrate the observations made about the experimental and numerical results it is important to establish a frame of reference. For the purpose of this discussion the hemispherical part has been split into three distinct zones as illustrated in Figure 37. Zone I represents the flange area of the stamped part, Zone II is the area of the part that forms against the sidewall of the upper die cavity entrance, and Zone III represents the dome of the hemispherical part.

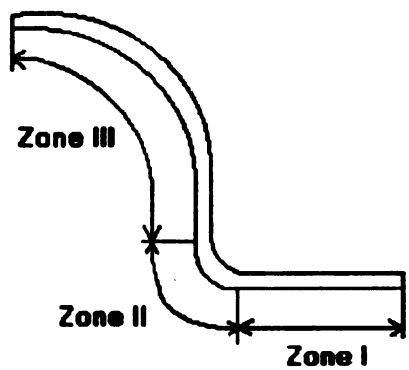

Figure 37. Zoned regions of the shaped hemispherical cups.

9.1.1. Experimental Results for R401-B01, Continuous Fiber Mat Reinforced Polypropylene Sheets

Three different materials were investigated for this validation of the numerical modeling. The first was the R401-B01, continuous fiber mat reinforced polypropylene sheet that was provided through a partnership with Azdel, Inc.

This material is manufactured with a random fiber orientation that, theoretically, is supposed to create a material that should behave in an isotropic manner. As illustrated in Chapter 8 there is some directionality associated with these materials and the experimental stamping results, illustrated in Figure 38, bear this out.

There is some significant wrinkling occurring within the flange area (zone I) of the part as it is formed. This is anticipated since there is indirect compression occurring within this area due to the tension of the material being drawn by the punch into the die chamber. As additional material is drawn into the chamber by the punch the material within the flange area must compress in the circumferential direction in order to flow over the lip of the die. This compressive stress is much larger than the material can withstand, especially at elevated temperatures so this leads to the wrinkling behavior exhibited by the stamped parts.

Once the material is drawn into the die chamber there is no mechanism, such as a counteracting hydrostatic pressure, that can be used to suppress the wrinkling behavior so naturally the wrinkling will remain within the part and will stretch throughout zone II. Figure 38(a) provides a good indication of this behavior but due to the complicated surface finish of the heated and stamped glass mat thermoplastic parts this wrinkling behavior was very difficult to capture adequately on camera.

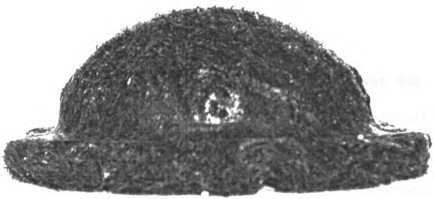

(a)

(b)

Figure 38. Experimental stamping results for R401, continuous fiber mat reinforced polypropylene, (a) side view, (b) top view.

9.1.2. Experimental Results for C321-B01, Chopped Fiber Mat Reinforced Polypropylene Sheets

The second material evaluated during this study was the C321-B01, chopped fiber glass mat fiber reinforced polypropylene also supplied through the partnership with Azdel, Inc. This material contains randomly arranged long chopped fibers where the term "long" implies fibers that are between 50-100 mm (2-4 in) in length. Figures 39 and 40 illustrate the experimental results for this material type.

The chopped fiber material proved to be more difficult to form in that, while the overall trends were the same, each experimental part provided slightly different results. The material exhibited wrinkling within zones I and II, similar to the continuous fiber material, but the overall wrinkling behavior was different for each chopped fiber case. For some parts there were a significant number of wrinkles forming within the flange area and for others there were a minimal number of buckling areas, but larger buckling regions.

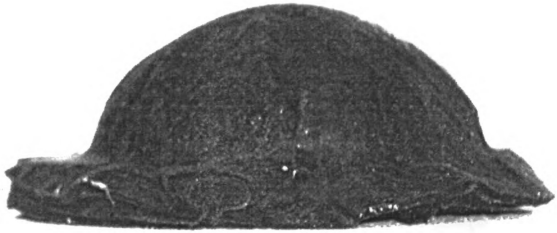

(a)

(b)

Figure 39. Experimental stamping results for sample A of C321, chopped fiber mat reinforced polypropylene, (a) side view, (b) top view.

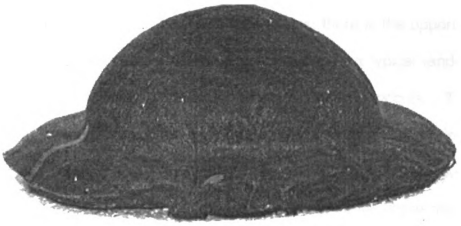

(a)

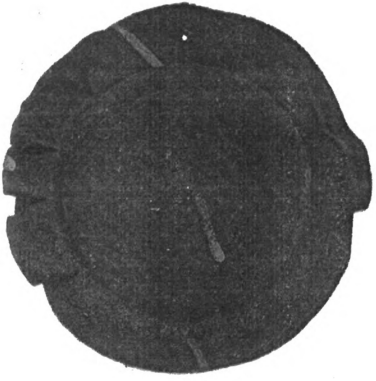

(b)

Figure 40. Experimental stamping results for sample B of C321, chopped fiber mat reinforced polypropylene, (a) side view, (b) top view.

The reasons for this disparity may be tracked to a couple of different factors; fiber alignment and fiber entanglement. Since the material consists of fibers that do not traverse the length of the material there is the opportunity for some fiber aligning as the part is being formed. Within a typical random fiber reinforced material there is some fiber entanglement that occurs. This fiber entanglement prevents the fibers from flowing freely during deformation of the continuous fiber reinforced materials. For the non-continuous fiber reinforcements, such as the long fibers used in this material, there may not be sufficient entanglement to prevent the fibers from flowing along with the matrix as the part is formed. This could lead to some fiber concentrations developing while other areas consist mainly of resin material. Therefore the material would not form in the same manner in each case but overall should provide the same general behavior.

9.1.3. Experimental Results for Woven Fabric Reinforced Polypropylene Sheets

The third material that was investigated as part of this research study was a plain weave fabric reinforced polypropylene material. This material is supplied as a dry fabric with impregnated matrix and is formed into layered thermoplastic sheets using a simple compression process under elevated temperature conditions prior to stamping. This material type was not characterized but was

used as an additional material that could potentially be modeled utilizing the updated material law with varying material properties.

Stamping experiments conducted using the woven fabric material had to be modified slightly due to the significant difference in material thickness between this material and the fiber mats used in the previous experiments. The woven fabrics are much thinner than the fiber mats so a gap between the blank holder and the rigid die of only 4mm (0.16 in) was needed in order to evaluate the wrinkling behavior of plain weave reinforced thermoplastic sheets.

Since the thermoplastic sheets were created in-house there was a significant amount of flexibility associated with the use of these materials. Samples could be created with a varying number of plies with varying directionality. The experimental stamping results for a single ply of orthogonal material can be found in Figure 41. The single ply plain weave specimens exhibited the same type of wrinkling behavior that was found in the mat fibers for the flange areas, just not as noticeable due to the significant differences in material thickness.

Within the wall area, zone II, instead of the continuous wrinkling patterns found in the mat fiber cases the woven fabric material exhibited some localized buckling that occurred during the forming process. Figure 41(a) and (c) capture this behavior quite adequately. This localized buckling can be attributed to the compressive stresses that are placed on the individual fibers during deformation.

As the punch draws more material into the chamber there is a significant amount of compressive stresses acting in the radial direction of the material. For the plain weave specimens this corresponds with the warp direction fibers and leads to the buckling behavior illustrated in Figure 41.

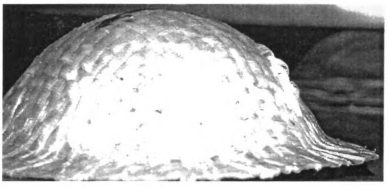

(a)

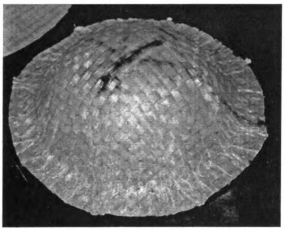

(b)

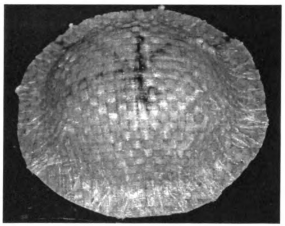

(c)

Figure 41. Experimental stamping results for single ply, plain weave fabric reinforced polypropylene, (a) side view, (b) and (c) top views illustrating the localized buckling effect within zone II.

9.2. Numerical Stamping Simulation

The numerical three-dimensional stamping simulations were created to mirror, as closely as possible, the experimental stamping process described in the previous section. Numerical modeling was accomplished utilizing the commercial code ABAQUS/Explicit with the updated material law being implemented through a user subroutine, VUMAT. The goal of the numerical analysis was to accurately simulate the experimental stamping process for all three material types while also trying to assess the validity of the newly developed constitutive relationship for modeling the deformation behavior of random mat fiber reinforced thermoplastics.

One of the goals when designing a numerical simulation is to minimize the time required to achieve a valid solution. This can sometimes prove to be very challenging when modeling a dynamic system such as the stamping of composite material with an explicit code. The explicit codes are very useful for solving static problems and they have proven to very adept at handling contact issues between surfaces such as a punch and a sheet of material. So, in order to obtain an economical solution there are some accelerating factors that must be considered while still maintaining quasi-static modeling conditions.

Various accelerating ideas were attempted in an effort to speed up the processing including changes to the mass scaling of the model, the total

modeling time, the loading rate and the number of elements within the mesh. Each of these changes had varying effects on the behavior of the model, with the most common problem encountered being that the problem did not remain quasi-static during processing, hence negating the results.

Due to the antisymmetric nature of the mat fiber reinforced materials there were very few geometrical factors that allowed for simplifying the analysis, therefore, full models were created to represent the stamping process. Each simulation utilized a mesh containing 5700 four-node shell elements, unless stated otherwise during the discussion. CPU time varied greatly for each model ranging from a low of 49 minutes all the way up to four days. No mass scaling was used but the effects of varying both the loading rate and number of elements was investigated. The results shown in the following sections were based on the models that took the shortest amount of CPU time while still remaining quasi-static.

9.3. Numerical Results – Isotropic Material Model

Theoretically, a composite material with a truly random fiber arrangement should provide a material with isotropic properties. So in an effort to determine the applicability of this type of modeling behavior to the stamping of fiber mat reinforced thermoplastics an isotropic material model was attempted. Material

properties used for this model were an average of the material properties listed in Table 1 for the R401, continuous fiber mat reinforced thermoplastics.

The results for this model, shown in Figure 42, demonstrate that by using an isotropic material behavior law the instabilities that occur during processing will not be captured such as the wrinkling within the flange area illustrated in Figure 38(b). Therefore, a more realistic material model is needed to accurately model the deformation behavior of mat fiber reinforced materials.

Figure 42. Numerical results for R401, continuous fiber mat reinforced polypropylene using an isotropic material model.

9.4. Numerical Results – Orthotropic Material Model

An orthotropic material model was created for these materials in order to provide a baseline to compare against the constitutive modeling results. The orthotropic consideration assumes that there are two preferred fiber directions, both mutually perpendicular to one another, even after deformation. The material properties required for the ABAQUS/Explicit orthotropic model included the Young's modulus in both the longitudinal and transverse directions, E_{11} and E_{22}, the in plane Poisson's ratio, ν_{12}, and the longitudinal and transverse shear moduli G_{12}, G_{13} and G_{23}. For the orthotropic model the transverse shear moduli are used for calculating the transverse shear deformation in the shell. All material property values were taken from Table 1, except for the transverse shear moduli, G_{13} and G_{23}, which were taken as constants of 65 kPa (9.4 psi).

Results for the R401, continuous fiber mat reinforced thermoplastic can be found in Figure 43, while the results for the C321, chopped fiber mat can be found in Figure 44. Similar to the isotropic model it is apparent that the orthotropic model cannot accurately capture the instabilities that arise in these materials during forming. While the flange area, zone I, begins to exhibit some minor instabilities, there are still no buckling regions within the cup wall, zone II. Therefore there is a need for a more accurate material model to accurately capture the behavior of the mat fiber reinforced material during deformation.

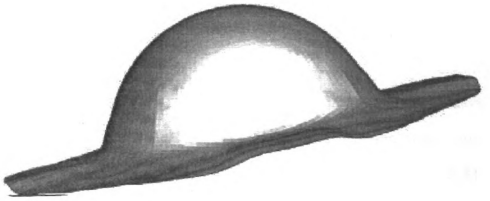

Figure 43. Numerical results for R401, continuous fiber mat reinforced polypropylene using an orthotropic material model.

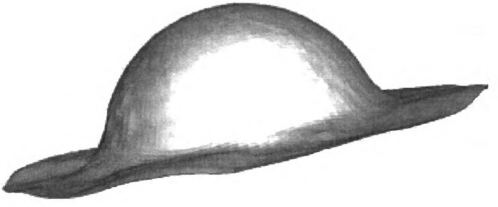

Figure 44. Numerical results for C321, chopped fiber mat reinforced polypropylene using an orthotropic material model.

9.5. Numerical Results – Updated Material Law with Varying Material Properties

The updated material law with varying material properties constitutive model was implemented into ABAQUS/Explicit using a material user subroutine, VUMAT, based on the theory outlined in Chapters 5and 6. The VUMAT was designed to model materials that contained either two or three preferred fiber orientations; orientations which did not need to start out, or even remain, mutually orthogonal. Material properties were taken from Table 1 in Chapter 8.

The models that were created for this section address only single layer modeling. Multi-layer modeling would require a constitutive relationship for the interaction between the material layers. For both of the glass mat reinforced materials there are approximately 18-20 mat layers that are compressed together to create the sample that was studied experimentally. A single layer mat impregnated with resin was not available for experimental evaluation.

9.5.1. Continuous Fiber Mat Reinforced Thermoplastics with a Random Fiber Orientation

The first material to be addressed is the R401, randomly distributed continuous fiber mat reinforced polypropylene supplied by Azdel. The material was modeled using both two preferred fiber orientations of 0° and 90° and as a

material with three preferred fiber orientations of 0°, 60° and 90°. The results for the two preferred fiber orientation model can be found in Figure 45 while the results for the three preferred fiber orientation model are illustrated in Figure 46. Both of these models are able to capture the instabilities that are occurring during the stamping process. When comparing these two models against one another it is readily apparent that the three preferred fiber orientation model predicts buckling instabilities further into the cup region.

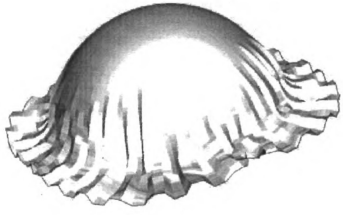

Figure 45. Numerical results for R401, continuous fiber mat reinforced polypropylene using the updated material law with varying material properties and two preferred fiber orientations.

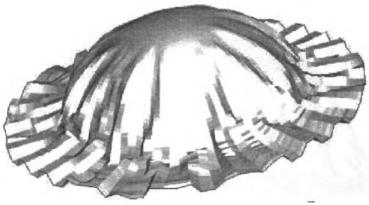

Figure 46. Numerical results for R401, continuous fiber mat reinforced polypropylene using the updated material law with varying material properties and three preferred fiber orientations.

Figure 47 contrasts a side view of the numerical results for the two preferred fiber orientation modeling results versus the experimental results. These pictures demonstrate that the two preferred fiber orientation model can qualitatively capture the behavior of the material within the flange. Figure 48 illustrates the same view for the three preferred fiber orientation model also versus the experimental results. This model also captures the behavior of the material within the flange. In addition, the three preferred fiber model also captures the behavior of the material within the cup wall with fairly good accuracy.

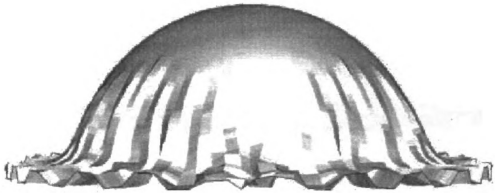

(a)

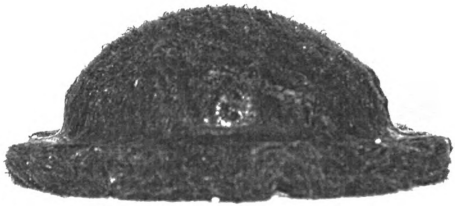

(b)

Figure 47. Side view of the numerical (a) versus experimental (b) results for R401, continuous fiber mat reinforced polypropylene using the updated material law with varying material properties and two preferred fiber orientations.

(a)

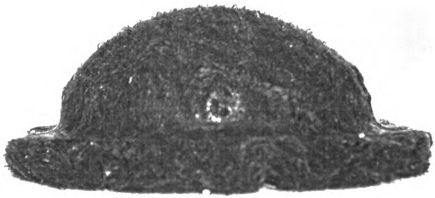

(b)

Figure 48. Side view of the numerical (a) versus experimental (b) results for R401, continuous fiber mat reinforced polypropylene using the updated material law with varying material properties and three preferred fiber orientations.

Figures 49 and 50 illustrate a top view of the numerical results versus the experimental results for the two and three preferred fiber orientation models, respectively. For both models there is some disparity between the predicted behavior of the material at the boundary and the actual behavior. The two preferred fiber orientation model appears to better represent the overall shape of the boundary and includes instability effects such as the severe buckling regions. The three preferred fiber orientation model more accurately represents the

locations of the buckling areas and provides an overall shape that is more indicative of the finished experimental part.

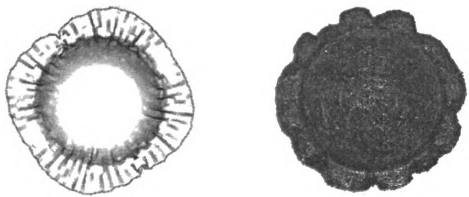

(a) (b)

Figure 49. Top view of the numerical (a) versus experimental (b) results for R401, continuous fiber mat reinforced polypropylene using the updated material law with varying material properties and two preferred fiber orientations.

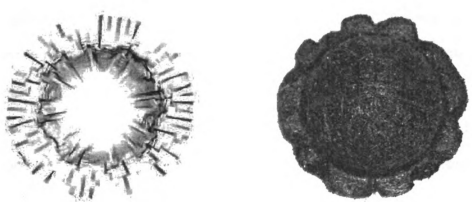

(a) (b)

Figure 50. Top view of the numerical (a) versus experimental (b) results for R401, continuous fiber mat reinforced polypropylene using the updated material law with varying material properties and three preferred fiber orientations.

While the two preferred fiber orientation model is better suited than either the isotropic or the orthotropic models for capturing deformation behavior the three preferred fiber orientation model provides an even better solution. Both models qualitatively represent the location and behavior of the wrinkling instabilities but there is still some disparity. Some of this is easily attributed to the fact that the current model accounts for only one layer of the mat fiber reinforcement. In actuality there are approximately 18-20 layers of the mats that are compressed together during the manufacturing process to create one single sheet. These additional layers impart some through-thickness stiffness to the layers that may lead to the discrepancies found between the modeling and the experimental results.

Another factor that may contribute to some of this disparity is material characterization. The uniaxial tensile tests conducted in Chapter 8 were conducted at room temperature while the experimental parts were formed at an elevated temperature. This could lead to a disparity between what the numerical simulation predicts and what actually occurs during experimentation. Elevated temperature uniaxial tensile tests were attempted as part of this study but due to limitations with the equipment and with the laser extensometer the tests could not be completed with confidence.

A third reason could be attributed to the loading rate used for the model. Currently the two preferred fiber orientation model takes 6 hours of CPU time

running at a loading rate of 0.1 seconds. The actual processing time is 40 hours based on processor speed and number of ABAQUS jobs being processed. When the loading rate is extended to 1 second, the total CPU time becomes 30 hours with an actual processing time of 4 days. Figure 51 compares the numerical results for a part run at a loading rate of 0.1 seconds versus a part formed utilizing a loading rate of 1 second. As illustrated in Figure 51, the longer loading rate may provide a little more accuracy in the results but it needs to be weighed against the significant difference in processing time.

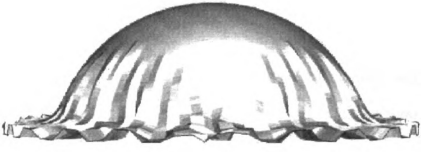

0.1 Second Time Step

1 Second Time Step

Figure 51. Comparison of changes made to the numerical loading rate during the numerical stamping process. Comparison based on the two preferred fiber orientation model for the R401-B01 continuous fiber mat reinforced thermoplastic.

Another possible source of the discrepancy could be attributed to the mesh density of the model. Figure 52 demonstrates the effect on the model of varying the mesh density from 3000 elements up to 8100 elements. The results are incrementally improved as the mesh density increases but the CPU time is significantly different for each case. The model with 3000 elements runs in a little over 90 minutes, the model with 5700 elements runs in a little over 4 hours and the model with 8100 elements runs in approximately a day and a half. So, once again the benefit of the increased mesh density needs to be weighed against the CPU time required to complete the analysis.

Overall, the updated material law constitutive relationship applied to the stamping of continuous fiber mat reinforced thermoplastics showed consistent results that qualitatively captured the deformation behavior during processing. The next logical progression is to determine a quantifiable method to assess the validity of the model. This was accomplished by comparing the force versus displacement behavior for both the numerical simulation and the experimental process as illustrated in Figure 53.

From Figure 53 it is apparent that there is very good agreement between the experimental and numerical behavior until the part reaches a draw depth of a 35.5 mm (1.4 in). At this point the experimental force increases dramatically while the numerical force stays relatively constant as highlighted in Figure 54.

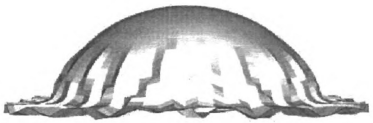

3000 Elements

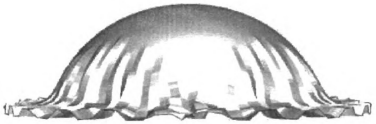

5700 Elements

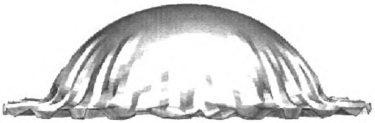

8100 Elements

Figure 52. Comparison of changes made to the mesh density during the numerical stamping process. Comparison based on the two preferred fiber orientation model for the R401-B01 continuous fiber mat reinforced thermoplastic.

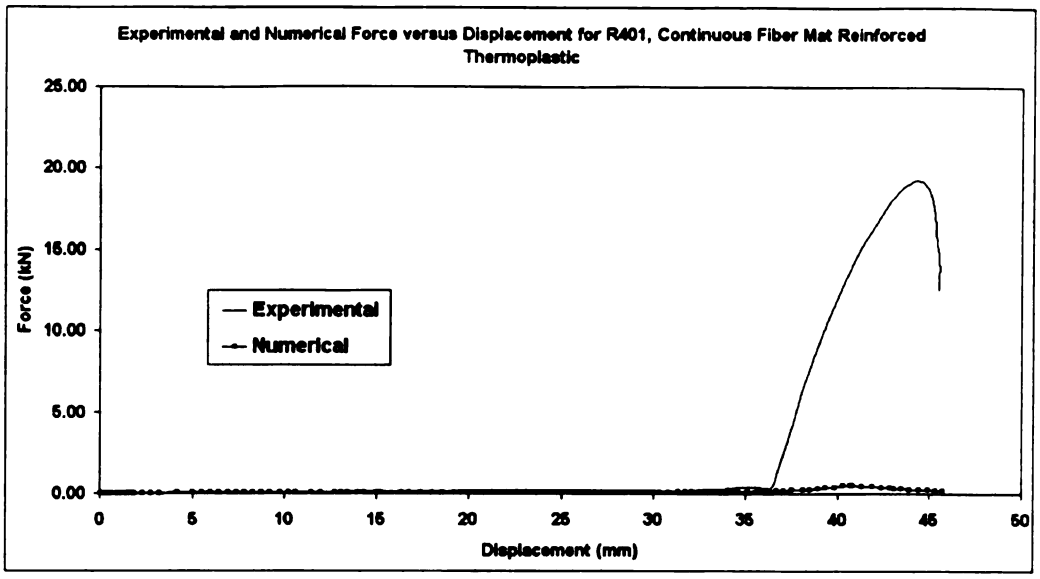

Figure 53. Experimental and numerical force versus displacement for R401, continuous fiber mat reinforced thermoplastic with a random orientation, full scale.

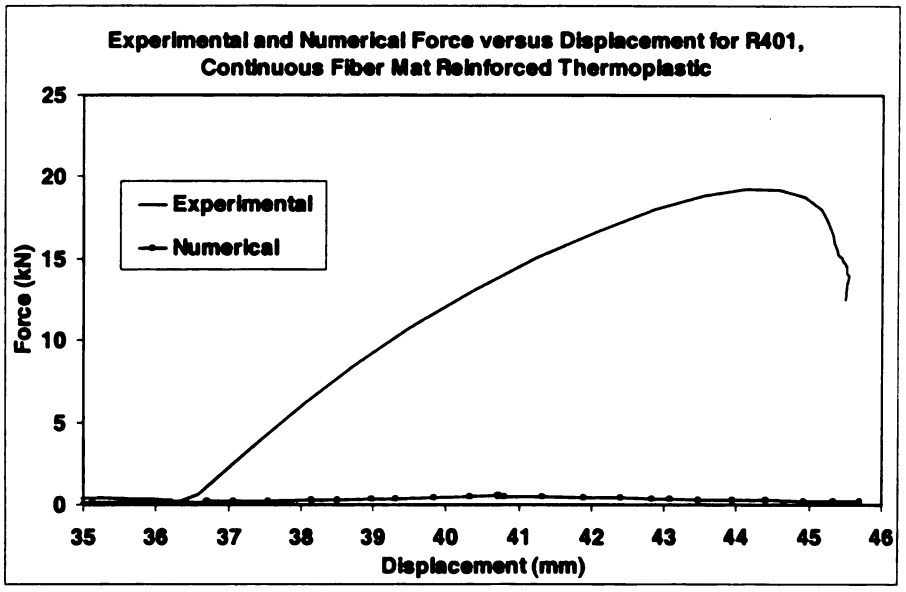

Figure 54. Experimental and numerical force versus displacement for R401, continuous fiber mat reinforced thermoplastic with a random orientation, zoomed in to illustrate the diverging path.

The main reason for this discrepancy can be attributed to the experimental set-up that was used to conduct these tests. To perform these tests the lower clamp had to be placed in displacement control and maintained at a distance of 19 mm (0.75 in) from the upper clamp. With this type of gap between the lower and upper die there is a very limited travel distance for the punch load cell. When the punch reaches a depth of 35.5 mm (1.4 in) the punch load cell will come into contact with the lower die, thereby adding a force to the total that is not indicative of the actual force being applied to the material. This additional force is not taken into account during the numerical analysis so a discrepancy is introduced.

By comparing the force/displacement behavior prior to the contact between the load cell and the clamp there seems to be a fairly decent correlation between the numerical and experimental results, illustrated in Figure 55. From this figure it is apparent that the error between the experimental and numerical force/displacement plots ranges from 5% up to over 48%. While there does seem to be a large amount of disparity between the experimental and numerical results it is important to recall that the model does only account for a single layer of the fiber mat materials. Additional layers would naturally increase the force required to form the material hence reducing the error between the predicted and actual force displacement plots.

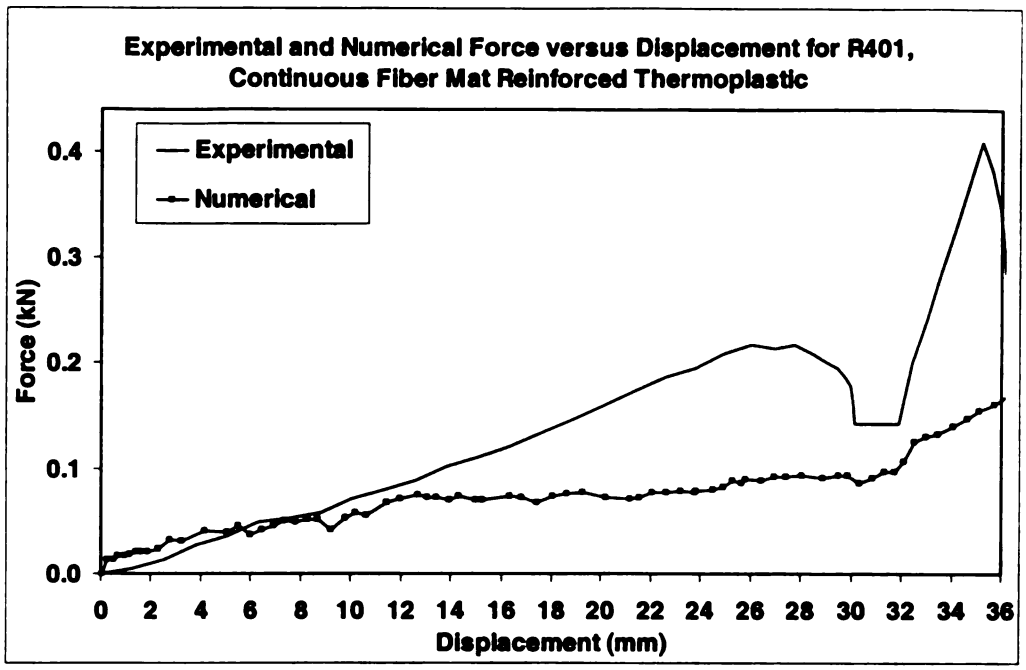

Figure 55. Experimental and numerical force versus displacement for R401, continuous fiber mat reinforced thermoplastic with a random orientation, up to a draw depth of 36 mm.

9.5.2. Chopped Fiber Mat Reinforced Thermoplastics with a Random Fiber Orientation

The second material that was evaluated during this study was the C321, chopped fiber mat reinforced polypropylene with a random fiber orientation. The material was modeled using only two preferred fiber orientations of 30° and 105° with the results illustrated in Figure 56. When compared against the orthotropic case from Figure 44 the two preferred fiber orientation model more accurately represented the material instabilities within both the flange and cup wall.

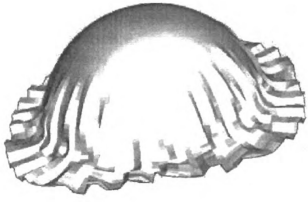

Figure 56. Numerical results for C321, chopped fiber mat reinforced polypropylene using the updated material law with varying material properties and two preferred fiber orientations.

Figure 57 illustrates a side view of the numerical versus experimental results for the chopped fiber material. As with the previous material the two preferred fiber orientation model was able to qualitatively capture the buckling instabilities that occurred within the flange area of the material. Very good accuracy is found when looking at the buckling that occurs along the wall of the hemispherical cup. The model is able to accurately predict the location and behavior of the deformation during the stamping process.

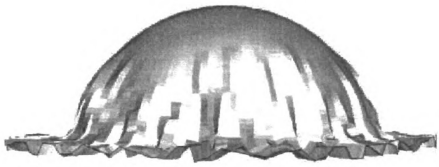

(a)

(b)

Figure 57. Side view of the numerical (a) versus experimental (b) results for C321, chopped fiber mat reinforced polypropylene using the updated material law with varying material properties and two preferred fiber orientations.

Figure 58 represents a view from the top of both the numerical and experimental results. As with the two preferred fiber orientation applied to the continuous fiber reinforcement there is some disparity between the predicted boundary behavior of the material and the actual behavior. There are a couple of reasons that could be attributed to this discrepancy regarding the behavior at the boundary. The first is due to the varying nature of the experimental results. As mentioned in Chapter 9.1.2 there were some differences between the

experimental stamping parts formed using the chopped fiber mats. This could lead to problems with trying to validate the numerical model. Without accurate experimental data it is very difficult to confirm the accuracy of a numerical model. On top of the experimental issues are the problems that could arise from either single layer versus multiple layer modeling or from the loading rate used in the simulation, both of which were discussed previously.

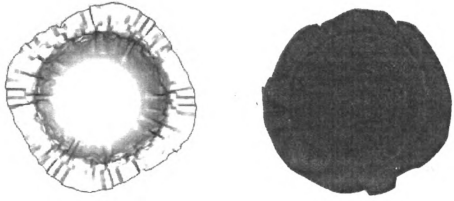

(a) (b)

Figure 58. Top view of the numerical (a) versus experimental (b) results for C321, chopped fiber mat reinforced polypropylene using the updated material law with varying material properties and two preferred fiber orientations.

The two preferred fiber orientation model was able to accurately predict the location of the wrinkling instabilities but was unable to reconcile the material behavior along the outer edge of the sheet. Overall the two preferred fiber orientation model is a much better choice than the orthotropic model but could use some refinement for this case. This was again verified when an attempt was made to quantify the difference between the predicted and actual behavior of the

chopped fiber mat reinforced thermoplastics. Force versus displacement for both the experimental and numerical analysis were plotted to try to determine the accuracy of the model for predicting the behavior of this material type, Figures 59 through 61.

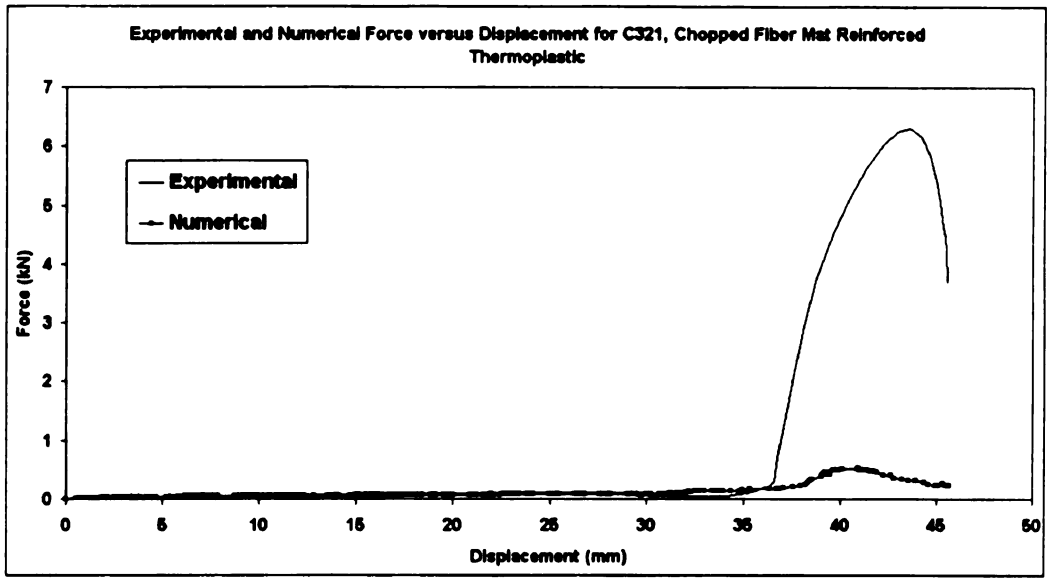

Figure 59. Experimental and numerical force versus displacement for C321, chopped fiber mat reinforced thermoplastic with a random orientation, full scale.

As discussed in the previous section there was a discrepancy between the numerical and experimental results, especially at the 35.5 mm draw depth. As with the previous material type, while the errors for the portion prior to the contact of the load cell and the clamp (draw depth less than 35.5 mm) seem high it is important to reiterate that the current model was created to model the behavior of a single layer of material whereas the parts that were experimentally evaluated consisted of between 18-20 layers.

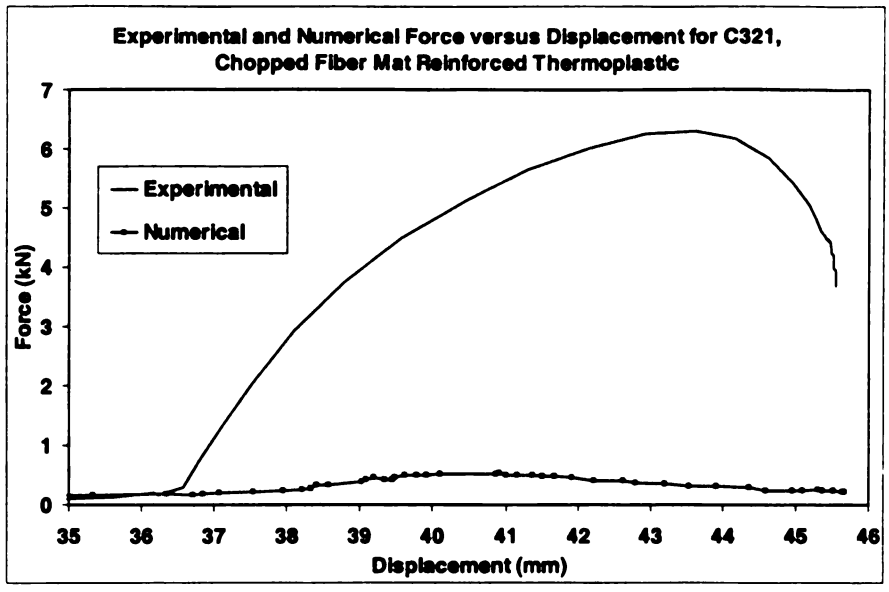

Figure 60. Experimental and numerical force versus displacement for C321, chopped fiber mat reinforced thermoplastic with a random orientation, zoomed in to illustrate the diverging path.

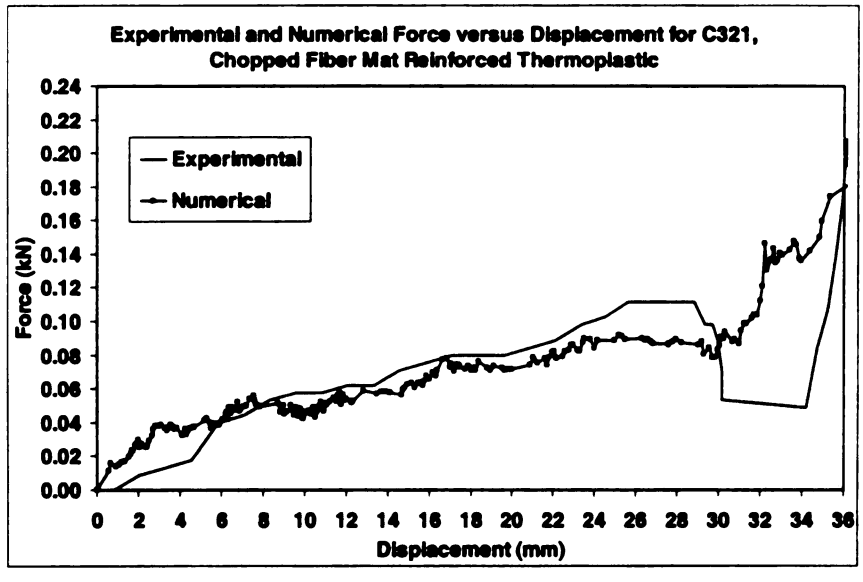

Figure 61. Experimental and numerical force versus displacement for C321, chopped fiber mat reinforced thermoplastic with a random orientation, up to a draw depth of 36 mm.

9.5.3. Woven Fabric Reinforced Thermoplastics

In addition to the fiber mat reinforced materials, the deformation behavior of a plain weave fabric reinforced thermoplastic material was also investigated using the two preferred fiber orientation model. Two preferred fiber orientations of 0° and 90° were used to build the numerical simulation with the material properties that were used to implement this model listed in Table 2.

Table 2. Material properties used as modeling input for the plain weave reinforced polypropylene.

Plain Weave	
$E_{f,0}$	19 GPa
$E_{f,90}$	19 GPa
$E_{m,all}$	76 MPa
$\nu_{f,all}$	0.22
$\nu_{m,all}$	0.1
$G_{f,all}$	2 GPa
$G_{m,all}$	0.2 MPa

A couple of reasons for choosing this material type for this investigation were; (a) that it provides a different type of material so that the validity of the updated material law could be investigated and (b) since the laminates were created in-house there existed the capability to perform experiments on a single ply. A comparison between the side view of the numerical results and side view of the experimental results is shown in Figure 62.

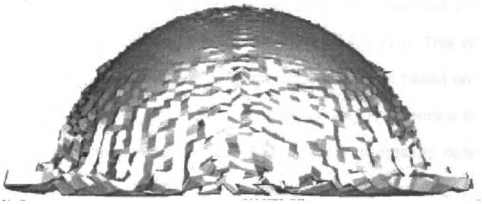

(a)

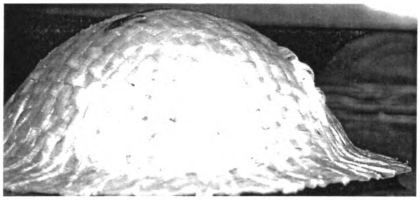

(b)

Figure 62. Side view of the numerical (a) versus experimental (b) results for woven fabric reinforced polypropylene using the updated material law with varying material properties and two preferred fiber orientations.

The comparison illustrated in Figure 62 demonstrates that the updated material law, specifically the two preferred fiber orientation, can qualitatively predict the localized buckling that occurs during the stamping of a single ply of the plain weave specimen. While the location and magnitude of the buckling differs, the model is able to predict this type of deformation behavior. One of the

major reasons for this discrepancy can probably be attributed to the choice of the material properties. Some assumptions regarding the properties had to be made, especially in regard to the in plane shear modulus, G_{12}. This value was derived through an extensive search of material handbooks based on a given range of values that was considerable. The proper way to determine this value would be to perform a series of picture frame tests in order to determine a material property that is specific to the material that is being modeled.

Chapter 10

STAMP THERMO-HYDROFORMING LITERATURE REVIEW

Through a thorough literature review there were no investigations found concerning the use of the hydroforming as a means for processing either thermoplastic or thermoset composite materials. Therefore, the main emphasis of the remaining literature review focused on the most recent experimental and numerical developments in the sheet metal hydroforming processes as well as the current state of experimental and numerical methods used for the processing of thermoplastic composites, specifically stamp forming and thermoforming.

10.1. Sheet Metal Literature Review

Based on the success found with using a hydrostatic pressure to delay the onset of fracture within metallic materials the same idea was extrapolated to the possible use of a hydrostatic force during the processing of thermoplastic materials. This led to the idea of adopting the use of sheet hydroforming currently used by sheet metal industries as a means of processing fiber reinforced thermoplastic composite sheets. In order to better understand the hydroforming process the literature review began by evaluating the current state of both the experimental and numerical sheet metal stamp hydroforming operations.

Yossifon and Tirosh (1977–1988) [56-60] published a series of articles dealing with the analysis of the hydroforming deep drawing process as applied to the formation of cups from metallic materials such as copper, aluminum, steel and stainless steel. The goal of the studies was to establish a hydroforming fluid pressure path, relative to the punch stroke, that would prevent part failure due to rupture or to wrinkling. Their earlier studies demonstrated the effect that excessive and insufficient fluid pressures have on the premature failure of hydroformed parts (rupture and wrinkling respectively). The purpose of the later investigations was to determine a predetermined path that can be followed to produce parts that are free from these types of defects.

In order to minimize wrinkling instabilities the fluid pressure was held to the minimum possible. The pressure relationship, based on equating the bending energy of the buckled plate and the work against lateral load (spring-type blank holder or fluid pressure) to the work done by the in-plane compressive membrane forces, included the governing parameters of friction coefficient and anisotropy. Through their work they were able to show that rupture instabilities occur when the fluid pressure being used for the hydroforming process was too high. The fluid pressure constrained the motion of the part and forced the punch through the material. The fluid pressure to prevent rupture was evaluated in terms of average friction coefficient, material properties, and geometrical considerations. Using these two fluid pressure values a range was determined that allowed for the manufacture of parts without the occurrence of wrinkling or

rupturing. This theory was tested experimentally and the results were very favorable with the predicted outcomes.

Lo et al. (1993) [61] expanded upon the earlier work of Yossifon and Tirosh [56-60] by applying the deep drawing hydroforming theory to the analysis of the hemispherical punch hydroforming process. The purpose of this work was to determine a theoretical method of predicting failure due to wrinkling (buckling) or rupture (tensile instability) during the punch hydroforming of hemispherical cups. This work was basically an extension of the work done by Yossifon and Tirosh [56-60] by incorporating a general friction-force expression into the analysis and expanding to more complicated geometries.

In order to predict failure the part was split into three regions based on the geometric characteristics of this operation. First there was a region where the part was free from contact with the die, a second region that consisted of the unsupported area termed the "lip area", and the third region that was the area of the part that had already come into contact with the surface of the punch. Along with the determination of the failure areas, the study also attempted to identify an upper and lower bound for manufacturing, a region termed the "work zone". It was proposed that if processes were run within these limits then there should be limited potential for failure. They were able to conclude that the working zone could be expanded by low friction forces, high strain hardening exponents, small drawing ratios, thick sheets, and through the use of orthotropic materials.

Hsu et al. (1996) [62] attempted to verify the theory developed by Lo et al. [61] through a series of experimental procedures. The purpose was the validation and verification of the failure prediction method for wrinkling and rupture instabilities during the punch hydroforming of sheet metal hemispherical cups. Various hydroforming pressure paths were tested during the process to validate the theory. They determined conclusively that a path that intersected the lower boundary of the working zone would lead to premature material failure due to wrinkling in every case. The same result was found for the pressure paths that intersected the upper boundary of the working zone. Through a series of varying parameter experiments the results achieved experimentally were very comparable to the theoretical predicted results.

Gelin et al. (1994) [63] experimentally and numerically studied the effects of process parameters during the aquadraw deep drawing process. The purpose of the study was to determine the main parameters that influence the aquadraw deep drawing process, specifically, the determination of the pressure in the cavity and under the blank holder as functions of process geometry, material parameters, and fluid parameters. Aquadraw deep drawing compared to hydroforming differs due to the use of a thin layer of water, subjected to fluid flow, that replaces the thin rubber diaphragm between the material and the die cavity. The investigation, limited to axisymmetric sheet metal materials, proposed a

cavity pressure modeling technique based on the optimal parameters of the process instead of being modeled by the Reynolds equation.

A relationship to determine the cavity pressure was based on the material behavior, the material thickness, the die entrance radius, and the drawing ratio. The value determined was always the maximum value. The paper evaluated the influence of each of these parameters on the overall cavity pressure determination. The study referenced other experiments performed that demonstrate the effectiveness of these parameters on the determination of this cavity pressure, but no experiments were performed that physically validated the new relationships proposed through this investigation.

For the numerical analysis portion of the investigation the finite element modeling code POLYFORM was utilized to simulate the deep drawing process in order to validate these relationships. Overall, the predicted behavior was comparable to the experimental behavior for the parts analyzed.

Gelin et al. (1998) [64] and Baida et al. (1999) [65] both expanded upon the earlier numerical work dealing with the aquadraw deep drawing process. These two investigations expanded upon the numerical work by adding the process parameters monitoring, identification tools and general sensitivity analyses to the numerical method used as a predictor of the die cavity pressure during the deep

drawing process. Overall their respective results showed very good correlation between the numerical and experimental behavior of the material.

Shang et al. (1997) [66] spent time on the evaluation of the copper spherical shell hydroforming process by studying the effects of intermittent draw-in during the operation. The purpose of this investigation was to examine, experimentally and numerically, the effects these intermittent changes would have on the formability of the blank material. During the processing of the cups there were two main formability factors that were investigated; the radius of the die shoulder and the blank holding force. Reducing the die shoulder radius increased formability but the use of a small radius had the potential of causing premature tearing of the blank along the die shoulder. Reducing the blank holding load encouraged draw-in, inward flow of the flange material, thereby increasing the average thickness of the product and delayed the onset of material failure.

Since the radius of the die shoulder is normally fixed or limited by the product specifications then the logical approach to increasing formability would be to vary the blank holding load. During this study the copper material was formed into a nearly spherical shell using four different approaches. The first approach was a single-stage hydroforming process using two different deformation paths, one that allowed for the draw-in of the flange, and one that did not allow the draw-in to occur. The second approach evaluated the effect of a double-stage hydroforming process also using two different flow paths. The first path allowed

for the draw-in during the first stage, and restricted it in the second. The second path was just the opposite, draw-in was not allowed during the first stage yet was permitted during the second stage. The results showed that during the single-stage hydroforming process, the formability of the material was greatly improved. For the double-stage hydroforming operation, the best results were achieved during the path that did not allow for the draw-in of the flange during the first stage, but did during the second stage.

10.2. Thermoplastic Forming Literature Review

Hou et al. (1991) [67] investigated the development of a thermoplastic composite stamp forming process for carbon fiber reinforced polypropylene. The main goals of the research were the establishment of a useful processing technique and the control of the parameters that led to the production of a quality composite part. The useful processing conditions included process temperature, cycle time, stamping velocity and stamping pressure. The experiments were conducted using a right angle matched tool forming parts from a continuous carbon fiber reinforced polypropylene composite material. Important conclusions drawn were that the stamping pressure is related to the stacking sequence of the laminates, it decreases with an increase in the number of 90° lay-ups due to transverse flow. The stamping temperature was determined to be at a range that is slightly higher than the melting temperature of polypropylene and that the

stamping pressure had more influence on the final part properties than the stamping velocities.

Hou (1997) [68] continued the earlier work by applying the same concepts and principles to the stamp forming of continuous unidirectional glass fiber reinforced polypropylene composite materials. The goal was the same as before, to establish a useful processing technique that leads to the production of a quality part. Experimentally the hold-down pressure became the limiting factor for the stamp forming process.

Harper (1992) [69] investigated the most recent developments of the thermoforming processing methods for shaping thermoplastic matrix composites. Some of the major disadvantages associated with the thermoforming method were discussed and addressed. The disadvantages included: the difficulty of stretching the material when trying to clamp it to the frame, the possibility for the material to be incompressible in thickness due to the density of the packed continuous fibers, buckling concerns, the speed of the forming requirements and the difficulties associated with the control of the fiber placement.

Pegoretti et al. (1997) [70] evaluated the anisotropic fracture behavior of polypropylene cups created by a vacuum thermoforming process. The anisotropic behavior was studied through an elasto-plastic fracture mechanics approach. Experiments were conducted using samples with high length/width

ratios drawn to depths of 100 and 58 mm. Results illustrated that the anisotropic behavior of the polypropylene was pronounced as the thermoforming draw-ratio increased. In all cases, the yield strength was found to be higher along the drawing direction

O' Bradaigh et al. (1993) [71] studied a general-purpose finite element simulation code that predicted the stresses and deformations in a composite sheet subject to, predominantly, planar forming forces during a diaphragm forming operation. The numerical analysis method incorporated the kinematics and rate dependence of the instabilities encountered during manufacturing, while still allowing for geometric generality. The two most limiting modeling assumptions made through this study were the planar restrictions and the purely viscous response assumptions. The finite element modeling was accomplished utilizing FEFORM, based on the finite element analysis (FEA) code PCFEAP.

In conjunction with the FEA analysis, experimentation was performed using a heated circular punch and mold. The objective was to investigate the stress and deformation states of the composite sheet and to draw conclusions regarding the sensitivity of the shear-buckling phenomenon to the different process parameters that could be varied including the uniform radial velocity, the uniform radial pressure, and pressure loading. The results showed very good agreement between the FEA modeling and the experimental results in the fiber direction. Somewhat poorer results were found in the transverse direction.

McGuinness et al. (1995) [72], through experimental and numerical work, focused on the occurrence of buckling during sheet forming of fiber reinforced composite materials into a hemispherical mold. The purpose of this experimental procedure was to study the effect that changes to the preform shape would have on the buckling patterns observed during the forming of quasi-isotropic laminates. More specifically, the goal was to determine if a square laminate was less prone to buckling at the 45º point than at the 0 and 90º points.

The physical portion of the experiment was accomplished using a computer-controlled thermoforming autoclave; the parts were not mechanically stamped but were formed by utilizing a pressure differential. Four types of preform shapes were evaluated; square, large rectangular, small rectangular and a truncated square preform achieved by cutting two corners off the square preform. No definitive conclusions were drawn from the experimental study about which shape outperformed the other. The numerical analysis results showed very good correlation with the experimental results. Overall conclusions of the study illustrated that for unidirectional and cross-ply laminates the shear stress at 45 º to the fiber directions controlled the buckling pattern. For the quasi-isotropic laminates, the axial compressive stress of the fibers that ran tangent to the buckling site determined the occurrence of the instability.

Long et al. (1996) [73] were concerned with the development of mathematical modeling techniques that describe the deformation of continuous random fiber reinforced thermoplastic materials during preform manufacture. The investigation used a numerical finite differencing scheme developed to simulate the material's behavior. The local stresses and strains were derived from equilibrium of forces, mass continuity, and plasticity theory. The model was verified through an experimental axisymmetric stretch forming process using both a hemispherical and a wheel hub punch. The main goal of the study was to develop a modeling method that could be extended from the simple hemispherical and wheel hub punch geometries to more complex forming operations.

Overall, the results from the modeling process were relatively similar to the actual experimental results. The conclusions of the paper were that the results could be used for the material tested, but that the assumptions that went into the calculations should be re-evaluated before changing the material. This is due to the changing nature of different composites as they are manufactured.

Kozieyet al. (1997) [74] presented the advantages and disadvantages of various constitutive equations for the description of the extensional behavior of polymers. The study's purpose was to introduce and evaluate the following mathematical models for the prediction of wall thickness distributions for thermoformed parts: Mooney-Rivlin model, Ogden model, G'Shell model,

Modified G'Shell model and K-BKZ model. The conclusions drawn were that the best results were achieved through the Modified G'Shell model but that these results were still less than perfect. The reason for this discrepancy was attributed to the fact that uniaxial data was used in an attempt to predict biaxial deformations.

Hsiao et al. (1997) [4] developed a methodology of analyzing the deep drawing process for thermoplastic composite laminates where the processing governing equations and the corresponding material properties of the composites were derived by the homogenization method. The finite element modeling at the macroscopic and microscopic levels was then developed for the simulation of the deep drawing process. In this study, numerical results from this methodology were demonstrated and compared with experimental observations.

The study proposed to break the process into two distinct stages; Thermoforming and Cooling. The governing equations for each stage were developed and the homogenization method was utilized to make these equations adaptable to the FEA environment. The homogenization method was able to de-couple the governing equations into a set of microscopic and macroscopic equations. The microscopic equations accounted for the characteristic deformation within the microstructures while the macroscopic equations accounted for the average deformation for the composite structure. The

microscopic equations were solved and used as input information for solving the macroscopic equations within the FEA analysis.

The process was verified by running experiments utilizing cylindrical and square punches. The experimental results for the fiber orientation prediction compared very favorably with the predicted theoretical results for both punches. Overall the numerical analysis proposed showed good results for predicting the macroscopic and microscopic stresses and strains, the fiber orientation and the final shape.

Chapter 11

STAMP THERMO-HYDROFORMING

An important goal in composite processing research is determining an optimum method of production for a new product. This requires a thorough understanding of the manufacturing processes involved as well as a detailed understanding of the fundamentals of deformation mechanics involved in the processes. Through the constitutive modeling, the deformation mechanics should be clearly identified. The constitutive model will need to be verified to ensure that it can accurately predict the behavior of the composite material during these processing operations.

The first step of this verification was addressed in previous chapters and is the development of the constitutive model for predicting the deformation behavior of fiber reinforced thermoplastics with multiple preferred fiber orientations. The experimental work will be used in order to evaluate the new constitutive models by comparing the numerical results with stamping experiments. The preliminary results from these experiments will be used to fine-tune the constitutive models and changes may be made to the model depending on the agreement found between the numerical and experimental portions of the research work.

Initially experiments will focus on forming hemispherical cups but once good agreement between the modeling and experiments is found the work could be

expanded and optimized with complex geometries such as elliptical and tapered square punches, eventually moving to parts that are very complex with different regions of concavity.

So, in addition to the constitutive modeling aspect of this work there is also an experimental portion that deals with the developing, designing, building and testing of a new processing method for the shaping and forming of fiber reinforced thermoplastic materials, stamp thermo-hydroforming. Since the stamp thermo-hydroforming process had never been attempted for the shaping and forming of composite materials, a fair amount of time was spent building and refining the process. The following sections will address the background of the process as well as the experimental set up and some experimental results.

11.1. Stamp Thermo-Hydroforming Background

The idea behind this experimental research effort started with a simple analysis of composite shaping techniques such as thermoforming and vacuum bag molding. The thought was that there are a variety of methods that can be used to shape and process fiber reinforced thermoplastic and thermoset composite materials but that each method had its distinct drawbacks such as economic cycle time concerns. The initial goal was to review these different processing methods and to identify areas that could be improved upon.

One of the processes that were evaluated was the thermoplastic sheet forming method commonly referred to as thermoforming or vacuum forming. In thermoforming, illustrated in Figure 63, the thermoplastic sheet is clamped above a negative, or female, mold and the sheet is heated. After the material is softened to its forming temperature the air beneath the sheet is evacuated through small holes that are machined into the mold. By evacuating the air from the chamber the thermoplastic material is sucked down into the mold thereby taking the required shape. Typically this process can be just a straight vacuum operation or may use a ram or plug to assist the processing (plug assisted method is illustrated in Figure 63).

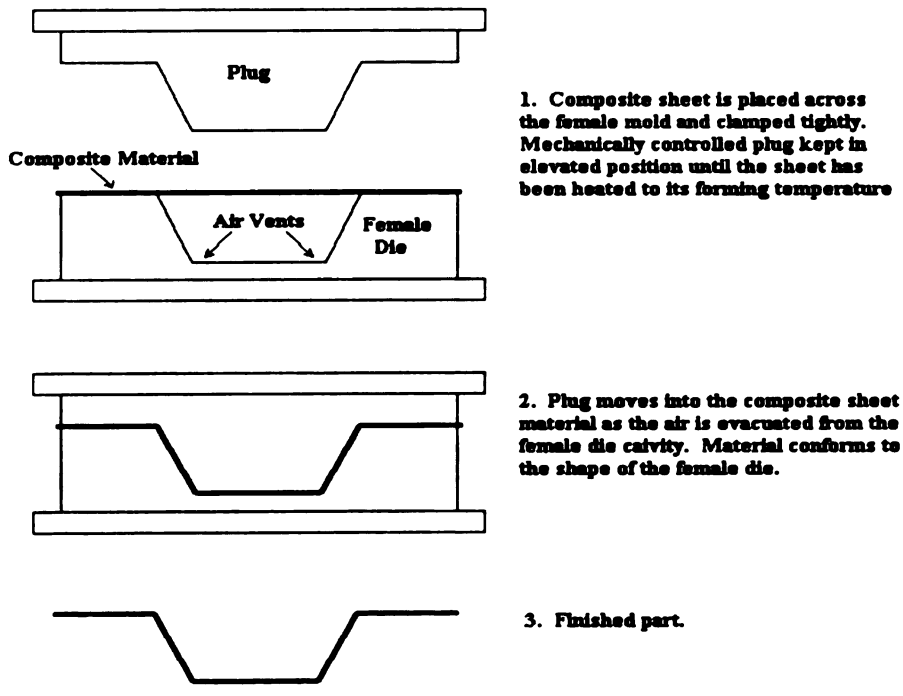

Figure 63. Illustration of the plug-assisted thermoforming processing method for thermoplastic composite materials.

While the thermoforming method is quite simple and relatively inexpensive, there are some disadvantages associated with the process. First off is that the material is very difficult to control as it moves through the lower chamber. This has the tendency to create parts that may have varying wall thickness and poor material distribution. The process has a considerable amount of waste associated with it and a fair amount of finishing is required at the completion of the process. In addition the range of shapes is limited and the ability to create parts with great detail is not attainable (McCrum et al., 1992 [75]).

In general, the most important complication associated with the thermoforming process is the ability to control the onset of both rupturing and wrinkling instabilities. These instabilities typically occur due to the nature of the process. As the air is evacuated from the female die chamber the material is drawn into the chamber and conforms to the shape of the female die. One of the obstacles is the uncontrolled nature of the material movement through the chamber. The thermoforming method requires very accurate control of both the draw rate and the clamping force used to hold the material in place. In addition, the thermoforming process as shown in Figure 63 allows for the formation of parts due to pure stretch only, no material draw-in is allowed.

An evaluation of the rupturing instabilities began with an investigation into the general manner in which thermoplastic material may fracture. In the most generic sense, the first step of the fracturing process is void formation. As the

material undergoes deformation the matrix and fiber material will begin to move, sometimes independent of one another. As the stress in the part increases the voids that were created during the manufacturing process will begin to grow in size. As they grow they start to come in contact with other voids, eventually, as the deformation of the part continues, enough voids will form to propagate across the part and will lead to material fracture.

The next step was to try to evaluate methods that could be used to alleviate the onset of rupturing within the framework of the thermoforming process. The attention turned to the control of fracture within the sheet metal industry. McClintock (1968) [12] and Rice et al. (1969) [13] conducted studies on sheet metal blanks that demonstrated rapidly decreasing fracture ductility as a hydrostatic pressure, applied across the material, was increased. Clift et al. (1990) [14] and Hartley et al. (1992) [15] demonstrated that for sheet metal draw blanks, the use of a hydrostatic pressure prevented the initiation and spreading of microcracks within the metallic material.

This finding led to the idea of using a hydrostatic pressure as a means of controlling material fracture during the processing of thermoplastic materials. One method of hydrostatic pressure application that was investigated was the use of stamp hydroforming as a means for processing composite parts. In addition to the fracture control the use of the hydrostatic pressure has the benefit of aiding in the reduction of wrinkling during the forming process.

The stamp hydroforming process is used for the shaping of sheet metal parts but no information could be located about the application of the hydroforming method to the shaping and processing of thermoplastic composite materials. Therefore, it was concluded that the study of the stamp hydroforming process, as a viable alternative to the conventional processing methods such as thermoforming and stamp forming, as a means for processing thermoplastic composite materials was warranted.

11.2. Stamp Thermo-Hydroforming Introduction

Stamp hydroforming utilizes a controllable pressurized fluid acting against the sheet to aid in the forming of the final part. The fluid is pressurized in an attempt to force the material to conform to shape of the punch. In addition, the fluidized pressure may also be used as a self-adjusted holding force for the material draw blank. Hydroforming differs from the conventional drawing process due to the presence of this pressurized fluid that replaces the female die typically associated with the process.

The advantages of such a process are numerous and the process is receiving significant attention from both the automotive and aerospace industries. Some of these advantages, Table 3, include highly improved drawability of the blank due to the applied pressure by the fluid, low wear rate of dies and punch, reduced

thinning in the final product when compared to conventional drawing, significant economic savings associated with the decreased tooling, and the potential for reducing the amount of finishing work required (Okine et al., 1990 [76]).

Table 3. Advantages and disadvantages of the stamp thermo-hydroforming process.

Advantages	
Improved drawability	Applied pressure delays fracture onset (see Figure 2)
Low wear rate of tooling	Eliminates contact between forming tools
Reduced thinning in final part	Pressure aids in the uniform distribution of strains
Significant economic savings	Eliminates the need for a female die and curing oven
Environmentally friendly	Consolidates multiple stamping operations, eliminates some finishing operations and reduces scrap/waste
Optimized processing	Better finish and all inclusive forming/curing process
Complex shapes	Could process complex parts with convex contours
Disadvantages	
Cycle time	Longer than stamping and thermoforming
Temperature challenges	Balance between material, fluid and tool temperature
Fluid pressure punch stroke	Optimal path may be part specific

The hydroforming process, as shown in Figure 64, represents a part that is being formed by a simple hemispherical punch. Prior to the start of the process the thermoplastic composite material is heated in an oven to bring the material to its forming temperature. Once the part has been heated to the appropriate temperature the sheet is transferred to the stamping press and is placed on the

clamping mechanism, as shown in Figure 64.1. Figure 64.2 shows the upper fluid chamber being lowered and the sheet being clamped securely between the two die halves, creating a seal for the upper fluid chamber. The fluid is then injected into the chamber and is given an initial pressurization.

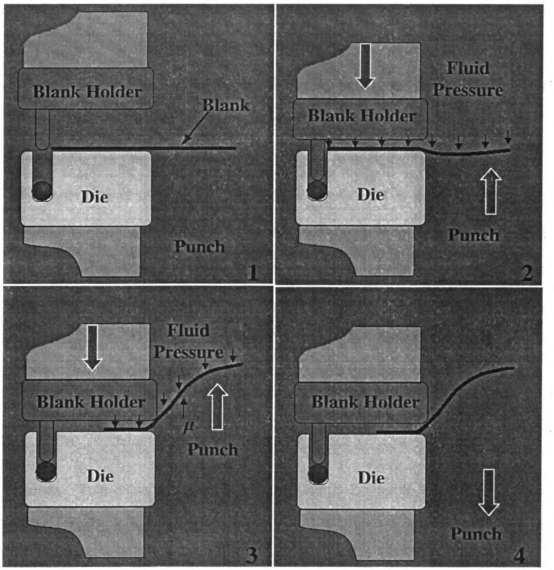

Figure 64. Schematic of the stamp thermo-hydroforming process.

As the punch travels the sheet begins to deform into a hemispherical shape initially, and finally deforms into a fully formed part after the punch penetrates deeper into the blank, Figure 64.3. While the punch is deforming the sheet the fluid volume within the upper chamber is decreasing, thereby causing the pressure within the upper chamber to increase. This increased pressure is used as a means of forcing the material to conform to the shape of the punch.

Once the punch has reached the prescribed draw depth, the fluid can be drained and the chamber can be raised, Figure 64.4. If the part has solidified adequately the punch can be retracted and the part can be removed, if more solidification time is required, the punch can be left in place until the part has achieved solidification. If the environmental surroundings are not adequate for the part solidification then the upper fluid chamber can be drained and either cool fluid or air can be injected to help decrease the finished parts total solidification time.

The process of hydroforming, unlike conventional stamping, involves supporting the bottom of the sheet with a bed of viscous fluid during the stamping process. This external support provides a through-thickness compressive stress that will improve the formability of the sheet by delaying the tensile instability (i.e. necking). Also, this external support reduces the formation of wrinkles due to tensile frictional forces.

In the stamp hydroforming of sheet metals, and the same issue will arise for composite materials, the difficulty lies in finding an appropriate fluid pressure-punch stroke path which will avoid rupture of the material yet control the onset of wrinkling instabilities. Yossifon and Tirosh (1977 – 1988) [56-60], Lo et al. (1993) [61] and Hsu et al. (1996) [62] performed a series of experiments and analyses that established this fluid pressure-punch stroke path for the stamp hydroforming of metallic hemispherical cups.

The stamp hydroforming process, when applied to composites, must be modified slightly due to the inherent differences between polymers and metals. Heat must be applied in order to reduce the stiffness of the thermoplastic matrix by increasing its temperature between the glass transition point and the melting point. Increasing the temperature of the pressurized fluid will allow the application of heat to the composite sheet. Since a heated fluid is used to shape the piece, good productivity can be expected from hydroforming due to the high heat transfer coefficient of the fluid.

Finally, a significant problem with stamping of composite sheets is to maintain the blank in place by using clamps. If the load needed to draw the sheet is higher than the shear yield stress of the composite, the sheet will slide from under the clamps (Hsiao et al., 1997 [4]). Hydroforming requires significantly less force, if the sheet is to be clamped at all, as the hydrostatic pressure is often sufficient to

hold the sheet in place. This last problem is often significant with composites as the polymer matrix can yield easily in the clamped region.

11.3. Experimental Apparatus

The experimental apparatus was built around an Interlaken 75 double action servo press, shown in Figure 65, where the double action refers to the clamping mechanism moving independently of the punch mechanism. The ability to independently control both the clamp and the punch affords the opportunity for various modifications of the experimental procedure. The experimental process started with a few modifications that were made to a limiting dome height (LDH) test setup, including drilling ports for pressure measurement, removing the air during the filling process and for filling and draining the fluid chamber. Figures 66 and 67 are pictures of the in-house designed dies that have been used to study the stamp thermo-hydroforming process.

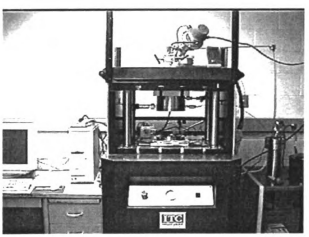

Figure 65. Stamp thermo-hydroforming experimental set-up.

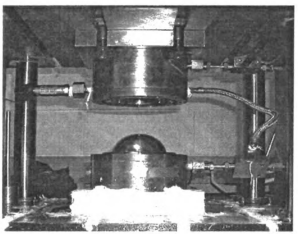

Figure 66. Die created to apply fluid pressure form either one or both sides of the composite sheet [77].

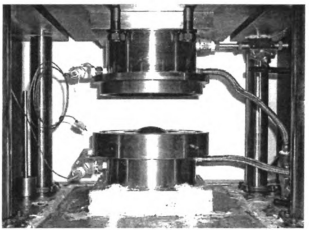

Figure 67. Die created for evaluating wrinkling behavior [77].

The experimental set-up was designed to fabricate 100 mm (4 in) diameter hemispherical cups using glass mat fiber reinforced polypropylene thermoplastic material that was supplied through a partnership with Azdel Inc. The experiments that can be conducted can be broken down into three major

categories, fluid pressure applied from one side of the material and fluid pressure applied from both sides of the sheet, and application of a fluid differential during processing.

Three different types of experiments can be performed under each fluid pressure category: pure stretching experiments, draw-in experiments (the material is not rigidly clamped, thereby allowing the material to draw-in to the chamber during forming), and experiments where a combination of pure stretch and draw-in are performed. In addition the three different categories can be further evaluated using a constant fluid pressure or a varying fluid pressure.

11.4. Hydroforming Challenges

One of the major obstacles that must be overcome with the stamp thermo-hydroforming process is the difficulty associated with finding an appropriate fluid pressure-punch stroke path that will avoid rupture of the material yet control the onset of wrinkling instabilities. For the stamp thermo-hydroforming of thermoplastic composite sheets the determination of this optimal path will be dependent on a number of factors but can be classified into three main categories: material, fluid and temperature. Therefore, there is the need to establish an upper and lower limit on the fluid pressure, as it relates to the punch stroke, to determine an optimum fluid pressure punch stroke path to ensure

limited rupturing and wrinkling failures of the finished part. A generalized curve is illustrated in Figure 68

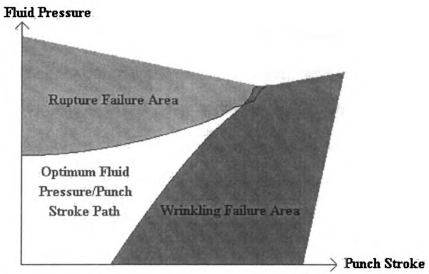

Figure 68. Generalized optimum fluid pressure punch stroke path for processing glass mat reinforced thermoplastics to avoid both rupturing and wrinkling.

The first category to be discussed refers to the choice and behavior of the composite sheet material. One of the major challenges with the material concerns the delicate balance between the fluid pressure and the ductility of the material chosen for the hydroforming process. The fluid pressure needs to be high enough to bend the work piece through its radius of curvature to conform to the shape of the punch yet the material needs to be ductile enough to take this bend without rupturing.

Another material challenge concerns the macroscopic and microscopic behavior of the material. The behavior of the thermoplastic materials during the processing operation is not easily predicted using just the macroscopic properties of the material. When dealing with the composite materials, the better predictor of overall material behavior comes from a very thorough understanding of the microstructural behavior of the material. It is important to understand how each fiber moves in relation to the other fibers and how their movement affects the overall matrix in order to predict the overall shape of the finished part. It is also important to recognize that these microscopic changes in material behavior are dependent not only on the punch displacement but also on the fluid pressure alterations.

The second category to be evaluated in regard to hydroforming challenges is the choice of an appropriate fluid and fluid pressure. As illustrated by Yossifon et al. (1977-1988) [56-60] fluid pressures within the upper fluid chamber that are too high will cause the material to move through the radius of curvature much faster than the ductility of the material will allow. This will lead to premature rupturing of the draw blank material. On the other hand, if the fluid pressure is too low then there is not enough stretching being forced to occur during the process and the material will be prone to wrinkling. In addition to the fluid pressure it is also very important to choose an appropriate fluid for the process. The fluid needs to be incompressible and able to handle the temperature needed to maintain the

composite material at or above it glass transition temperature to ensure the part can be formed.

The third category of the hydroforming challenges is the temperature associated with the processing. Thermoplastic materials at room temperature are very brittle and will shatter if put through the stamping process. In order to shape thermoplastic materials they must first be heated at, or above, the glass transition temperature. The glass transition temperature of the material refers to the temperature at which the matrix has become malleable and can easily be shaped. The fluid that is going to be injected into the fluid chamber also needs to be heated prior to starting the forming process. The fluid temperature must be at or above the forming temperature of the material to ensure that the draw blank material does not drop below the glass transition temperature. Simultaneously, a heating system is placed around the upper and lower chambers in order to preheat the metallic surfaces prior to the start of the hydroforming process. The challenge is the timing involved with all these systems. The thermoplastic material does not retain heat for long periods of time and can typically lose between 15 – 30 ºC during the transfer between the oven and the die as illustrated in Figure 69. Therefore it is important to keep the transfer time to a minimum while ensuring that the die and fluid will not remove heat from the material before it has been shaped by the punch.

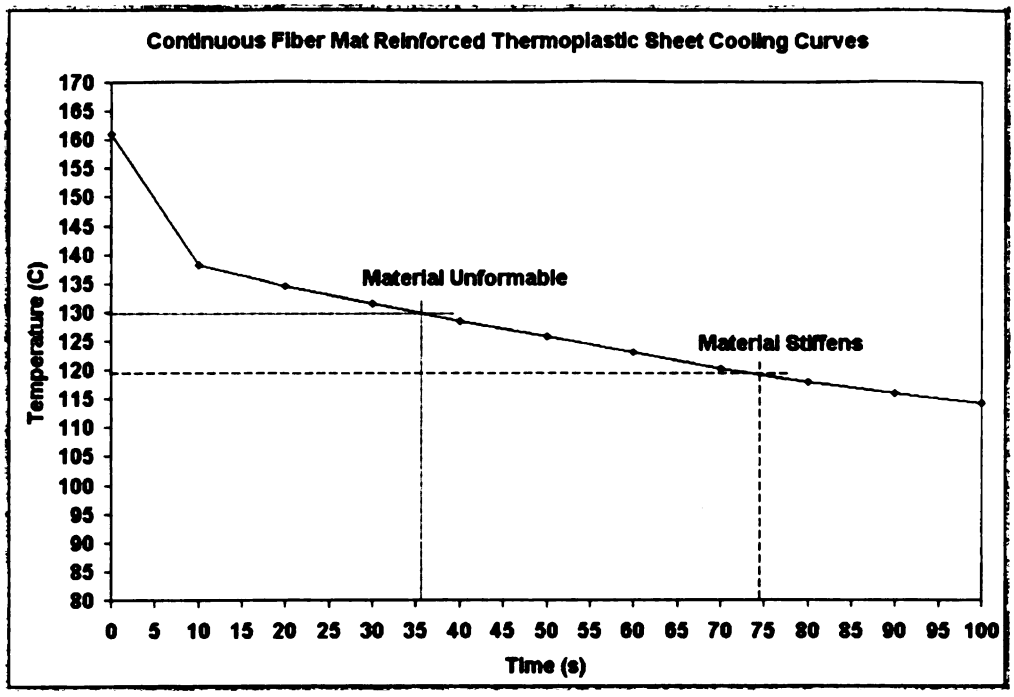

Figure 69. Cooling curve for a continuous fiber reinforced glass mat with a random orientation.

Finally, a significant problem with the stamp thermo-hydroforming of composite sheets is to maintain the sheet in place using clamps. If the load needed to draw the sheet is higher than the shear yield stress of the composite, the sheet will slide from under the clamps (Hsiao et al., 1997 [4]). Hydroforming requires significantly less force, if the sheet is to be clamped at all, as the hydrostatic pressure is often sufficient to hold the sheet in place. This is often significant with composites as the polymer matrix can yield easily in the clamped region.

11.5. Experimental Results

The initial results for the constant fluid pressure applied from one side undergoing pure stretch can be found in Figure 70. From these results a 7-10 percent increase in draw depth can be found when applying small levels of counteracting pressure.

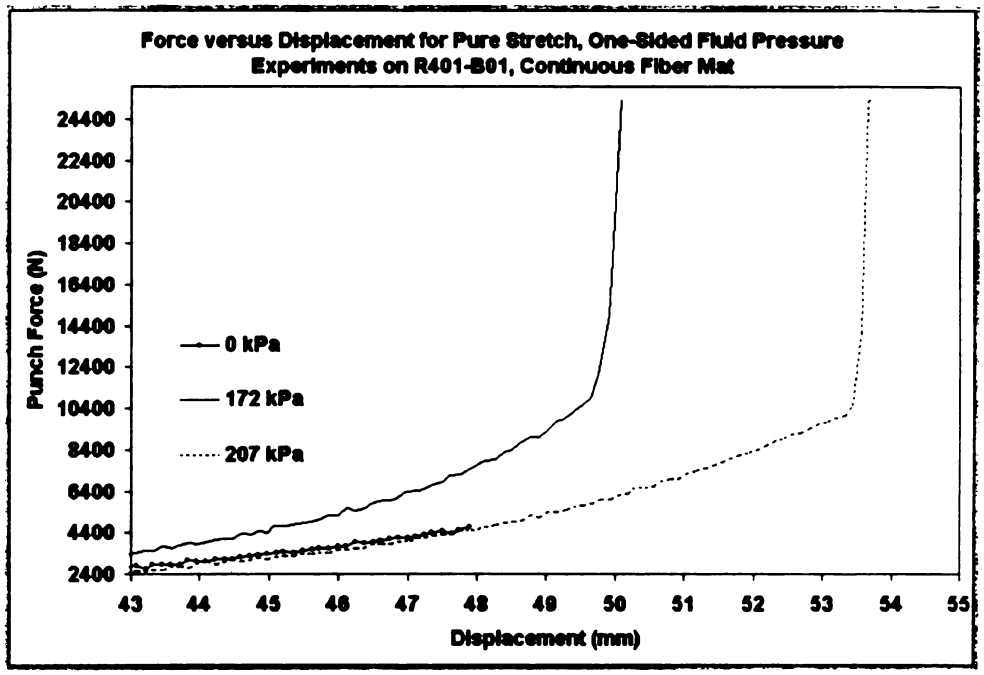

Figure 70. Draw depth results for glass mat fiber reinforced thermoplastics during stamp thermo-hydroforming.

In addition to the draw depth improvements the use of a counteracting hydrostatic pressure during forming has also led to less delamination of the material as evidenced by Figures 71 and 72. When there is no applied fluid

pressure the fibers within the material are allowed to pull out of the matrix as they reach their termination point. When the pressure is applied the fibers will fracture before pulling out of the matrix. Overall this provides more strength to the fractured areas since the fibers remain imbedded within the matrix.

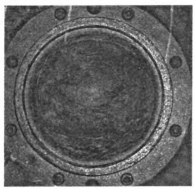

(a)

(b)

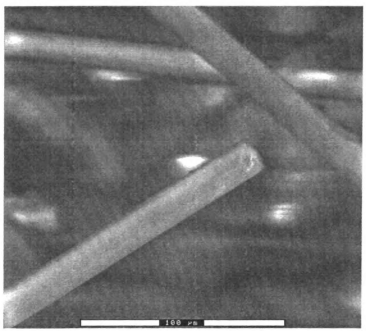

(c)

Figure 71. Delamination picture for 0 kPa case, a) top view of hemispherical part, b) side view of part, c) environmental scanning electron microscopy (ESEM) picture of glass fiber pulled out of the matrix.

(a)

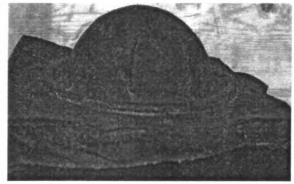

(b)

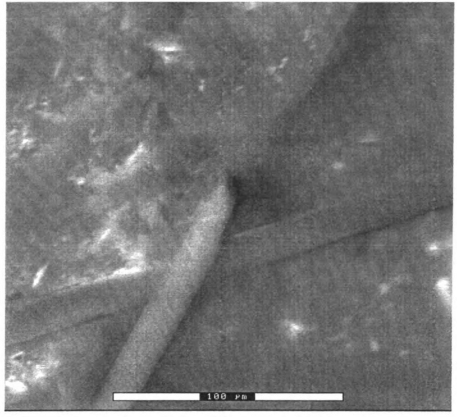

(c)

Figure 72. Delamination picture for an applied fluid pressure of 207 kPa (30 psi); a) top view of hemispherical part, b) side view of part, c) environmental scanning electron microscopy (ESEM) picture of glass fiber fracture.

11.6. Numerical Wrinkling Behavior Investigation

The experiments that were performed were used to investigate the effects of an applied fluid pressure during pure stretching. This type of testing allows for the investigation of the rupture characteristics of the material but since the material is rigidly clamped it does not allow for the investigation of the material's wrinkling behavior. One of the goals during the development of the updated material law was to use the constitutive relationship as a tool for eliminating some of the trial and error associated with the experimental process. So to this end the wrinkling behavior of the mat fiber reinforced materials was investigated numerically.

The main goal of this investigation was to determine whether an applied hydrostatic pressure would actually reduce the buckling that is occurring during the stamping process. This initial investigation was just to determine what type of effect the applied pressure would have on the wrinkling behavior of the material, not to try to optimize the pressure loading to achieve the optimal shape.

Figure 73 illustrates a continuous fiber mat reinforced material that was formed using a wide range of counteracting hydrostatic fluid pressures. From Figure 73 it is apparent that the applied pressure significantly reduces the wrinkles that are forming, especially within the flange of the material. The pressures applied in these investigations were constant and applied uniformly

over the part from the first step until the completion of the stamping process. A more realistic situation, and the one that showed the best results for aluminum samples (Zampaloni et al., (2002) [78, 79, 80] and Abedrabbo et al. (2003) [81]) would be the application of a varying pressure profile. A varying pressure profile typically starts out at a low pressure and increases throughout the processing, reaching its maximum at the final draw depth to ensure a properly formed part. Further work would need to be accomplished to optimize the pressure profile that should result in a better overall shape that minimizes wrinkling behavior for the fiber mat reinforced materials.

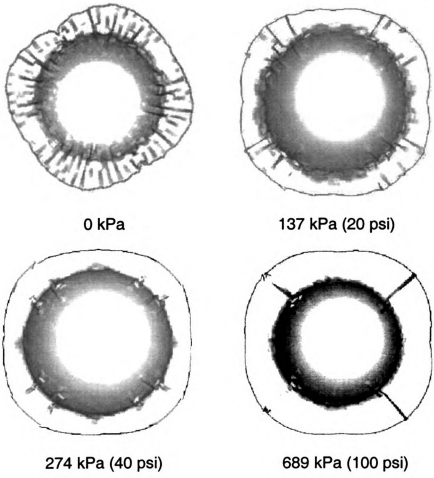

Figure 73. Numerical results of the stamp thermo-hydroforming process with constant fluid pressure.

Chapter 12

CONCLUSIONS

An important goal in composite processing research is determining an optimum method of production for a new product. This requires a thorough understanding of the manufacturing processes involved as well as a detailed understanding of the fundamentals of the deformation mechanics involved in the processes. Through the constitutive modeling, the deformation mechanics should be clearly identified and verified to ensure that it can accurately predict the deformation behavior of a composite material during processing operations.

This research work developed a constitutive model that accounted for the deformation behavior of the fiber mat reinforced thermoplastics with a random orientation. The model is based on multiple preferred fiber orientations, none of which are mutually perpendicular prior to or during deformation.

Two different types of mat fiber reinforced material were investigated. One was a continuous fiber mat reinforced polypropylene, while the other was a long, chopped fiber mat reinforced polypropylene. Both materials were characterized through a series of squeeze flow and uniaxial tensile tests. From these tests the preferred fiber orientations as well as the material properties were determined.

The constitutive model was implemented through a user-subroutine into the commercial finite element analysis code ABAQUS/Explicit. Numerical results were validated against experimental stamping results. Overall the updated material law constitutive relationship was able to accurately capture the material instabilities that occurred during the stamping process.

Since the mat fiber reinforced materials have not been extensively investigated this research creates one of the building blocks that can be used to develop more accurate models in the future. The model was developed for the single layer behavior so with the addition of a constitutive relationship for the interaction between the layers a constitutive relationship for the full sheet could be developed. In addition, the model focused only on the deformation behavior of the mat fiber reinforced materials and not on failure methods such as delamination or fracture.

In addition to the constitutive modeling aspect of this work there is also an experimental portion that deals with the development, design, build and verification of a new processing method for the shaping and forming of fiber reinforced thermoplastic materials, stamp thermo-hydroforming. Since the stamp thermo-hydroforming process had never been attempted for the shaping and forming of composite materials, a fair amount of time was spent building and refining the process.

Overall the process demonstrated a 7-10 percent increase in draw depth when applying small levels of counteracting pressure. In addition to the draw depth improvements the use of a counteracting hydrostatic pressure during forming led to less delamination of the material.

The wrinkling behavior of the mat fiber reinforced material was investigated numerically utilizing the updated material law constitutive relationship. Results showed that an increase of fluid pressure during forming significantly reduces the wrinkling instabilities occurring within the part and leads to a better formed part.

Chapter 13

RECOMMENDATIONS FOR FURTHER WORK

13.1. Constitutive Modeling/Numerical Analysis

Since the mat fiber reinforced materials have not been extensively investigated this research creates one of the building blocks that can be used to develop more accurate models in the future. The model was developed for the single layer behavior so with the addition of a constitutive relationship for the interaction between the layers a constitutive relationship for the full sheet could be developed. In addition, the model focused only on the deformation behavior of the mat fiber reinforced materials and not on failure methods such as delamination or fracture.

Further studies should be conducted on the applicability of this material model to other types of structures or to materials with more than three preferred fiber orientations. The logical extension is to apply this model to the chopped fiber mat reinforced thermoplastics using the four material directions that were characterized. Only two directions were utilized for this study based on the varying nature of the experimental stamping results.

13.2. Material Characterization

Further characterization needs to be investigated for the chopped fiber mat reinforced thermoplastics. Based on the experimental results the deformation mechanics of the chopped fiber mats is not captured as accurately. This might be attributed to the empirical relationships used to determine some of the material properties. For fibers that are not continuous, better empirical relationships might exist that would more accurately reflect the nature of the changing material properties.

Another material characterization issue that should be addressed is the area of elevated uniaxial tensile tests. The tests conducted in Chapter 8 were conducted at room temperature. The experimental parts were formed at an elevated temperature so this could lead to a disparity between what the numerical simulation predicts and what actually occurs during experimentation. Elevated temperature uniaxial tensile tests were attempted as part of this study but due to limitations with the equipment and with the laser extensometer the tests could not be completed with confidence.

APPENDIX

Appendix A

NON-ORTHOGONAL MODEL WITH TWO PREFERRED FIBER ORIENTATIONS

A non-orthogonal constitutive model for the deformation behavior of woven fabric reinforced thermoplastics was developed as a precursor to this work This constitutive model will be discussed here briefly just to give an overview of the work being conducted. The full details of this model, including a discussion of the results and applications, can be found in the papers by Yu et al. (2002 and 2003) [47, 48].

A linearized and incremental constitutive equation was derived by considering the structural unit of deforming woven FRT (Yu, 2001a, 2001b [49, 50]). Two assumptions were made: 1) the intersection points between two preferred directions can rotate freely, and 2) the fibers are attached to the resin matrix implying that the structural unit shares a common uniform strain. By applying mechanical properties to the fibers and the matrix, the total force and stresses are calculated considering the information on the structural parameters (thickness, structural unit dimension and fiber angle) and fiber properties. The material stiffness (relating strains and stresses) is then calculated using the kinematics and force equilibrium of the structural unit. The constitutive equation that was developed is shown in Equation 34.

$$\begin{bmatrix}\Delta\sigma_{xx}\\ \Delta\sigma_{yy}\\ \Delta\sigma_{xy}\end{bmatrix}=\begin{bmatrix}\frac{\tilde{E}^{\alpha}}{bc}+\Gamma\left(\frac{a}{\bar{h}}\right)\left(\frac{a^2}{c}\right)+\frac{2}{3}E^{M} & \Gamma\left(\frac{a}{\bar{h}}\right)\left(\frac{b^2}{c}\right) & \Gamma\left(\frac{a}{\bar{h}}\right)\left(\frac{ab}{c}\right)\\ \Gamma\left(\frac{b}{\bar{a}}\right)\left(\frac{a^2}{c}\right) & \Gamma\left(\frac{b}{\bar{a}}\right)\left(\frac{b^2}{c}\right)+\frac{\tilde{E}^{\beta}}{ac}+\frac{2}{3}E^{M} & \Gamma\left(\frac{b}{\bar{a}}\right)\left(\frac{ab}{c}\right)\\ \Gamma\left(\frac{b}{\bar{h}}\right)\left(\frac{a^2}{c}\right) & \Gamma\left(\frac{b}{\bar{h}}\right)\left(\frac{b^2}{c}\right) & \Gamma\left(\frac{b}{\bar{h}}\right)\left(\frac{ab}{c}\right)+\frac{1}{3}E^{M}\end{bmatrix}\begin{bmatrix}\Delta\varepsilon_{xx}\\ \Delta\varepsilon_{yy}\\ 2\Delta\varepsilon_{xy}\end{bmatrix} \quad (34)$$

Where $\tilde{E}^{\alpha}=E^{\alpha}A^{\alpha}$ and $\Gamma=A^{\gamma}E^{\gamma}/\left(a^2+b^2\right)^{3/2}$. Here a, b, and c are geometrical parameters of FRT composites, representing projected lengths of woven unit, and thickness. Fiber moduli in the two fiber directions and in the resin were symbolized by E^{α}, E^{β}, and E^{M} with the area variables of A^{α} and A^{β}.

The model was validated against a series of uniaxial tensile tests, picture frame tests and through sheet stamping processes. The numerical results showed good correlation with the experimental behavior. A full discussion of the derivation and of the modeling and experimental results can be found in references [47] and [48].

REFERENCES

REFERENCES

[1] Mallick, P. K., 1993, "Fiber-Reinforced Composites: Materials, Manufacturing, and Design", M. Dekker, New York, NY, pp. 1-175, 1993.

[2] Dweib, M.A. and O'Bradaigh, C.M., 1998, "Anisotropic Modeling of Isothermal Squeezing Flow of Glass-Mat Reinforced Thermoplastics (GMT)", *Polymer Composites*, Vol. 19, No. 8, pp. 588-599.

[3] Margolis, J.M., 1991, "Economics of Automotive Composite Applications", Composites in Manufacturing: Case Studies, edited by Strong, A.B., Society of Manufacturing Engineers, 1st Ed., pp.291-307.

[4] Hsiao, S.W.and Kikuchi, N., 1999, "Numerical Analysis and Optimal Design of Composite Thermoforming Process", *Computational Methods and Applied Mechanics and Engineering*, Vol. 177, pp.1-34.

[5] Fejes-Kozma, Z. and Karger-Kocsis, J., 1994, "Fracture Mechanical Characterization of a Glass Fiber Mat-Reinforced Polypropylene by Instrumented Impact Bending", *Journal of Reinforced Plastics and Composites*, Vol. 13, pp. 822-834.

[6] Czigany, T., Marosfalvi, J. and Karger-Kocsis, J., 2000, "An Acoustic Emission Study of the Temperature-Dependent Fracture Behavior of Polypropylene Composites Reinforced by Continuous and Discontinuous Fiber Mats", *Composites Science and Technology*, Vol. 60, pp. 1203-1212.

[7] Chow, S., Lussier, D.S. and Chen, J., 2001, "Shear and Friction Response of Co-Mingled Glass/Polypropylene Fabrics during Stamping", Proceedings of the 16th Technical Conference of the American Society for Composites, September.

[8] Gorczyca, J.L., Sherwood, J.A. and Chen, J., 2001, "Finite Element Modeling of the Shear Behavior of Woven Co-Mingled Glass/Thermoplastic Composites", Proceedings of the 16th Technical Conference of the American Society for Composites, September.

[9] Davis, S.M. and Mcalea, K.P., 1990, "Stamping Rheology of Glass Mat Reinforced Thermoplastics", *Polymer Composites*, Vol. 11, No. 6, pp. 368-378.

[10] Chen, J.L. and Sun, C.T., 1993, "A Plastic Potential Function Suitable for Anisotropic Fiber Composites", *Journal of Composite Materials*, Vol. 27, No. 14, pp. 1379-1390.

[11] Zinoviev, P.A., Tsvetkov, S.V., Kulish, G.G., van den Berg, R.W. and Van Schepdael, L.J.M.M., 2001, "The Behavior of High-Strength Unidirectional Composites under tension with Superposed Hydrostatic Pressure", *Composite Science and Technology*, Vol. 61, pp. 1151-1156.

[12] McClintock, F.A., 1968, "A Criterion for Ductile Fracture by the Growth of Holes", *Journal of Applied Mechanics*, Vol. 35, pp. 363-371.

[13] Rice, J.R., and Tracey, D.M., 1969 "On the Ductile Enlargement of Voids on Triaxial Stress Fields", *Journal of Mechanical Physics and Solids*, Vol. 17, pp. 201-217, 1969.

[14] Clift, S.E., Hartley, P., Sturgess, C.E.N., and Rowe, G.W., 1990 "Fracture Prediction in Plastic Deformation Process", *International Journal of Mechanical Science*, Vol. 32, No. 1, pp. 1-17.

[15] Hartley, P., Pillinger, I., and Sturgess, C., 1992 "Numerical Modeling of Material Deformation Processes Research Development and Applications", Springer-Verlag.

[16] Breen, D.E., House, D.H., and Wozny, M.J., 1994, "A Particle-Based Model for Simulating the Draping Behavior of Woven Cloth", *Textile Research Journal*, Vol. 64, No.11, pp.663-685.

[17] Sidhu, R.M.J.S., Averill, R.C., Riaz, M., and Pourboghrat, F., 2001, "Finite Element Analysis of Textile Composite Preform Stamping", *Composite Structures*, Vol.52, pp.483-497.

[18] Billoet, J.L. and Cherouat, A., 2000, "New numerical model of composite fabric behavior: simulation of manufacturing of thin composite part", *Advanced Composite Letters*, Vol.9, No.3, pp.167-179.

[19] Luca, P. de, Lefebure, P., and Pickett, A.K., 1998, "Numerical and Experimental Investigation of Some Press Forming Parameters of Two Fiber Reinforced Thermoplastics: APC2-AS4 and PEI-CETEX", *Composites Part A*, Vol.29, pp.101-110.

[20] Dong, L., Lekakou, C., and Bader, M.G., 2001, "Processing of Composites: Simulations of the Draping of Fabrics with Updated Material Behaviour Law", *Journal of Composite Material*, Vol. 35, pp.138-163.

[21] O'Bradaigh, C.M., and Pipes, R.B., 1991, "Finite element analysis of composite sheet-forming process", *Composites Manufacturing*, Vol. 2, No.3/4, pp.161-170.

[22] Spencer, A.J.M., 2000, "Theory of Fabric-Reinforced Viscous Fluids", *Composites Part A*, Vol.31, pp.1311-1321.

[23] Takano, N., Uetsuji, Y., Kahiwagi, Y., and Zako, M., 1999, "Hierarchical Modeling of Textile Composite Materials and Structures by the Homogenization Method", *Modeling and Simulation in Materials Science and Engineering*, Vol. 7, pp.207-231.

[24] Peng, X.Q. and Cao, J., 2000, "Numerical Determination of Mechanical Elastic Constants of Textile Composites", *International Symposium on Affordable Composites Manufacturing*, pp.677-686.

[25] Dweib, M.A. and O'Bradaigh, C.M., 1999, "Extensional and Shearing Flow of a Glass-Mat Reinforced Thermoplastics (GMT) Material as a Non-Newtonian Viscous Fluid", *Composites Science and Technology*, Vol. 59, pp. 1399-1410.

[26] Rogers, T.G., 1989, "Rheological characterization of anisotropic materials", *Composites*, Vol.20, No. 1, pp.21-27.

[27] Dweib, M.A., Vahlund, C.F. and O'Bradaigh, C.M., 2000, "Fibre Structure and Anisotropy of Glass Reinforced Thermoplastics", *Composites Part A*, Vol. 31, pp. 235-244.

[28] Lee, N.J. and Jang, J., 1999, "The Effect of Fibre Content on the Mechanical Properties of Glass Fibre Mat/Polypropylene Composites", *Composites Part A*, Vol. 30, pp. 815-822

[29] Lee, D.H. and Carnaby, G.A., 1992a, "Compressional Energy of the Random Fiber Assembly Part I: Theory", *Textile Research Journal*, Vol. 64, No. 4, pp. 185-191.

[30] Lee, D.H., Carnaby, G.A. and Tandon, S.K., 1992b, "Compressional Energy of the Random Fiber Assembly Part II: Evaluation", *Textile Research Journal*, Vol. 64, No. 4, pp. 258-265.

[31] McGee, S.H. and McCullough, R.L., 1984, "Characterisation of Orientation in Short-Fibre Composites", *Journal of Applied Physics*, Vol. 55, No. 5, pp. 1394-1403.

[32] Advani, S.G. and Tucker, C.L., 1987, "The Use of Tensors to Describe and Predict Fiber Orientation in Short Fiber Composites", *Journal of Rheology*, Vol. 31, No. 8, pp. 751-784.

[33] Kitano, T., Haghani, E., Tanegashima, T. and Saha, P., 2000, "Mechanical Properties of Glass Fiber/Organic Fiber Mixed-Mat Reinforced Thermoplastic Composites", *Polymer Composites*, Vol. 21, No. 4, pp. 493-505.

[34] Pillai, K.M., Tucker, C.L. and Phelan, F.R., 2001, "Numerical Simulation of Injection/Compression Liquid Composite Molding Part 2: Preform Compression", *Composites Part A*, Vol. 32, pp. 207-220.

[35] Ebewele, R.O., 2000, "Polymer Science and Technology", CRC Press LLC. Boca Raton, Florida.

[36] Goldberg, R.K. and Murthy, P.L.N., 2000, "Strain Rate Dependent Analysis of Polymer Matrix Composite Laminates Utilizing a Micromechanics Approach", Proceedings of the 15th Technical Conference of the American Society for Composites, College Station, Texas.

[37] Goldberg, R.K., 2001, "Implementation of Fiber Substructuring Into Strain Rate Dependent Micromechanics Analysis of Polymer Matrix Composites", Proceedings of the 16th Technical Conference of the American Society for Composites, Blacksburg, Virginia.

[38] Tsai, J. and Sun, C.T., 2000, "Nonlinear Constitutive Model for High Strain Rate Response in Polymeric Composites", Proceedings of the 15th Technical Conference of the American Society for Composites, September.

[39] Wang, C. and Sun, C.T., 1997, "Experimental Characterization of Constitutive Models of PEEK Thermoplastic Composite at Heating Stage During Forming", *Journal of Composite Materials*, Vol. 31, No.15, pp.1480-1506.

[40] Thiruppukuzhi, S.V. and Sun, C.T., 2001, "Models for the Strain-Rate-Dependent Behavior of Polymer Composites", *Composites Science and Technology*, Vol. 61, pp. 1-12.

[41] McGuinness, G.B., and O'Bradaigh, C.M., 1997a, "Characterisation of Thermoplastic Composite Melts in Rhombus-shear: the picture-frame experiment", *Composites Part A*, pp. 115-132.

[42] McGuinness, G.B. and O'Bradaigh, C.M., 1997b, "Development of Rheological Models for Forming Flows and Picture-Frame Shear Testing of Fabric Reinforced Thermoplastic Sheets", *Journal of Non-Newtonian Fluid Mechanics*, Vol.73, pp.1-28.

[43] Tsai, S.W., 1966, "Mechanics of Composite Materials," Part II, Technical Report AFML-TR-66-149.

[44] Halpin, J.C., 1984, "Primer on Composite Materials Analysis", 2nd Edition, Technomic Publishing Company, Inc., Lancaster, PA 17604.

[45] Potter, K.D., 1970, "The Influence of Accurate Stretch Data for Reinforcements on the Production of Complex Structural Mouldings", *Composites*, Vol. 10, pp. 161-167.

[46] Mohammed, U., Lekakou, C. and Bader, M.G., 2000, "Experimental Studies and Analysis of the Draping of Woven Fabrics", *Composites Part A*, pp. 1409-1420.

[47] Yu, W.R., F. Pourboghrat, K. Chung, M. Zampaloni, and T.J. Kang, "Non-orthogonal Constitutive Equation for Woven Fabric Reinforced Thermoplastic Composites", *Composites: Part A: Applied Science and Manufacturing*, Vol. 33, No. 8, pp. 67-77, September 2002.

[48] Yu, W.R., Zampaloni, M., Pourboghrat, F., Chung, K. and Kang, T. J., (2003) "Numerical Study of Stamp Thermo-Hydroforming Applied to Woven FRT, Comparison between Symmetric and Anti-Symmetric Deformation", accepted for publication in *Composites Structures*.

[49] Yu, W.R., Chung, K., Pourboghrat, F., Zampaloni, M., and Kang, T.J., 2001a, "A Constitutive Equation for Fabric Reinforced Thermoplastic Composites" 33rd International SAMPE Technical Conference (ISTC), SAMPE, Seattle, Washington, USA.

[50] Yu, W.R., Zampaloni, M. and Pourboghrat, F., 2001b, "Stamping of Woven Fabric Reinforced Thermoplastic Composites", Automotive Composite Conference, Society of Plastic Engineers, Michigan, USA, September.

[51] Okoli, O.I. and Smith, G.F., 2000, "Development of a Semi-Empirical Method for Obtaining the Dynamic Young's Modulus in Random Continuous Reinforced Glass/Epoxy Composites", *Journal of Reinforced Plastics and Composites*, Vol. 19, No. 4, pp. 292-300.

[52] Pinfold, M., 1995, "Composite Mechanical Properties for Use in Structural Analysis", PhD Thesis, University of Warwick.

[53] Nielsen, L.E., 1974, "Mechanical Properties of Polymers and Composites, Vol. 2", Marcel Dekker Inc., New York.

[54] Halpin, J.C. and Tsai, S.W., 1969, "Effects of Environmental Factors on Composite Materials", Air Force Technical Report, AFML-TR-67-423.

[55] Hewitt, R.L. and De Malherbe, M.C., 1970, "An Approximation for Longitudinal Shear Modulus of Continuous Fibre Composites", *Journal of Composite Materials*, Vol. 4, pp280-282.

[56] Tirosh, J., Yossifon, S., Eshel, R., and Betzer, A. "Hydroforming Process of Uniform Wall Thickness Products", *ASME Journal of Engineering for Industry*, Vol. 99, pp. 685-691, 1977.

[57] Yossifon, S., Tirosh, J., and Kochavi, E. "On Suppression of Plastic Buckling in Hydroforming Processes", *International Journal of Mechanical Science*, Vol. 26, pp. 389-402, 1984.

[58] Yossifon, S., and Tirosh, J. "Rupture Instability in Hydroforming Deep-Drawing Process", *International Journal of Mechanical Science*, Vol. 27, pp. 559-570, 1985.

[59] Yossifon, S., and Tirosh, J. "Buckling Prevention by Lateral Fluid Pressure in Deep Drawing", *International Journal of Mechanical Science*, Vol. 27, pp. 177-185, 1985.

[60] Yossifon, S. and Tirosh, J. "On the Permissible Fluid-Pressure Path in Hydroforming Deep Drawing Processes - Analysis of Failures and Experiments", *Journal of Engineering for Industry*, Vol. 110, pp. 146-152, 1988.

[61] Lo, S.W., Hsu, T.C. and Wilson, W.R.D. "An Analysis of the Hemispherical-Punch Hydroforming Process", *Journal of Materials Processing Technology*, Vol. 37, pp.225-239, 1993.

[62] Hsu, T.C. and Hsieh, S.J. "Theoretical and Experimental Analysis of Failure for the Hemisphere Punch Hydroforming Processes", *Journal of Manufacturing Science and Engineering*, Vol. 118, pp. 434-438, 1996.

[63] Gelin, J.C., Delassus, P. and Fontaine, J.F. "Experimental and Numerical Modeling of the Effects of Process Parameters in the Aquadraw Deep Drawing", *Journal of Materials Processing Technology*, Vol. 45, pp. 329-334, 1994.

[64] Gelin, J.C., Ghouati, O., and Paquier, P. "Modeling and Control of Hydroforming Processes for Flanges Forming", *CIRP Annals - Manufacturing Technology* , Hallwag Publ Ltd, Berne, Switzerland, Vol. 47, No. 1, p 213-216, 1998.

[65] Baida, M., Gelin, J.C. and Ghouati, O., 1999, "Modeling the Hydroforming of Thin Metallic Components", Proceedings of the Seventh International Symposium on Plasticity and Its Current Applications (PLASTICITY '99), Edited by Khan A., Cancun, Mexico, January 5-13, pp. 293-296.

[66] Shang, H.M., Qin, S. and Tay, C.J. "Hydroforming Sheet Metal with Intermittent Changes in the Draw-In Condition of the Flange", *Journal of Materials Processing Technology*, Vol. 63, pp. 72-76, 1997.

[67] Hou, M., and Friedrich, K. "Stamp Forming of Continuous Carbon Fibre/Polypropylene Composites", *Composites Manufacturing*, Vol. 2, No. 1, pp. 3-9, 1991.

[68] Hou, M. "Stamp Forming of Continuous Glass Fibre Reinforced Polypropylene", *Composites Part A-Applied Science and Manufacturing*, Vol. 28, No. 8, pp. 695-702, 1997.

[69] Harper, R.C. "Thermoforming of Thermoplastic Matrix Composites", *SAMPE Journal*, Vol. 28, No. 2, pp. 9-17, 1992.

[70] Pegoretti, A., Marchi, A., and Ricco, T. "Determination of the Fracture Toughness of Thermoformed Polypropylene Cups by the Essential Work Method", *Polymer Engineering and Science*, Vol. 37, No. 6, pp. 1045-1052, 1997.

[71] O' Bradaigh, C.M., McGuinness, G.B., and Pipes, R.B. "Numerical Analysis of Stresses and Deformations in Composite Materials Sheet Forming: Central Indentation of a Circular Sheet", *Composites Manufacturing*, Vol. 4, No. 2, pp. 67-83, 1993.

[72] McGuinness, G. B. and O Bradaigh, C. M. "Effect of Preform Shape on Buckling of Quasi-Isotropic Thermoplastic Composite Laminates During Sheet Forming," *Composites Manufacturing*, Vol. 6, No. 3-4, pp.269-280, 1995.

[73] Long, A.C., Rudd, C.D., and Middleton, V. "Modeling the Deformation of Thermoformable Fiber Reinforcements During Preform Manufacture", *Polymer Composites*, Vol. 17, No. 3, pp. 321-331, 1996.

[74] Koziey, B., Pocher, J., Tian, J.J., and Vlachopoulos, J. "New Results in Finite Element Analysis of Thermoforming", Annual Technical Conference - ANTEC, Conference Proceedings, Proceedings of the 1997 55th Annual Technical Conference, ANTEC, Apr 27-May 2 1997, pp. 714-719, 1997.

[75] McCrum, N.G., Buckley, C.P., and Bucknall, C.B., "Principles of Polymer Engineering", Oxford University Press, New York, NY, pp. 167-319, 1992.

[76] Okine, R.K., Edison, D.H., and Little, N.K. "Properties and formability of an aligned discontinuous fiber thermoplastic composite sheet", *Journal of Reinforced Plastics and Composites*, Vol. 8, p. 70, 1990.

[77] United States and Foreign Patents Pending, "Hydroforming of Composite Materials" Pourboghrat, F., Zampaloni, M. and Benard, A., Submitted December 2000.

[78] Zampaloni, M., Abedrabbo, N. and Pourboghrat, F., 2002, "Experimental and Numerical Study of Stamp Hydroforming of Sheet Metals", submitted to *International Journal of Mechanical Sciences.*

[79] Zampaloni, M., Yu, W.R. and Pourboghrat, F., 2002, "Part I of Stamp Thermo-Hydroforming for Shaping and Forming Glass Mat Fiber Reinforced Thermoplastics", submitted to *Journal of Thermoplastic Composites Materials.*

[80] Zampaloni, M., Yu, W.R. and Pourboghrat, F., 2001, "Experimental and Numerical Study of Stamp Thermo-Hydroforming for Shaping Glass Mat Fiber Reinforced Thermoplastic Sheets into Hemispherical Cups", Automotive Composite Conference, Society of Plastic Engineers, Michigan, USA.

[81] Abedrabbo, N., M. Zampaloni, and F. Pourboghrat, 2002, Numerical Study of Wrinkling Behavior of AL6111-T4 in Stamp Hydroforming", presented at NUMISHEET 2002, Jeju Island, South Korea.

[82] Sikarskie, D.L., 1998, "Strength Prediction of Random Fiber Composites", 3rd Annual Research Report submitted to the National Center for Manufacturing Science.